Modeling of Thermal Stress Cycling in Refractory Materials

by

Abhijit Pandhari

A THESIS SUBMITTED IN PARTIAL FULFILLMENT OF

THE REQUIREMENTS FOR THE DEGREE OF

DOCTOR OF PHILOSOPHY

in

The Faculty of Graduate and Postdoctoral Studies

(Materials Engineering)

THE UNIVERSITY OF BRITISH COLUMBIA

(Vancouver)

July 2017

Abstract

In metallurgical reactors, the thermal stress field of refractories always changes with the heat transfer conditions at the hot-face. It is suggested that 'thermally induced refractory cracking' is often the primary cause of in-service refractory failure but quantitative support for this is lacking. The current work is focussed on studying this aspect by developing an experimentally validated thermomechanical model that considers refractory strength degradation under repeated thermal cycling.

A thermo-mechanical model has been developed with ABAQUS to predict thermal stress and damage in a refractory specimen subjected to thermal cycling. An experiment based on the "contact-conduction method" that uses a hot/cold metal block to heat/cool a refractory specimen was carried out to validate the model. The experiments were run for up to 3-cycles starting from cold- and hot-refractory specimens. Thermocouples were used to gather temperature data from refractory and steel block. An inverse heat conduction model was developed to predict the heat flux applied to the refractory specimen by the steel block based on the temperature history from the steel block. Ultrasonic testing was carried out on the refractory specimens before and after the thermal cycling tests.

The contact-conduction method was successful in creating significant thermal gradients in the refractory specimens. Thermocouples on refractory located at 1cm from the steel-refractory show temperature variation of about 500°C and 575°C for cold- and hot-refractory specimen, respectively after 3-cycles.

The model was capable of predicting the temperature changes and damage in the refractory material after multiple cycles. Ultrasonic velocity tests show significant change in the sound velocities in the areas experiencing thermal cycling, indicating significant micro-cracking damage in those areas. It was seen that with multiple cycles the damage penetrated further into the specimen, however the magnitude of the damage does not increase significantly.

Application to an example tundish operation indicated that the model was capable of analyzing an ideal preheating schedule and was capable of predicting the effect of idle time and multiple thermal cycles on the damage in refractories. However, to predict thermal spalling more precisely, an integrated model that considers the effect of thermal gradients, chemical reactions and mechanical loads is needed.

Lay Summary

In the metallurgical reactors, a special type of insulting material known as “refractory” is used in the furnace-lining. While in service, refractories undergo alternate heating-cooling schedules due to the rotation of the furnace, charging-discharging and so forth. This process induces stress, known as “thermal stress” in the material that is considered to be one of the reasons to cause cracking in refractories. This work is focussed to study this aspect.

A new computer-based modeling methodology is developed to predict when and where the refractory material will crack while in service. A novel experimental technique is designed to create industry-like operating conditions to physically test the material in the lab and to validate the model. The results indicate that the model is successful in predicting cracking in refractories.

When applied, this mathematical model can be used to provide a guideline for the furnace operation so that refractory losses are minimized.

Preface

This research work was collaboration between TRB Refractories, France and The University of British Columbia. The former provided the refractory material used in this work. Many people have contributed in this work including Dr. Daan M. Maijer, Dr. Peter Barr and Simon Chiartano.

I was responsible for developing the models, preparation of the refractory samples, carrying out thermal cycling tests on refractories and collecting the data.

Part of Chapter7 has been published and presented:

-Pandhari A. A. , Barr P. V., Maijer D. M. and Chiartano S., "Modeling Cracking in Refractory Materials Due to Thermal Cycling", Proceedings of the Unified International Technical Conference on Refractories (Unitecr 2013) Victoria, Canada, pp.805-810.

Table of Contents

List of Tables

List of Figures

List of Symbols

Symbol	Units	Description
α	m^2/s	Thermal diffusivity
k	W/m/K	Thermal conductivity
$\boldsymbol{\rho}$	kg/m^3	Density
C_p	J/kg/K	Specific heat
E	GPa	Modulus of Elasticity
v	m/s	Velocity of sound
ν	--	Poisson's ratio
E_0	GPa	Elastic modulus of an undamaged material
σ_{t0}	N/m^2 (Pa)	Peak tensile stress
ε_{0t}^{el}	_	Elastic strain of an undamaged material in tension
ε_{t}^{el}	_	Elastic strain of a damaged material in tension
ε_{0c}^{el}	_	Elastic strain of an undamaged material in compression
ε_{c}^{el}	_	Elastic strain of a damaged material in compression
ε_{t}^{ck}	_	Cracking strain of an undamaged material
ε_{t}^{pl}	_	Plastic strain of damaged material in tension
ε_{c}^{in}	_	Inelastic strain of an undamaged material
ε_{c}^{pl}	_	Plastic strain of damaged material in compression
d_t	_	Damage parameter in tension
d_c	_	Damage parameter in compression

Acknowledgements

I would like to express my deepest sense of gratitude towards my supervisors Dr. Daan M. Maijer and Dr. Peter Barr for their immense help, guidance and financial assistance during this research work. Without their patience and motivation, this work would not have been possible. They were a constant source of encouragement and inspiration for me throughout this program.

I would also like to thank my committee members Dr. Tom Troczynski and Dr. Steve Cockcroft for their invaluable comments and critical remarks regarding the project work. They have always been very supportive throughout this work. I really appreciate Dr. George Opera and Dr. Ainul Akhtar for being resourceful and encouraging.

I appreciate the help and the research collaboration with Mr. Simon Chiartano (TRB Refractories, France). I am thankful to TRB Refractories for supplying the refractory material.

I am very thankful to Gary Lockhart and Harish Gautam for their immense help with the thermocouples. I am sincerely thankful to Ross, Carl and Dave from the machine shop for their help with the experimental set-up. I would especially like to thank Michelle Tierney for always being helpful during my studies.

I especially would like to thank Dr. Dick Hasselman for being a great motivation to me. His advice regarding looking at a “big picture” during the research work was very practical. I am also very grateful to Dr. Ian Okabe for his practical advice and moral support.

My father Prof. Arun Pandhari and mother Prof. Anjali Pandhari were the immense source of encouragement and motivation. Their unconditional love and support cannot be

described in words. I would like to thank them from the bottom of my heart. I would especially like to thank Mr. Mukundraj Moholkar and Mrs. Rukmali Moholkar for their care, love and support.

Last but not the least, without my friends and colleagues, this research would not have been a fun experience. I thank my friends Sina Shahendeh. Rahul Lodha and Aniruddha Chatterjee. They were always the “helping hand” during the work. I would especially like to thank Padmesh Rajput, Geetanjali Kharmate, Emtiyaz Khan and Sarah Meli for their constant encouragement. Special thanks to all of my friends, especially to Tim Sexton, Judith Bosire, Enkhgerel Gerelchuluun, Priyanka Chakarabarti, Natalie Johnston, Shannon Aines, Josh Rudolph and Guillaume Lefebvre for being optimistic about my work over the years during the PhD.

To my Parents

1. Introduction

Refractory materials are used to line the interior of metallurgical furnaces, reactors and other processing units because of their insulating capabilities. Ideally, refractory materials are chemically inert in the environment they are used in, as well as, being capable of withstanding the thermal shock at the temperatures that they are subjected to without losing their structural integrity during service.

The worldwide refractory consumption is significant because of their widespread use in various industries such as steel and non-ferrous alloy production, glass manufacturing, waste incineration, and lime / cement production. The largest consumer of refractory materials is the steel industry [1]. Today, advances in refractory technology have reduced refractory consumption in the steel industry to almost $1/3^{rd}$ of that required thirty years ago. Still for every ton of steel produced, 10 kg of refractory is consumed. For every ton of glass and non-ferrous metals produced 4 kg and 2.7 kg of refractory is consumed, respectively [2]. The global demand of refractory materials is significant: ~$28 billion or ~45 million tons (for the year 2012) and it is expected to grow [1].

Even though the global refractory production is less than that of the other industries (e.g. steel industry), the role of the refractory materials is immensely important. High-quality steel production is now possible because of the developments in the secondary steel-making. One of the major developments in this area has been improvements to the gas purging / injection systems that employ high-quality refractories in the gas-purging cones. The weight of these cones is ~30 kg, which is significantly smaller than the total weight of the ladle (~600 tons) with

250 tons of steel-making capacity [2]. Thus, refractory components that represent only ~0.01% of the weight of the ladle greatly improve steel quality. It is therefore important to understand refractory failure.

Metallurgical reactors especially used for the smelting operations expose their refractory linings to hostile environments that challenge their survival. Refractory degradation originates from a variety of mechanisms, e.g., mechanical abrasion, chemical attack and phase instabilities. These phenomena are superimposed on thermally induced stress/strain fields caused by differential thermal expansion (macroscopic scale) or local mismatches in the coefficient of thermal expansion (CTE) between the grain and matrix materials. Thermal gradients in the refractory will also induce a state of internal stress. When significant, thermal gradients as well as local mismatches in CTEs can cause cracking. Transients occur in the thermal stress field when the surface heat-transfer conditions change. Batch processes involving distinct charge-tap-rotation events result in thermal cycling on the hot-face and impose a transient stress field on the underlying ‘steady-state’ condition of the refractory, i.e., the residual effects of bringing the refractory up to temperature and the prevailing thermal gradient between the hot and cold faces.

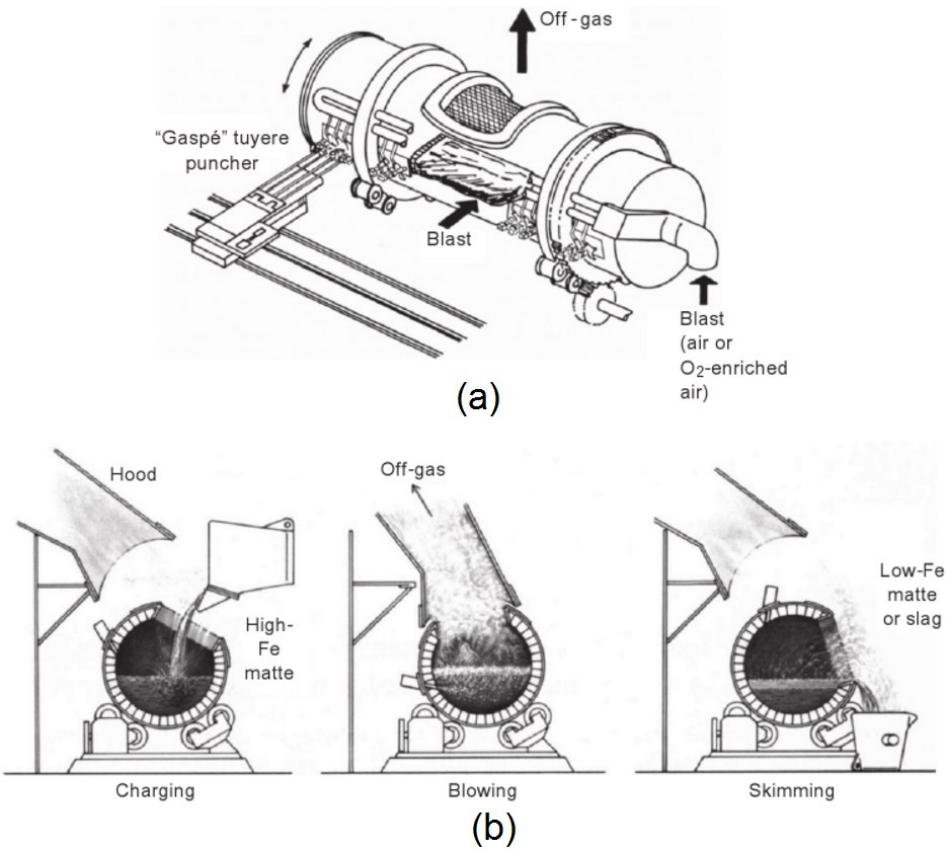

Figure 1.1: Thermal cycling in Peirce-Smith (P-S) Converter Lining (a) Schematic of P-S converter (b) Different positions of the converter [3].

An example of a process exhibiting transients related to batch processing is the Pierce-Smith converter used for copper converting. As shown in Figure 1.1(b), during the blowing phase of operation, a portion of the refractory lining is under the bath while air is injected in the matte. When the reactor is rotated for tapping, the refractory previously submerged beneath the bath is exposed to the converter gas or even ambient conditions via radiative heat transfer through the converter mouth, i.e., cooling conditions. After tapping, the converter is recharged before it is returned to the blowing position and the hottest section of the refractory is again under the bath, i.e., subjected to heating conditions. Each cooling-heating

cycle results in a thermal stress cycle and repeated cycling can cause progressive damage accumulation and eventual failure of the refractory.

Excessive refractory loss can lead to complete refractory lining failure resulting in metal breakout due to the direct contact between the molten metal and the steel shell of the process vessel. Apart from the safety issues, the introduction of refractory materials into the melt can cause undesirable chemical reactions and can interfere with the predetermined chemistry of the molten metal. This can cause inclusions in the material altering the mechanical properties of the final product.

When refractory loss is significant, reactor operation is stopped to allow for relining. Due to differences in reactor type and the refractory being used, the lining life varies. For example, the lining life for an oxygen steel-making furnace (BOF) is about 1500-15000 heats, whereas for an argon oxygen decarburization reactor (AOD), it is about 30-50 heats for small (<50 tons) vessels and is about 120 heats for large (>90 tons) vessels [4]. Wear of the refractory lining is often the sole factor dictating the campaign life of the reactor [4].

From an economic point of view, refractory loss is detrimental in two ways: 1) frequent relining reduces the furnace availability affecting productivity and 2) increased consumption of refractory increases the cost of production. In order to improve the lining life of a reactor it is important to understand the factors that lead to failure during cyclic heating/cooling. The goal of this thesis is to study the thermal cycling of refractories through experiment and mathematical modeling. The next chapter focuses on the previous work in this area.

2. Literature Review

Refractory degradation in pyrometallurgical reactors is a significant problem. The fact that thermal stress and thermal stress cycling plays a role in degradation of these materials is acknowledged but quantitative understanding of the phenomenon remains incomplete. To understand the thermally-assisted mechanisms of refractory failure, it is crucial to know the temperature history of the refractory, the associated stress response and the eventual damage in the material. With that in mind, previous work in the areas of thermal modeling, thermal stress modeling and refractory damage will be reviewed in this chapter.

1) Thermal modelling of the refractory: Investigations in this area focus on the thermal cycling experienced by the lining during operation. The investigations include mathematical models of the heat transfer occurring within the refractory subject to specified thermal boundary conditions. Although, these models are largely un-validated, they provide insight into the thermal conditions in the refractory lining during the operation.

2) Thermal stress modelling of refractories: These investigations quantify the thermal stresses generated in the lining for several reactors by means of finite element based models and laboratory scale experimentation.

3) Damage in refractories: Previous work in this area includes theoretical and analytical work to understand the fracture and the mechanical behaviour of refractories. Various experimental and modeling techniques have been used to study the damage.

2.1 Heat Transfer in Refractories

2.1.1 Thermal Cycling in Refractory Linings

Thermal cycling of the refractory hot-face occurs in reactors operating in 'batch' mode due to charging, discharging, tilting, rotation, etc. Bustos et al. [5] developed a mathematical model for the refractory in the Peirce-Smith converter to quantify the cooling occurring during the idle time of the reactor between the two operating cycles known as the out-of-stack time. Figure 2.1 shows the predicted temperature profiles of the lining in front of the converter mouth for several out-of-stack times. It is evident that significant cooling of the surface occurs while out-of-stack. As is typical of transient heat transfer conditions, the steepest thermal gradients occur initially at the hot-face and the gradient declines over time.

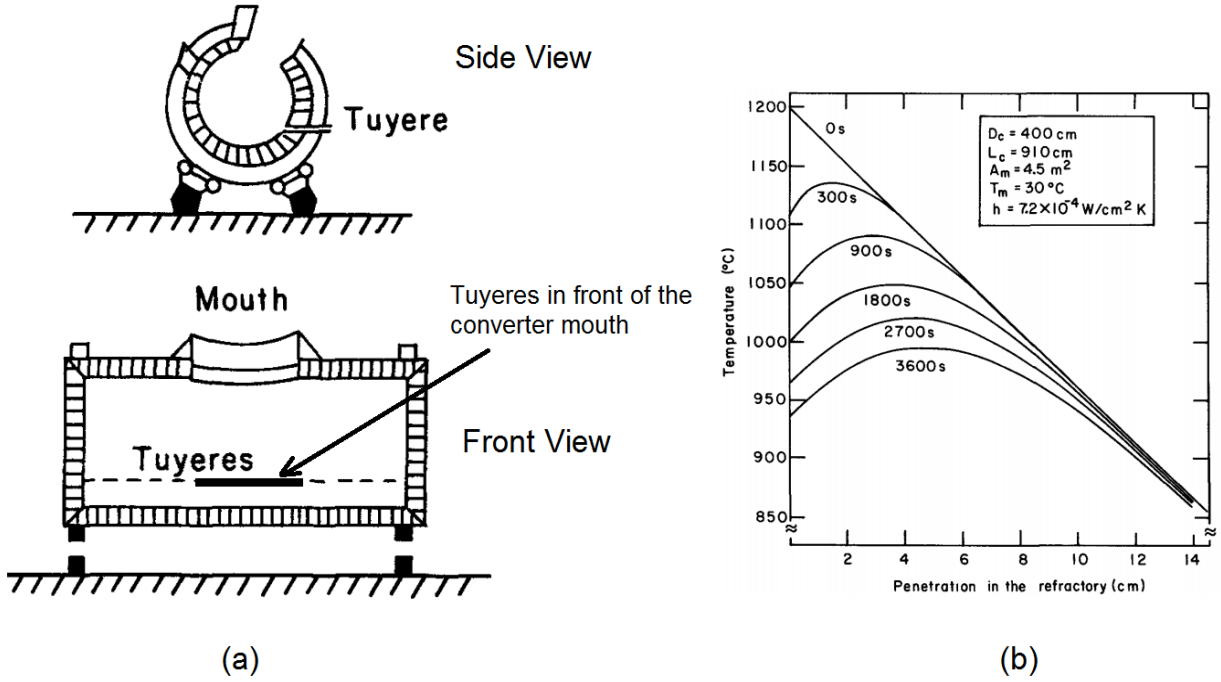

Figure 2.1: (a) Tuyere locations in the Pierce-Smith converter (b) Temperature profiles inside the lining of a tuyere in front of the converter mouth for different out-of-stack times [5]

The low thermal diffusivity (~5 x 10^{-7} m^2/s) of the refractory material means that transient effects require significant time to penetrate beyond the hot-face, i.e., at one hour the 'thermally active zone' is only about 10cm. When the converter is returned to service, the temperature profile returns to the initial quasi-steady-state, but in doing so the hot liquid matte will subject the hot face to aggressive heating conditions.

When the free expansion due to uneven temperature distribution within the material is restrained, the so-called thermal stress is induced in the material. Due to this thermal cycling, thermal stress cycling also occurs [6] throughout the thermally active zone. Origin of the thermal stress is discussed in details in section 2.2.1.

It should also be noted that at 0s the magnitude of the thermal gradient is constant and would result in a steady-state thermal stress state. Upon cooling and heating, the magnitude and direction of the thermal gradient changes within the thermally active zone. Thus, thermal cycling not only generates steep thermal stress gradients but it also changes the direction of the thermal stresses.

Wang et al. [7] developed a finite element based mathematical model for the heat transfer in the wall of the stack region in a blast furnace. The model was validated by comparison to temperature data measured with thermocouples at four locations around the circumference of the lining, i.e., at 0°, 90°, 180° and 270° (denoted by 'East', 'North', 'West' and 'South' respectively.). Figure 2.2 summarizes the results generated by Wang et al. and clearly highlights the significance of the thermal gradients in the radial direction. The temperature changes ~100°C within a distance of just 50 mm (thermal gradient of about 2 °C/mm).

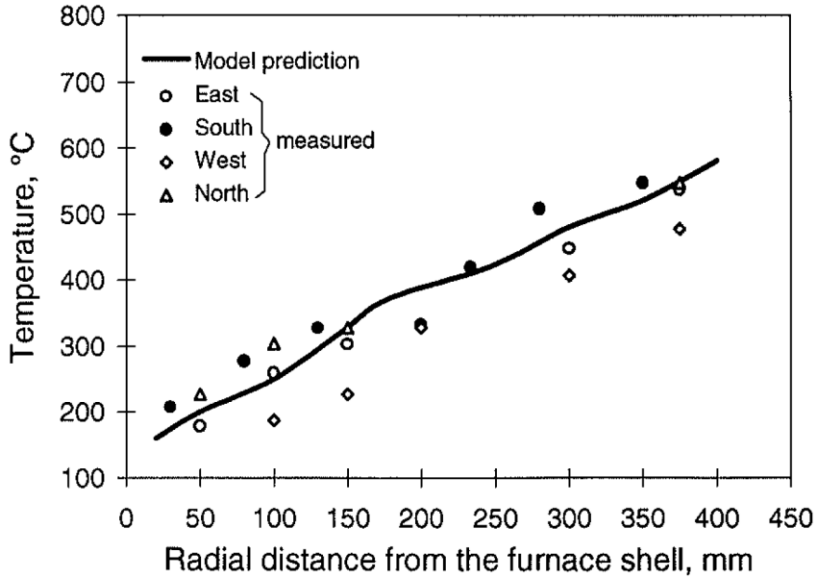

Figure 2.2: Measured and predicted temperature distributions in the radial direction of the blast furnace wall of the stack region [7]

Studies for various pyro-metallurgical reactors show that the thermal gradients during operation are significant in almost all of major reactors. Nieckele et al. [8] developed a mathematical model for an industrial aluminum melting furnace. Simulation of the oxy-fired combustion process showed a refractory hot zone in the region of the flame and strong localized thermal gradients. Khoei et al. [9] developed a 3-D mathematical model of an aluminum scrap melting rotary furnace to study the effect of thermal cycling on the lining due to the furnace rotation. Shubin [10] analyzed the one-dimensional heat flow in the radial direction of the refractory lining for a rotary cement kiln furnace to study thermal spalling.

Volkova [11] simulated the heat transfer in the lining of a steel ladle and incorporated the effects of lining wear rates. Xia et al. [12] numerically investigated heat flow in the working lining, safety lining, insulation layer and the outer steel shell of a steel ladle during the holding period between the completion of ladle operations and the start of metal pouring into a tundish. Zimmer et al. [13] quantified the heat losses through the refractory in a steel ladle during holding and vacuum periods based on the thermocouples inserted at various locations in the refractory lining. Hanifi et al. [14] simulated the thermal and thermal stress profiles in the refractory lining of a steel ladle during casting and during idle time after casting and converter tapping. Fredman [15] summarized the modeling and experimental work done in the refractory lining of a steel ladle. In all of these investigations, the thermal profiles during heating-cooling events of the lining show significant thermal variation.

In the above-mentioned investigations, various techniques have been used to quantify temperature changes in the refractories investigated. Apart from the use of thermocouples to track temperature changes, analytical methods have also been used. Since these techniques have

limitations, numerical methods such as finite element method (FEM) and finite difference method (FDM) appear to be the most commonly used.

Several investigations [16-18] have revealed the presence of significant thermal gradients in the tuyere region of submerged injection systems due to localized gas-cooling of the refractory. In summary, all of the investigations indicate that significant thermal gradients in the refractory lining are common in all of the pyro-metallurgical reactors and that the magnitude and direction of the thermal gradient changes during the operation. The effect of thermal gradients on the development of thermal stress is discussed in the next section.

2.2 Thermal Stresses in the Refractories

2.2.1 Origin of the Thermal Stresses

Early wok by Kingery [19] was focussed on the conditions that lead to thermal stresses and the parameters that influence their magnitude. Kingery suggested that, when the free expansion of each small unit volume of a material is restrained, thermal stresses arise in the material due to the differences in the thermal expansion within various parts of the body. In the material with thermal gradients, the difference in thermal expansion is due to differences in the temperature within various parts of the body. In an isothermal body of heterogeneous material, thermal stress arise due to expansion / contraction differences between the various components of the material (grains, phases, crystals and so forth). Kingery pointed out that in refractories, thermal stress can be the result of both inhomogeneity of the refractory material and the presence

of thermal gradients. On a microstructural level, refractories consist of different phases with variations in the grain size, reinforcing particles, etc. When the material is uniformly heated (or cooled), thermal stress arises due to differences in the expansion (or contraction) behaviour of these microstructural components. Kingery attempted to explain how thermal gradients generate thermal stress in the material with the help of Figure 2.3. The figure shows the typical stress distribution within a slab during (a) cooling and (b) heating. During cooling, the surface tries to contract and the sub-surface material resists the contraction. As a result, tensile stress occurs near the surface and compressive stress within the interior. The direction of stress is reversed during heating. In the case of refractory materials, the formation of tensile stress at the surface during cooling or in the lining during heating can lead to failure due to the low shear strength exhibited by refractories [19].

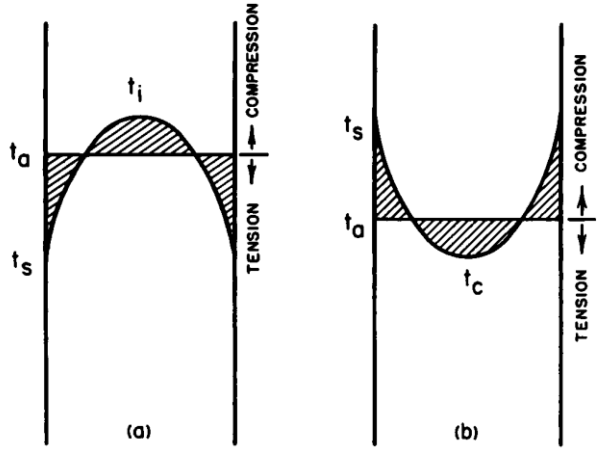

Figure 2.3: Schematic representation of the temperature profile and the direction thermal stresses in a slab during (a) cooling and (b) heating [19].

2.2.2 Influence of Thermal Gradients

As mentioned in the previous section, heating and cooling induces thermal stress in refractories. The distribution and severity of the stress also depends on the severity of heating and cooling. Tsibin et al. [6] explained this with the help of a schematic diagram (Figure 2.4) that shows a refractory material going through three different rates of heating. This situation is similar to the typical preheating of refractory lining. Figure 2.4 (a) shows the schematic representation of the temperature gradients generated in a lining when subjected to a convective boundary condition. τ_1, τ_2 and τ_3 indicate the times for which the convective heat flux is applied. It can be seen that the thermal gradient gets steeper from τ_3 to τ_1. Figure 2.4 (b-d) shows the thermal stress profiles corresponding to the times τ_1, τ_2 and τ_3. Zone I and Zone III are regions which exhibit compressive stresses, whereas, Zone II is a region with the tensile stresses. As the thermal gradients (at τ_1, τ_2 or τ_3) are small going away from the hot face, the magnitudes of the thermal stress (compressive or tensile) are also small, away from the hot face. The largest temperature change was observed for time τ_2 and this corresponds to the highest magnitude of thermal stresses among all three cases (τ_1, τ_2 and τ_3).

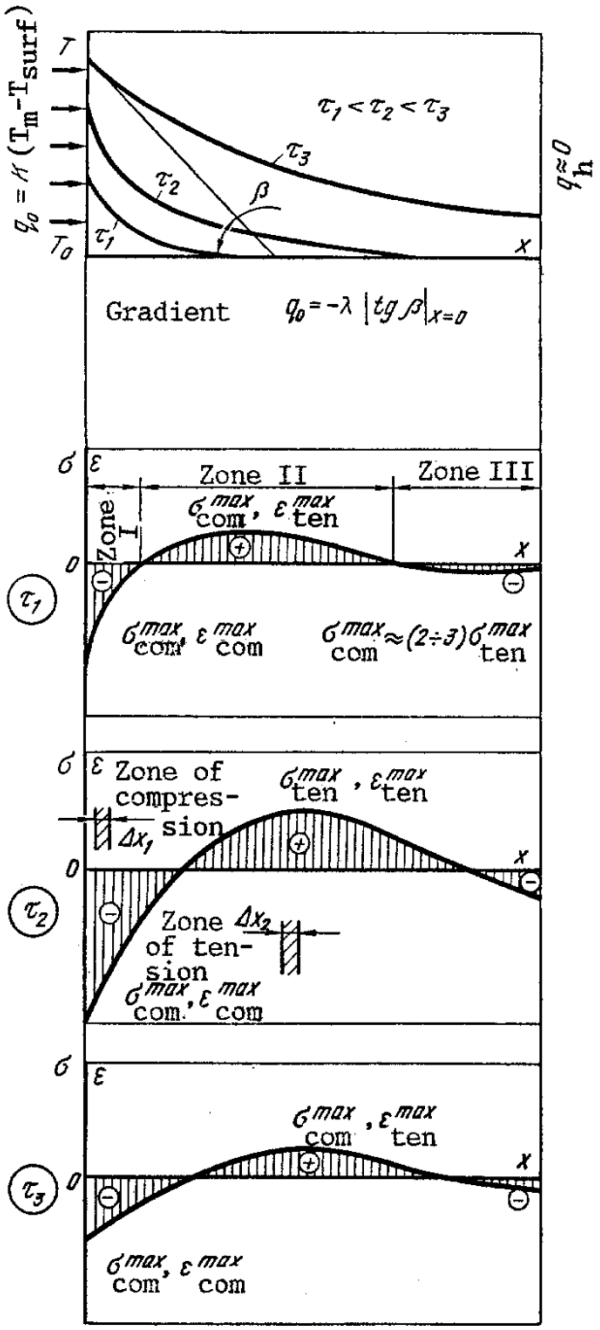

Figure 2.4: Schematic representation of the thermal stress distribution in a concrete lining with various temperature gradients [6] (a) Thermal profile in the lining after various times. Thermal stress distribution corresponding to times; (b) τ_1, (c) τ_2 and (d) τ_3

Chang et al. [20] developed a two-dimensional mathematical model based on the finite element method for a refractory brick. They considered the case where a refractory brick was being heated from one end. The results of this work are shown in Figure 2.5, which shows the temperature distribution and the associated longitudinal and transverse stress distribution after 3000s of heating. It can be seen that a biaxial state of stress is formed near the heated face of the brick. The locations of the maximum tensile stresses indicate regions of the possible crack formation. Figure 2.5 also indicates that the magnitude of the maximum longitudinal tensile stress (11.1MPa, See Figure 2.5(b)) is larger than the magnitude of the maximum transverse tensile stress (9.1MPa, See Figure 2.5(c)). Thus, if a crack formed, it would most likely propagate in the transverse direction. This study also showed that the stress distribution changes at shorter times when the temperature profile is steep. The transverse tensile stresses are higher than the longitudinal tensile stresses at shorter times indicating that if a crack formed it would most likely propagate in the longitudinal direction.

The magnitude of the thermal stress also depends strongly on the material properties [18, 21]. In the above-mentioned analysis, the material was assumed to be homogeneous and the material properties were assumed temperature independent. The thermophysical properties, i.e., conductivity, thermal diffusivity, density and specific heat affect the thermal profile in the material. Ganguly et al. [21] suggested that in refractory materials, temperature has a stronger effect on the thermal conductivity than the other material properties such as Poisson's ratio, modulus of elasticity and coefficient of thermal expansion. With the help of an analytical solution they showed that the thermal stress field is strongly dependent on the variation of thermal conductivity with temperature. The effect of heating and cooling on the Young's

modulus was studied by Joliff et al. [22] for a bi-phase material of spherical aluminum inclusions in a glass matrix. They reported an appreciable change in the Young's modulus when heated and then cooled down.

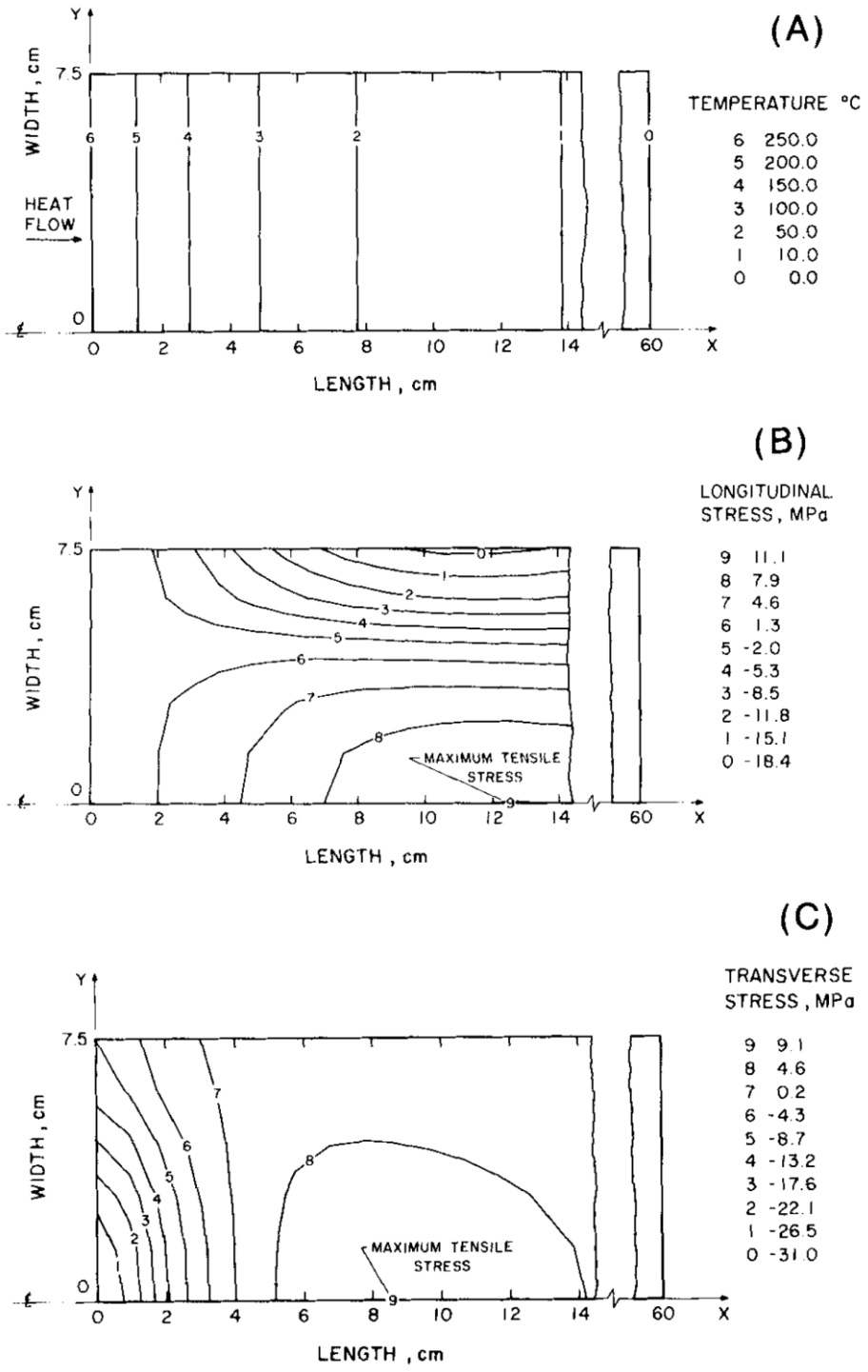

Figure 2.5: Temperature profile and associated plane stress thermal stress distribution in the brick that is subjected to heating. (a) Temperature profile (b) Longitudinal stress distribution (c) Transverse stress distribution [20].

2.2.3 Thermal Stresses Experienced in Industrial Operations

In industrial practice, heating and cooling conditions are aggressive and lead to very high thermal gradients in reactor linings. These aggressive thermal conditions are commonly known as ‘thermal shock’. Thermal shock is particularly problematic when heating refractory from a relatively low temperature by contact with hot liquid metal. Aggressive cooling occurs when the hot-face is exposed to a ‘cold’ environment with correspondingly high rates of convective and radiative heat transfer. Refractory materials, due to their inherently brittle nature, are susceptible to cracking under conditions of high heat transfer rates or rapid variations in heat transfer. To avoid the refractory failure, it is important to know the magnitude of thermal stress when refractories are subjected to the industrial operating conditions.

A significant amount of work has been done on quantifying thermal stress in lining materials for various reactors. Nikiforov et al.[23] attempted to specify safe heating rates for periclase-carbon refractory linings for steel ladles based on thermal and thermal stress calculations. They experimentally investigated the thermal variation on the inner surface of the lining during heating and numerically calculated the temperature variation through the lining thickness. The thermal stresses were calculated based on this temperature profile, assuming linear-elastic material behaviour with temperature independent material properties.

Figure 2.6 shows the calculated thermal and thermal-stress profiles along the thickness of the lining. The numbers over the curves show the time (in “h:min” format) after the start of the heating. Under these conditions, the stresses are compressive near the hot end and transition to tensile stresses moving away from the hot end. Assuming the tensile and compressive strengths

of the material are 25 MPa and 40 MPa, respectively, the authors predicted that cracking would take place in the material once the stresses exceed these limits.

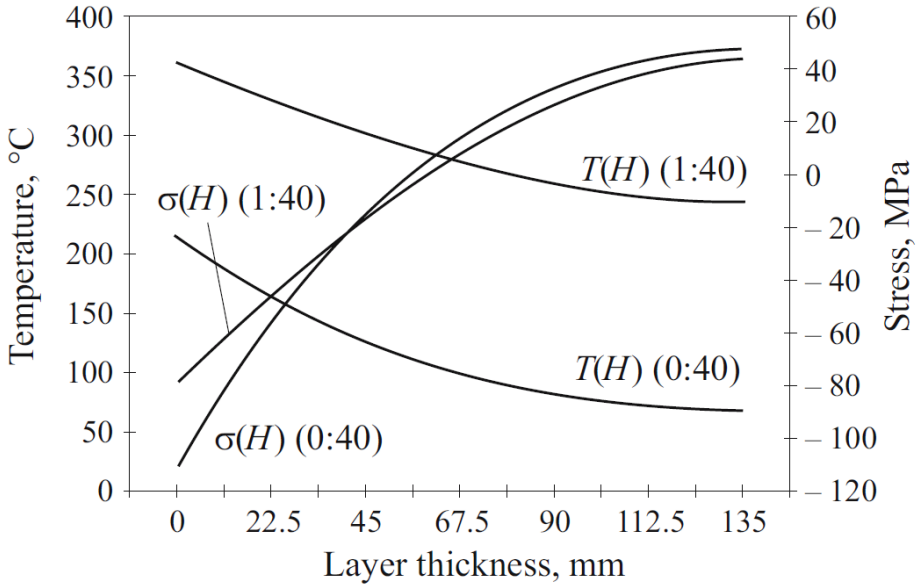

Figure 2.6: Predicted temperature and stress profiles in the refractory lining of the steel ladle at various times [23].

Gruber et al. [24] developed an FEM based axisymmetric mathematical model for a blast furnace lining that employed Ram Mix[1]. They assumed temperature dependent material properties and used a Von Mises plastic failure criterion for the Ram Mix and the Drucker-Prager plasticity model for the shaped refractory. Their work showed that the thickness and

[1] "Ram Mix" is a ready-to-use mixture of refractory aggregates and clay sold in a damp granular form that can be shaped with a pneumatic hammer or mallet to form a part of the refractory lining. Ram Mix is usually used as backup insulation behind the "working lining" that is in contact with the melt.

compressibility of the Ram Mix are key parameters for minimizing the compressive stress in the corundum bricks of the working lining that is in contact with the molten iron.

Liang et al. [25] attempted to quantify the transient stresses in the lining of a black liquor gasifier considering thermal and chemical factors. In their work, they assumed elastic-plastic material behaviour for the alumina refractories used in this application and predicted the influence of various process related factors on the refractory stress distribution.

Much of the above-mentioned work assumes simplistic (linear-elastic or elastic-plastic) material behaviour for the refractories and attempts to capture the ideal process conditions to avoid cracking based on the predicted magnitude of the thermal stresses. However, refractory cracking depends on many factors. The next section discusses about the damage in refractory material.

2.3 Thermally Induced Refractory Damage

Considering the productivity of any reactor, the main objective is to reduce the heating or cooling time of the refractory lining without inducing large thermal gradients or thermal shock in the lining that can cause cracking. Cracking, in any form in the lining, limits the refractory life. However, cracks which are produced normal to the hot face of the lining are less fatal than those produced parallel to the hot face. The parallel cracks are responsible for sudden loss of refractory material. The distance of these cracks from the hot face determines the extent of thermal spalling. Even though refractory materials are often capable of arresting the crack,

thermal spalling is still prevalent. It is therefore important to understand the cracking process in refractories.

A significant amount of theoretical and modeling work [25-38] has been done to understand and avoid refractory cracking during thermal shock. The early work by Schwartz [26] suggests that the resistance to cracking in refractories depends on the magnitude of thermal gradients and the material properties. It is however, accepted that cracking in refractories depends on two mechanisms:

1) Crack initiation
2) Crack propagation

Early design of refractories was based on increasing the resistance to crack initiation. The idea was to make sure the magnitude of thermal stress does not exceed the tensile strength of the refractories. The resistance to fracture initiation can be improved by increasing fracture strength, thermal conductivity and by decreasing the Young's modulus and the coefficient of thermal expansion [26,30]. Work has been done to characterize the resistance to crack initiation based on the bending strength after thermal shock using notched ceramic specimens [31].

However, increasing strength to avoid the initiation of fracture has a negative impact on crack propagation as it increases the elastically stored energy in the material. Given the heterogeneity and porosity in the refractory material, it is hard to resist the initiation of cracks in the refractory materials. If a crack is initiated, the energy acts as a driving force for crack propagation creating new fracture surfaces. If this energy is more than the total fracture energy required to propagate the crack over an equivalent cross sectional area of the specimen, then the

refractory experiences a catastrophic failure. If the elastic energy is less than the fracture energy, the failure is non-catastrophic [30]. Refractories do not exhibit a high resistance to fracture initiation, but they can possess a significant resistance to the crack propagation [27]. Therefore, the resistance to crack propagation can be improved by reducing the elastic energy of the material and can be achieved by decreasing the fracture strength and increasing the values of Poisson's ratio and the Young's modulus [28]. Hasselman [27,29] suggested "resistance parameters" in terms of material properties and thermal gradient target to control refractory cracking and also proposed a unified theory [30] that combines the phenomena of crack initiation and crack propagation.

Bradley et al. [34-36] developed a thermoelastic material model that employed the strain energy criteria to predict safe heating and cooling rates accounting for the material properties and the geometry of the specimen.

Significant efforts have been reported [38-44] that analyze cracking in refractories following various experiments. Harmuth et al. [38, 39] employed a wedge splitting test in order to have stable crack propagation. Fracture energy results were used to compare the resistance to thermal shock for various refractories. Boccaccini et al. [40] used a chevron notched specimen to determine the fracture toughness values of a refractory material after going through thermal cycling. They also studied surface damage using an image correlation technique after every thermal cycle. They considered three cordierite–mullite based refractory materials with varying silica and alkali contents, which form glassy material phases. The refractory with the highest amount of glassy phases showed the highest fracture toughness. Their work suggested that improved resistance to thermal shock can be realized by enhancing the glassy phase responsible

for crack bridging. Soboyejo et al. [42] observed cracking in a refractory specimen and confirmed the visco-elastic crack bridging phenomenon due to the glassy phase. They observed the fracture surface of the refractory specimen after thermal cycling with the help of an SEM. Figure 2.7 shows the bridges of the glassy phase connecting the cracked surfaces.

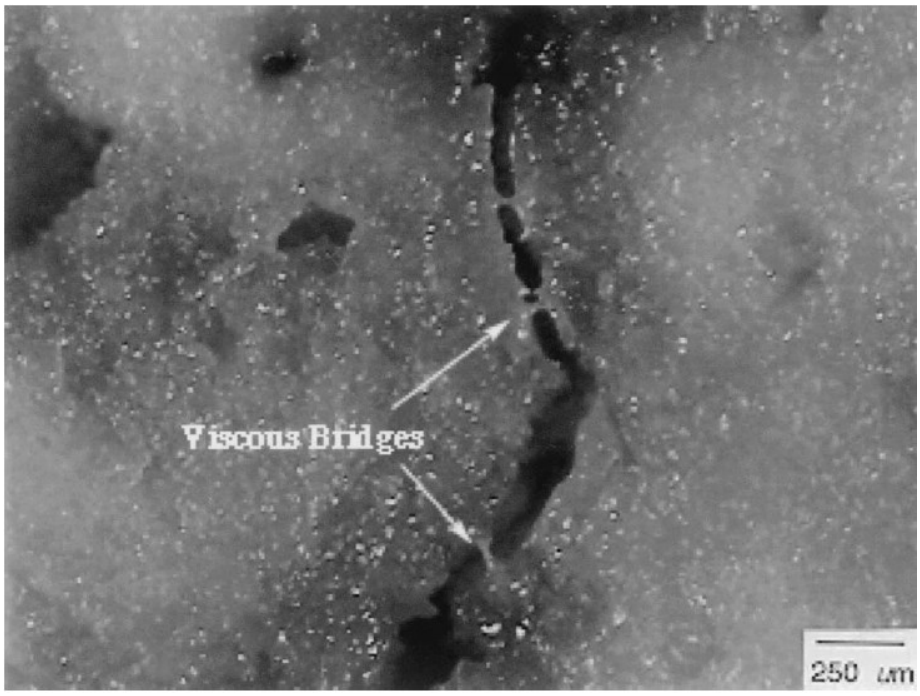

Figure 2.7: SEM micrograph of the viscous glassy phase responsible for crack bridging in a refractory specimen gone through thermal cycling [42].

The research work examined in this area focuses on understanding cracking in refractories in terms of material properties, process conditions and the geometry of the specimen. The majority of the experimental work has been aimed at thermal cycling of refractories and calculating parameters to enhance thermal shock resistance [42-44].

In an industrial operation, refractories experience repeated thermal cycling with essentially one-dimensional heat flow. The next section will describe the various experimental techniques used to carry out thermal cycling studies in refractories.

2.4 Thermal Cycling Experimentations

Due to their inherent brittleness, refractory materials are susceptible to catastrophic failure due to the thermal stress experienced during thermal cycling in the pyrometallurgical process conditions. It is therefore necessary to quantify the influence of material properties and process parameters on thermally induced refractory failure. One of the ways to do that is to subject the refractory material to thermal cycling and analyzing the material properties before, during and after the experiment. This test is called a 'thermal shock test' in the refractory literature. The analysis of such experiments is then used to compare various refractory materials for their resistance to failure. The tests are typically classified into ascending (heating) and descending (cooling) type of tests.

A large body of the early work in this area is concentrated on descending type of tests where, the refractory specimen is heated to a temperature of interest and then quenched in a quench media, most often water [23,43,45-52]. The retained strength after the quench is usually measured by a three-point bending test. The temperature difference between the heated block and the water at which the refractory loses a significant amount of strength is called the 'critical temperature difference (ΔT_c)', and is used as a measure of the thermal resistance of the material [45].

Singh et al. [45] conducted tests on alumina cylindrical rods with water and silicone oils with varying viscosities as quenching media. They analyzed the heat transfer characteristics of refractory samples immersed in the baths and studied the effect of bath temperature on ΔT_c. ΔT_c was determined based on visible cracking and three-point bending tests on the specimen. They found that baths with lower viscosity resulted in better heat transfer compared to high viscosity baths. Due to this, there was an increase in ΔT_c when the viscosity of the bath was increased. At higher bath temperatures, the viscosity of the quenching medium (silicone oil and water) reduces increasing the heat transfer coefficient and hence, reducing the ΔT_c as shown in Figure 2.8a. However, in the case of a water bath (2.8b), ΔT_c decreases initially with the bath temperature, but then increases after about 60°C. This is due to the occurrence of boiling phenomenon and the formation of a surface film which reduces the heat transfer coefficient, increasing ΔT_c.

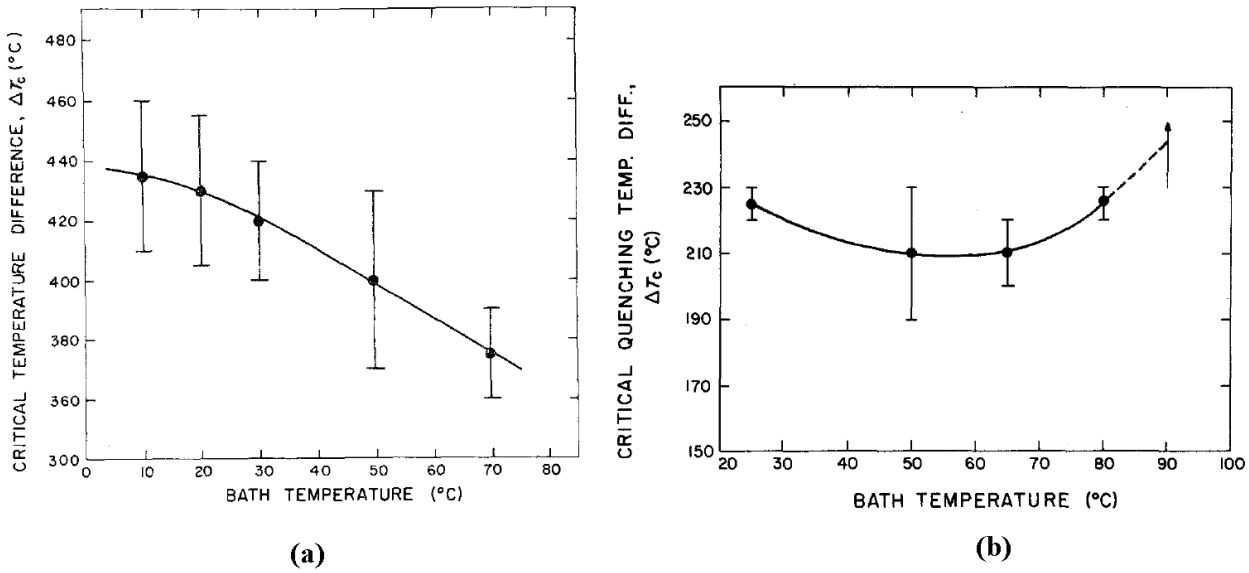

Figure 2.8: Effect of the critical temperature difference ΔT_c for cylindrical alumina rods on the bath temperature for (a) silicone oil bath (b) water bath [45].

Rendtorff et al. [50] attempted to study the effect of multiple thermal shock tests on mullite-zirconia-zircon refractories with varying zircon content. They heated prismatic bars to the temperature of interest, quenched in water and dried the refractory. They repeated this cycle and experimentally calculated the change in elastic modulus with the number of cycles for each type of refractory. They reported a reduction in the elastic modulus with an increase in the quenching temperature difference ΔT. They also reported that the values of the elastic modulus after each cycle that suggest the cracking in refractories is influenced by the number of heating/cooling cycles. Figure 2.9 shows the fractional change in the elastic modulus after each test cycle with the quenching temperature difference (ΔT) of 800°C. The severity of the cracking increases up to 3 cycles for these types of refractories. Their work did not explain the reason for this refractory degradation behaviour.

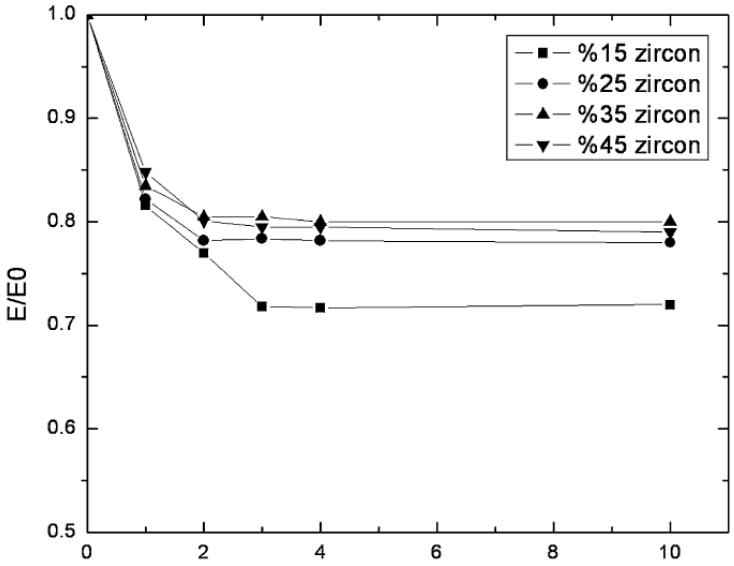

Figure 2.9**:** Effect of the number of thermal shock cycles with $\Delta T = 800^0 C$ on the fractional change in the elastic modulus for the mullite-zirconia-zircon refractories with varying zircon content [50].

To find out the effect of refractory degradation and its link to thermal cycling, Posarac et al. [51] studied the thermal shock resistance of a cordierite/silicon carbide composite material by quenching in water from 950°C. The test was repeated multiple times. The effects of testing were characterized using image analysis on the circular face of the cylindrical sample after every cycle, shown in Figure 2.10. The number of cycles required to damage the surface by 50 % or the total destruction of sample was considered as the criteria to judge the material. Their work clearly shows the degradation of the refractory material with multiple heating/cooling cycles.

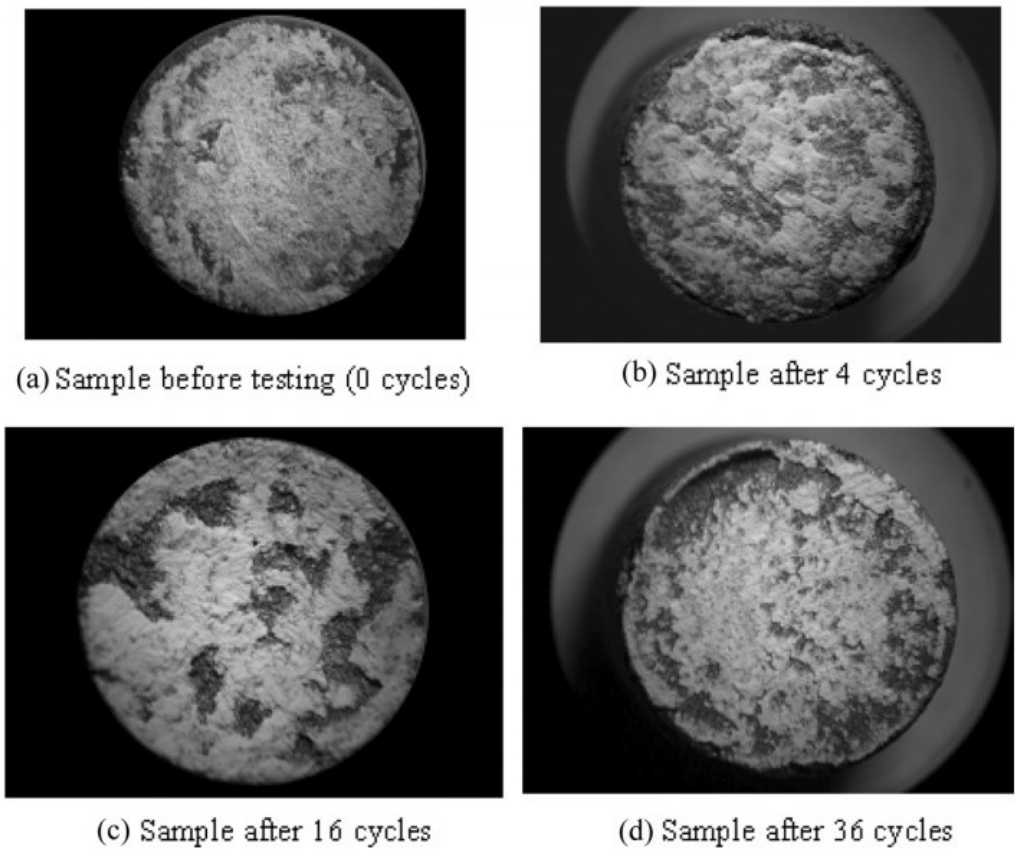

Figure 2.10: Effect of the number of cycles on surface damage for cordierite/silicon carbide composite material [51].

Significant modeling work has been performed to quantify thermal shock when the refractory is subjected to quenching in water. To study the thermal shock resistance of refractories under rapid cooling, Koksal et al. [52] developed a mathematical model of a rectangular block of refractory to calculate the thermal stress formed during water quenching. They considered cases where refractory materials were heated uniformly to three different temperatures (400°C, 600°C and 800°C) and then quenched in the water. The predicted temperatures, based on an assumed heat transfer coefficient of 5000 W/m^2K, and the longitudinal stresses at the center and surface are shown in Figure 2.11. These results show that due to cooling, tensile stresses develop on the surface and compressive stresses are generated at the center of the specimen. It is also evident that higher specimen temperatures result in higher thermal gradients and higher thermal stress.

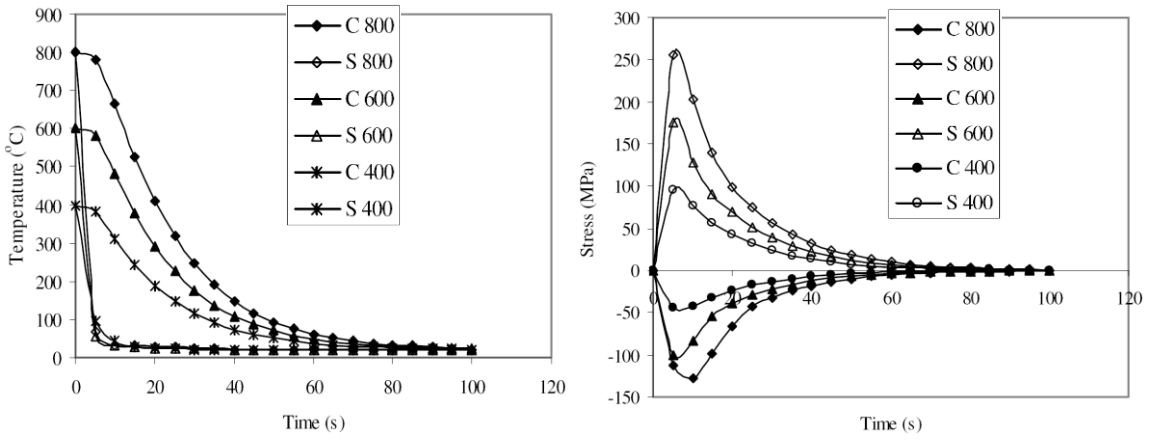

(a) (b)

Figure 2.11: Predictions of a thermo-mechanical model for a refractory material subjected to the sudden cooling. Abbreviations 'C' and 'S' represent the results at the center and at the surface respectively (a) Temperature changes with time at the center and at the surface, when refractories of 400°C, 600°C and 800°C are quenched in water (b) The corresponding stress distribution [52].

From the literature, it is evident that the critical quenching temperature difference ΔT_c appears to be the standard parameter used to quantify thermal shock resistance. However, results may not be reproducible using this as criteria unless all the process parameters are specified. This is especially true for the water quench tests where the phenomenon of boiling and steam formation also depends on the surface condition (e.g., roughness) of the sample [45]. Therefore, varying surface roughness etc. can cause varying thermal stress for the water based quenching tests. In addition, it is difficult to quantify the spatially varying heat transfer coefficient and reproduce the same conditions in the experiment.

Other quenching mediums have been used for these experiments. Soboyejo et al. [42] used a salt bath to cool refractories samples. They used a sodium nitrate and potassium nitrate containing salt solution with a melting point and a boiling point of ~275°C and ~550°C, respectively. Andalusite based burned refractory samples of size 57mm × 57mm × 76mm were thermally cycled. To carry out thermal cycling, the samples were heated to 1150°C or 1500°C in the furnace and then quenched in the salt bath which was maintained at ~400°C. A thermocouple was placed in contact with the specimen. The samples were quenched for ~7-10 min and then cooled in air. The process was repeated to carry out the desired number of thermal cycles. Although, the salt bath appeared to be a good quenching medium, a thermal analysis was not done to precisely quantify the heat flux. In addition, after quenching in the salt bath, the specimens needed to be cleaned in hot water because they absorbed salt (~40g).

Damhof et al. [54, 55] used a molten aluminum bath to heat refractory specimens. They used corundum refractory specimens with dimensions of 50mm × 50mm × 150mm in their thermal cycling experiments and studied the damage. They developed an experimental set-up to

create one-dimensional heat flow where one end of the specimen was quenched into the molten aluminum bath maintained at 1000°C while the other surfaces were insulated. For cooling, the specimen was exposed to the ambient air. Thermocouples were attached to the sample at various distances from the quenched end. The thermocouples were used to record the transient thermal changes at the specific locations on the specimen and the heat flux entering into the specimen was not quantified.

Other methods to subject refractories to thermal cycling have also been reported [44,56-58]. These methods have focused on disc shaped specimens. Tomba Martinex et al. [57] used a high velocity air jet to cool cordierite-based disc-shaped specimens. They attempted to quantify the thermal shock resistance following the critical temperature difference discussed earlier. Disc shaped specimens of ~17.5mm in radius and ~2.67mm in height were micro-indented on the surface. The specimen was heated in a furnace to the desired temperature and then cooled with a high velocity (330m/s) air jet at room temperature. This procedure was carried out a number of times by increasing the initial furnace temperature until cracks were visible. The difference between the furnace temperature and the temperature of the air jet (room temperature) was reported as the critical temperature difference to cause cracking. The issue with this method is that the cooling rates achieved with the air jet were not as severe as experienced in quench tests. Thus, higher furnace temperatures were required to cause failure of the specimen.

The disc shaped specimens were also used [44] to study crack initiation and propagation in graphite using an arc-discharge technique for heating. Panda et al. [56] developed testing equipment to carry out ascending type (heating) thermal shock tests on disc shaped specimens using an oxy-hydrogen flame on one side and water-cooled copper blocks in contact with the

specimen on the other side. Rogers et al. [58] developed a technique of using metal blocks directly in contact with the disc shaped refractory specimen to carry out descending (cooling) type thermal-shock tests. They heated soda-lime silicate glass specimens, 5.08cm in diameter and 0.159cm in thickness, in a furnace to various temperatures ranging from 400°C to 550°C. The center of the heated specimen was placed directly in contact with a brass rod of 2.5cm diameter that induces uniform, biaxial tensile thermal stresses at the center of the disk. A thermocouple attached to the center of the specimen opposite the brass rod was used to collect temperature data during the cooling. Acoustic emission sensors mounted to the end of the brass rod were used to record the cracking events in refractory specimen during the experiment (Figure 2.12). An FE model along with a statistical model of fracture was employed to predict the probability of the failure as a function of time for various initial specimen temperatures.

To ensure the success of a modeling exercise, attention must be paid to ensure proper quantification of the thermal boundary conditions. Even though this contact technique has only been used for the cooling tests, its potential for controlled, and readily quantifiable, heat transfer conditions makes it more attractive than the conventional quenching methods discussed above.

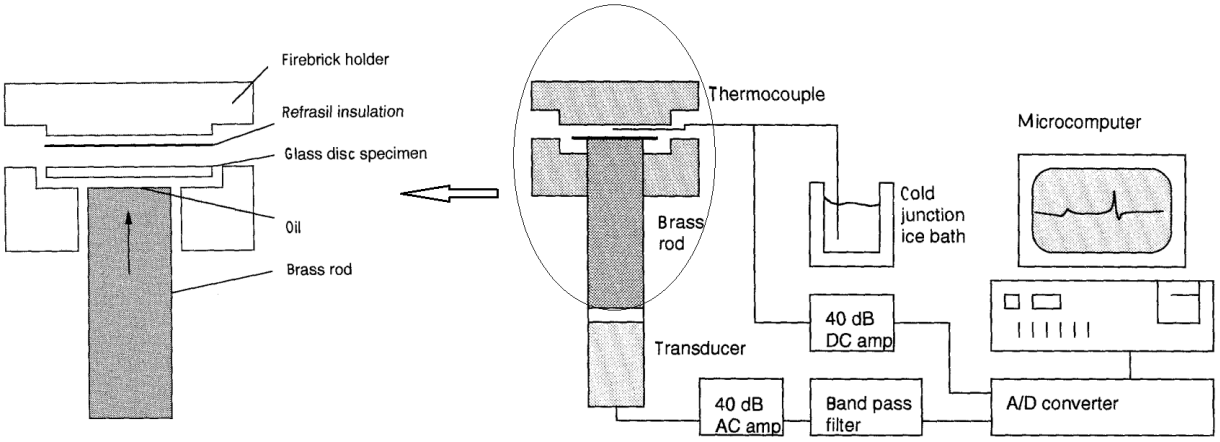

Figure 2.12**:** Schematic representation of the thermal-shock test using the "contact-cooling" method [58].

The refractory behaviour under thermal-shock conditions is connected to the complex material degradation behaviour. The previous work indicates that there is no unique way to study the thermal-shock behaviour quantitatively and extrapolate the results for the practical applications. The analysis of such data is difficult because the results from the tests are usually linked to the experimental details. Therefore, knowledge of temperature and the associated thermal stress are necessary to understand the complex refractory degradation behaviour. Numerical modeling could be an important tool to quantify the thermal stresses in the refractories going through the thermal-shock conditions. The next section is devoted to the numerical modeling to study the refractory damage.

2.5 Modeling Refractory Damage

Refractories are categorized as a special class of materials called “quasi-brittle materials”. The other materials in this category are structural ceramics, paper, coal, ice, rock and stiff clays. The “quasi-brittle” classification indicates that the material is not completely brittle and that linear elastic fracture mechanics (LEFM) do not apply. A significantly larger fracture zone occurs in quasi-brittle materials compared to that of brittle materials. Figure 2.13 shows a schematic of the stress distribution along a crack in these materials.

The area within the ellipse is called the fracture process zone in which the stress decreases non-linearly with increasing deformation (i.e. softening) until eventually complete fracture occurs (i.e. stress reaches zero). This zone is surrounded by (at the boundary of the elliptical surface) a zone of hardening where the stress increases non-linearly or remains constant with deformation. These two zones constitute the non-linear zone.

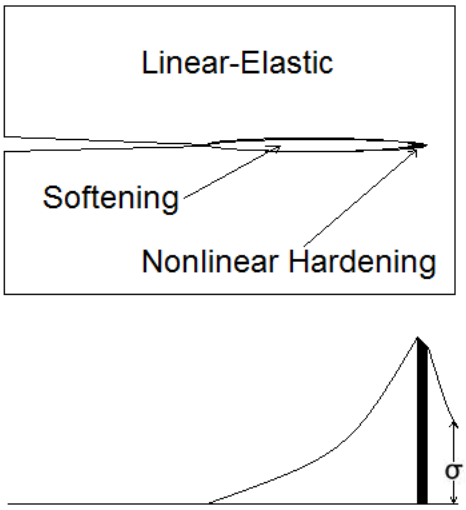

Figure 2.13: Schematic representation of the stress distribution along the crack in a typical quasi-brittle material. Adapted from [59].

In brittle materials (for which LEFM can be applied), the non-linear zone is very small and tending to be concentrated to a point. In ductile materials, the size of the non-linear zone is significantly larger than that of the brittle materials. Even though the fracture process zone is still very small, the hardening zone is large. In quasi-brittle materials, the hardening zone is often very small but the fracture process zone is large due to the damage associated with micro-cracking, voids and so forth [59].

Various approaches have been used to model damage accumulation in refractory materials. Andreev et al. [60] simulated cyclic thermo-mechanical behaviour of a single refractory brick based on conditions found in the steel industry. They employed a fictitious crack model for the tensile behaviour to simulate cracking. The initial linear portion of the stress-strain curve was modelled by assuming linear-elastic material behaviour. The non-linear portion was modelled by assuming an imaginary crack with cohesive forces acting between the crack surfaces. Since refractories exhibit plastic deformation when loaded in compression, the Drucker-Prager yield criterion was employed. They developed a 2-D model with a computation domain of 225mm×165mm, applied a heat flux boundary condition to generate 1-D heat transfer conditions and analysed the cracking pattern assuming no mechanical constraints on the brick.

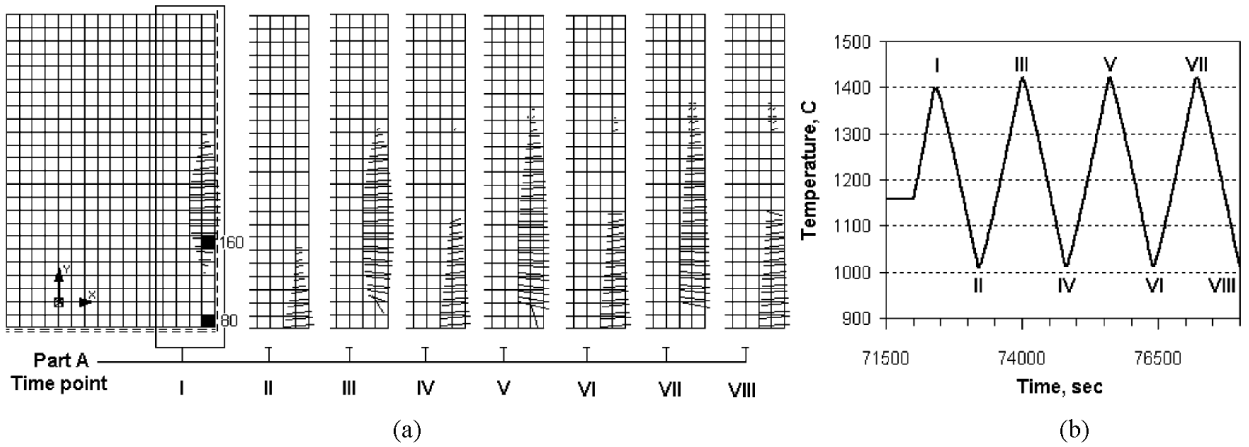

Figure 2.14: (a) Modeling results of the cracking pattern developed in refractory material with the cyclic thermal loading and (b) Temperature of the hot face [60].

Figure 2.14 (a) shows the predicted cracking pattern at specific times during a series of thermal loading cycles and Figure 2.14 (b) shows the hot face temperature. It was observed that even though the range of thermal cycling is constant for each cycle, damage in the form of cracks accumulates during each cycle. Initially, at stage I (in Figure 2.14) the cracks are opened due to tensile stresses. When a part of the brick is under compression in the next stage, the crack does not completely close due to the irreversible strains. During this stage, additional crack formation occurs near the hot surface because of thermal stresses induced by cooling. Again, in the next stage of heating, these cracks do not close in the areas loaded in compression due to the irreversible strains and thus the crack formation continues with additional number of cycles.

Gasser et al. [61] simulated cracking in refractories using a ‘smeared-crack model’ for tensile conditions to model the softening behaviour. Their results indicate that the first thermal cycle causes significant damage to refractory linings.

Approaches based on continuum damage mechanics (CDM) have been used by various researchers to model damage [62-64]. In the CDM approaches, damage, related to microcracking, porosity etc. is locally represented by a damage variable ranging from 0 (for undamaged material) to 1 (for a completely damaged material). The value of the damage variable is expressed in terms of a measurable physical quantity; usually it is the fractional loss in the elastic stiffness relative to the undamaged material.

Liang et al. [62] employed a CDM approach to model the failure associated with a cylindrically shaped black liquor gasifier lining. They considered the effects of thermal cycling as well as the effects of chemical reaction between melt and the refractory lining. The time and temperature dependent strain induced by the chemical reaction was included as an inelastic strain in the finite element formulation within ABAQUS. Their model, shown in Figure 2.15, considered a radial 2-D strip consisting of different layers of refractory bricks and the outer fibre-steel support. They applied a constant temperature (950°C) boundary condition at the inner surface of the lining and assumed the outer surface loses heat to the surrounding environment by natural convection and radiation. The outer steel shell was constrained in the radial direction.

The damage predicted by the model for conditions representing 3 months of operation is shown in Figure 2.16. The highest values of damage are 0.39 and 0.014 in compression and tension, respectively. The highest value of tensile damage occurs near the joints. The hot face of the lining also shows a high value of damage indicating cracking. Although, the predicted damage parameters were not validated against any experimental data, this model gives a general understanding about the possible locations of the cracks.

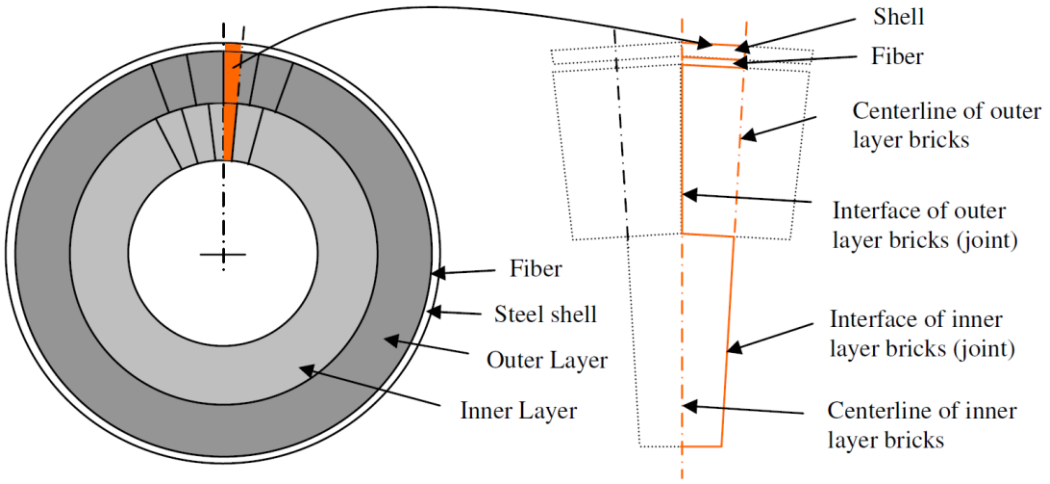

Figure 2.15: Schematic of the computation domain for the black liquor gasifier model [62].

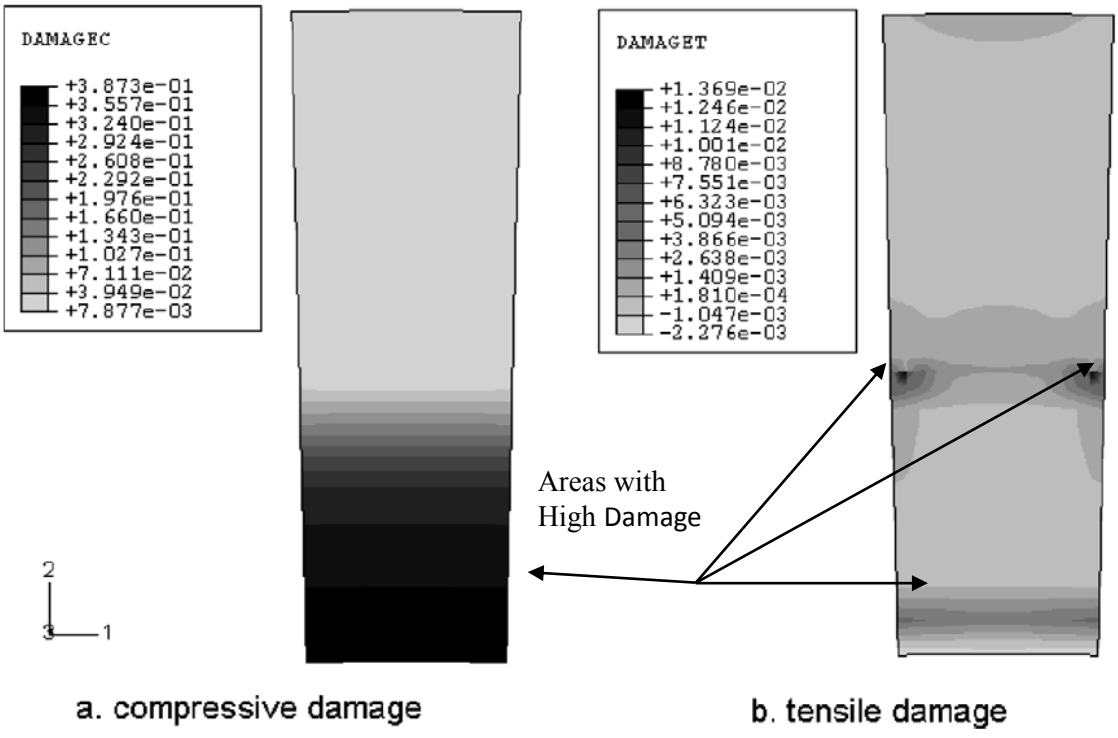

Figure 2.16: Predicted damage of the refractory lining after 3 months of operation [62]

Damhof et al. [54] developed a CDM-based finite element model that was capable of incorporating the thermal stresses in a coarse-grained material. They incorporated strains associated with the thermal gradient as well as the strains due to the external mechanical constraints on the refractory. The variables related to the microstructural inhomogeneity were assumed and later fit with the results from the thermal shock experiment. They considered a case where one end of a refractory bar initially at 20°C is suddenly immersed into the molten aluminum at 1000°C. Temperature data were obtained from thermocouples inserted along the centerline of the refractory bar at varying distances from the hot-face. Figure 2.17 shows the computation domain with the boundary conditions and the predicted damage evolution after 10 s of heating. Figure 2.17 (b) shows the contour plot of the damage variable. It shows that the maximum value of the damage parameter, ~0.4, occurs near the heated end on the surface. The value of the damage parameter indicates a 40% loss of stiffness compared to the undamaged material. This region indicates cracking after 10 s of heating.

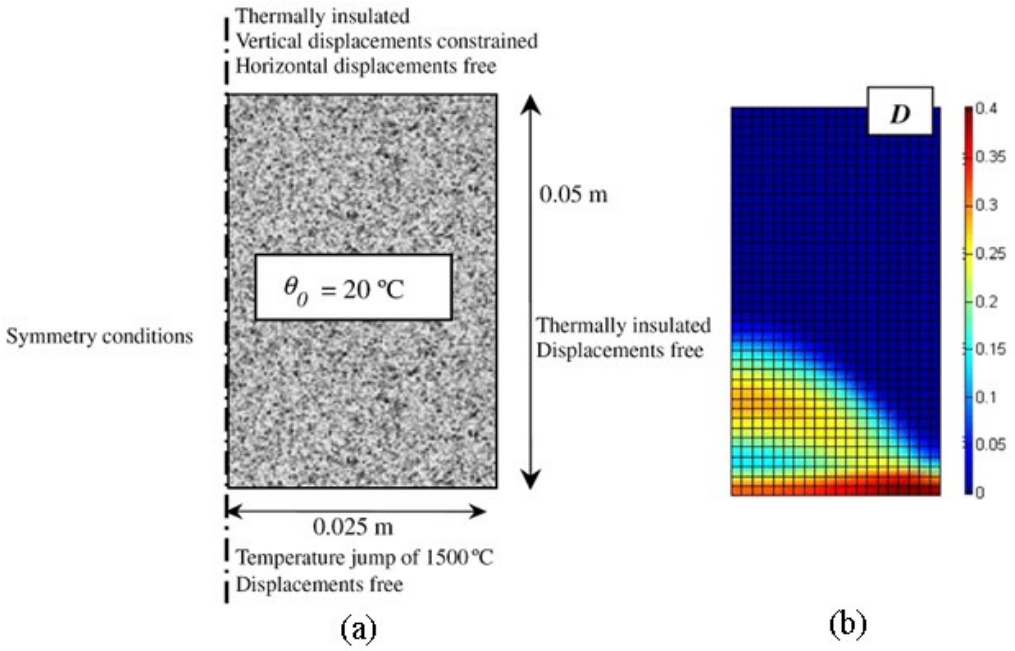

Figure 2.17: (a) Computation domain and boundary conditions used for the damage analysis and (b) Damage contour after 10 s of heating [54].

A more recent investigation by Henneberg et al. [65] in this area was targeted on incorporating fracture mechanics into the CDM approach in same the model. Their work provides a methodology to incorporate microcrack initiation and propagation phenomena into the CDM model. They simulated pulsed heating of a refractory specimen using an FE based model. Although, the results were not validated against experimental data, their simulation provides useful insights about the refractory cracking behaviour and indicates that longer duration heating causes damage effects to penetrate further into a specimen and also causes larger overall damage compared to shorter duration heating (i.e. 0.1s).

2.6 Summary

The previous work in the area of thermally induced refractory failure is summarized by the following points.

- Investigations in the area of heat transfer and thermal modeling highlighted that thermal cycling and the associated thermal gradients in a refractory lining during industrial operations can be severe. This is due to the very low value of thermal diffusivity of the refractory materials.
- Research considering the thermal stress in refractories indicates that during a single heating-cooling cycle both the direction (tensile versus compressive) and magnitude of the associated thermal stresses fluctuate. During heating compressive stresses are introduced near the surface and tensile stresses are introduced during cooling. Refractories exhibit lower strength in tension than in compression, therefore, tensile stresses are critical when considering thermal failure during the operation. Most of the modeling work reviewed has focused on a single heating or cooling event using FEM with the assumption of a linear-elastic material behaviour.
- Theoretical and analytical work in the area of refractory failure indicates that refractories have a low resistance to fracture initiation, but a significant resistance to the crack propagation. Parameters that predict crack initiation and propagation in terms of the material properties have been proposed. The bulk of the studies on refractory failure has concentrated on studying or estimating these parameters.

- Various experimental techniques were used to introduce sudden thermal cycling in refractories to study their failure behaviour. Most of the experiments reviewed involved quenching specimens in various media, which possesses issues related to quantifying, as well as, controlling the boundary conditions. In addition, most of these studies concentrated on only one heating or cooling event with multidimensional heat flow in the refractory specimen. Thus, these conditions diverge from the thermal conditions that are usually experienced during industrial operation. Experiments using a cold metal block in contact with a hot refractory specimen enable quantification and control of the thermal conditions.

- Due to their large fracture process zone, refractories are classified as "quasi-brittle materials" and the assumption of linear-elastic material behaviour does not apply to for characterizing damage. Approaches based on fracture and damage mechanics have been used to model damage in refractory materials. The CDM approach appears to be an effective means to quantify damage in laboratory scale experiments if the damage can be expressed in terms of a relatively easily quantifiable material properties such as elastic stiffness.

3. Scope and Objectives

The literature review indicates a need for quantifying the thermal degradation of refractories when subjected to multiple thermal cycles. One of the ways to do this is to develop an experimentally validated thermomechanical model that considers refractory strength degradation under the repeated thermal cycling that is typical of pyrometallurgical and other high temperature processes.

Considering the damage evolution in an entire lining would be difficult due to many factors. The design of the refractory lining varies from furnace-to-furnace as well as campaign-to-campaign. To develop a mathematical model of an industrial application, one would need to know the details of the design as well as the spatial and temporal boundary conditions that apply during operation. This data is difficult to acquire and not available in the literature. Additionally, simulating an entire lining with a damage-based thermomechanical model would be computationally expensive. Parameters such as size and shape of the refractories and the presence of refractory joints can complicate the analysis. Additionally, the data required to validate a thermal and thermomechanical model of an entire lining is difficult to acquire. A single refractory specimen has the distinct advantage of bypassing the above-mentioned issues. In addition, it allows one to consider the underlying refractory behaviour in the absence of complicating factors such as the brick installation pattern and joints.

Considering these factors, the overall objective of this thesis is to develop an experimentally validated thermomechanical model capable of predicting refractory degradation during thermal cycling. To accomplish this objective following tasks have been identified:

- Design an experimental set-up such that multiple thermal cycles can be induced on a single refractory specimen while controlling and quantifying the heat transfer conditions;
- Conduct thermal cycling experiments on refractory specimens and assess the thermally induced damage before and after the experiments;
- Develop a one-dimensional inverse heat conduction model to quantify the heat flux experienced by a refractory specimen during the thermal cycling experimentation.
- Develop a 3-D thermo-mechanical model with ABAQUS as a platform to predict transient thermal and thermal stress fields and damage accumulation accompanying both single and multiple thermal cycles.

4. Experimental Methodology

An experiment has been designed to perform thermal cycling (thermal shock) on the lab-scale. The experiment is used to study the thermomechanical response of a refractory material to thermal cycling. The first section of this chapter details the development of the experimental set-up and the second section provides the details of the instrumentation and characterization techniques used during and after the experiments.

4.1 Laboratory-Scale Thermal Cycling Experiments

The primary aim of the experiments performed in this work is to validate a damage based thermomechanical model for a single refractory specimen for conditions relevant to industrial operation. The experiments can also be used independently to study the damage resistance of refractory materials subjected to thermal cycling conditions. The experimental methodology was to be designed to promote one-dimensional heat flow in the refractory specimen. In addition, it was intended that the magnitude of the induced thermal stresses be large enough to cause damage in the refractory specimen. As discussed in the Literature Review, the technique of using hot and cold metal blocks to heat and cool the refractory specimen is a simple and effective methodology.

4.1.1 Experimental Procedure

In the initial form of the experiment, the baseline methodology was to place a hot (~1000°C) metal block in contact with a cold (room temperature) refractory specimen. After a specified amount of heating time the hot metal block would be replaced with a cold (room temperature) metal block. This procedure would be repeated for multiple heating / cooling cycles. The schematic of the "contact thermal cycling" experimental setup is shown in Figure 4.1.

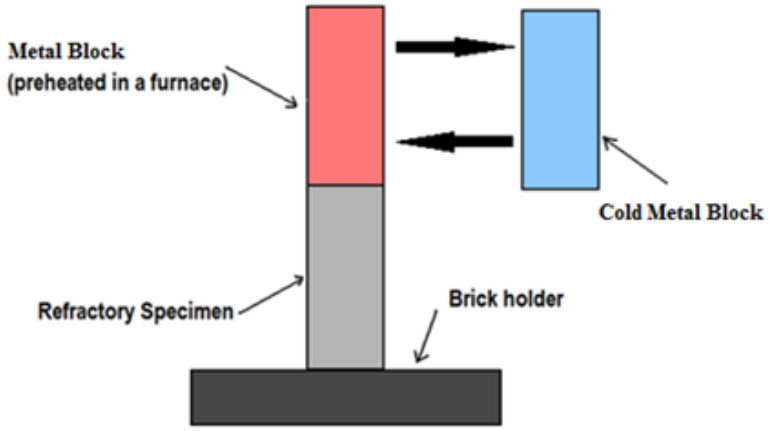

Figure 4.1: Schematic of the "contact thermal cycling" experiment

The experimental setup employs metal blocks for heating and cooling, as well as, other ancillary components to facilitate the testing. Various factors were considered in choosing the materials for the refractories and the metal blocks. These factors will be discussed in the next sections.

4.1.2 Choice of a Refractory Material

A refractory materials is defined as, “any non-metallic material capable of withstanding elevated temperatures, without destruction or deterioration (by fusion, sublimation, chemical-decomposition or physico-chemical transformations) so rapidly as to preclude its use in the construction of vessels, linings, furnace walls, flues etc., subjected to high temperatures [66].” These materials may be further classified into various categories. The classification can be based on the chemical composition (basic, acidic and neutral refractories), the operating temperature range, the method of manufacturing (power pressed, dry pressed, electrocast, wire cute etc.), or their physical appearance (shaped or unshaped). However, irrespective of the type, a refractory should possess adequate strength, resistance to mechanical and/or chemical attack and good insulating properties. Therefore, it is important to assess refractories to ensure they provide adequate properties relevant to their intended use. A significant amount of work has been done to investigate the thermo-physical properties of refractories. The testing methods are fairly well established and documented in the literature [67]. Hence, the data for thermo-physical properties for many refractories is readily available or easily acquired by testing. However, due to brittle and inhomogeneous nature of refractories, mechanical testing of refractories is difficult to perform. Gripping of the specimen (especially for tensile tests) requires special set-up. Furthermore, testing at elevated temperatures adds significant complexity.

To model the progressive damage that occurs in refractories during thermal cycling, cyclic mechanical testing at elevated temperatures is necessary. Acquiring this data is very difficult due to the factors mentioned above. Cyclic, uniaxial loading-unloading tests in tension as well as in compression at room temperature and at elevated temperatures are needed. Researchers at the Groupe d'Etude des Matériaux Hétérogènes (GEMH) lab in Limoges, France

have developed the equipment and methodologies necessary to perform these tests. Only a few refractories, tested with this methodology, have been reported in the open literature. The choice of the refractory material for this study was based on the availability of data for a high temperature refractory suitable for lining a metallurgical vessel. The material used for the current work was andalusite-based refractory concrete, manufactured by TRB Refractories, France (TRB). This material is being widely used in the secondary steel-making reactors. The same material from TRB has been tested and the damage-related property data is available in the literature.

The material studied in this work is a silica-aluminous refractory with low cement content. The material consists of ~7% high alumina cement (trade name "Secar 21") and ~93% aggregates of the andalusite mineral. The overall composition of this material is 58% Al_2O_3, 37.5% SiO_2, 2.3%CaO, 0.9% Fe_2O_3 and traces of impurities. The open porosity in the material is 6%. Figure 4.2 shows the microstructure of the material consisting of andalusite grains of 0.3-1.6mm in the cementitious matrix. Andalusite is an alumino-silicate mineral that typically contains 54-60% Al_2O_3 and 37-42% SiO_2, as well as traces of impurities such as Fe_2O_3, CaO, TiO_2, MgO, Na_2O and K_2O. It exhibits high thermal shock resistance at temperatures as high as 1250°C.

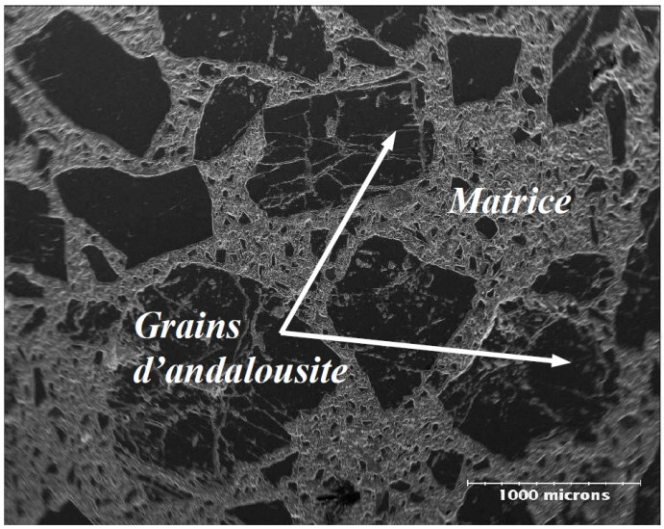

Figure 4.2: Microstructure of andalusite-based refractory concrete [67]

The matrix contributes to about 37.5% of the material by mass and maximum grain size is about 200μm. The matrix consists of 20% cement (Secar 21), 20% calcined alumina, 12.5% microsilica, 40% kerphalite (same composition as andalusite), 7.5% cyanite and traces of other impurities. The thermo-mechanical properties of this material are discussed in Chapter 6 as part of the model development.

4.1.3 Choice of a Material for Metal Blocks

The material selected for the metal blocks to heat and cool the refractory specimens was based primarily on the thermal diffusivity. Initially, copper blocks were considered due to copper's high diffusivity ($\alpha = 1.12 \times 10^{-4} m^2 / s$). However, two concerns were identified with the use of copper: 1) at high temperatures (~1000°C) deformation of the copper via creep may be

significant and 2) copper will oxidize significantly at high temperatures, which would affect heat transfer to the refractory specimen.

In order to minimize the creep and oxidation issues, the use of stainless steel was considered. Since stainless steel has a lower thermal diffusivity ($\alpha = \sim 1.1\times10^{-5} m^2/s$) than copper ($\alpha = \sim 1.1\times10^{-4} m^2/s$), it is important to assess the effect of this material choice on the resultant refractory thermal profile. A 2-D thermal model was developed in the commercial finite element software, ABAQUS. A contact interface boundary condition, assuming an interfacial heat transfer coefficient of 1000W/(m^{2}K), was applied to allow a qualitative comparison of different heating block materials. The computational domain and the boundary and initial conditions used in the model are shown in Figure 4.3. The material properties used for copper, stainless steel and refractory material used for the simulation are shown in Table 4.1.

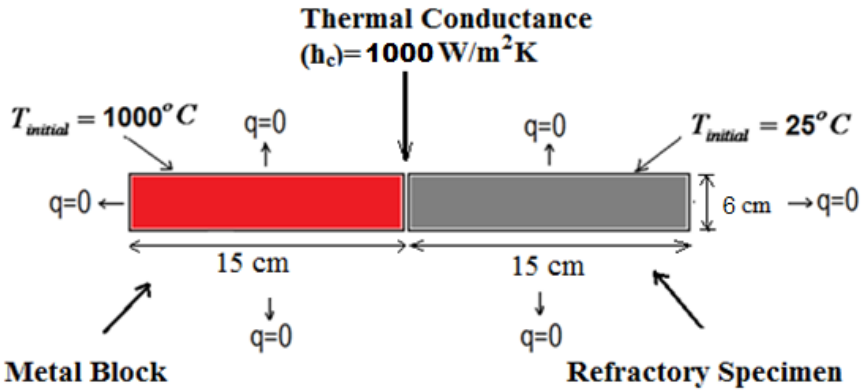

Figure 4.3: Schematic of the computational domain and the boundary conditions for a thermal model used to assess candidate heating block materials.

The model was run to predict the temperature profile in the metal heating block and the refractory specimen considering metal blocks manufactured from copper and steel. The initial

temperature of the metal blocks was assumed to be 1000°C. The resulting temperature profiles of the refractory specimen are plotted after 10min of heating for both the copper and steel blocks in Figure 4.4. The maximum difference (~70°C) between the two profiles is observed at the interface. However, the difference decreases with increasing distance from the metal-refractory interface. At 3cm from the interface, the temperature difference has decreased to about 30°C. Although the value of the interfacial heat transfer coefficient was assumed, the same value was applied for both candidate materials to facilitate a direct comparison. A larger value of the interfacial heat transfer coefficient implies more efficient heat conduction across the metal-refractory interface. It was observed that the difference between the thermal profiles was larger when larger values of the interfacial heat transfer coefficient were used. However, the differences showed less sensitivity when the interfacial heat transfer coefficient was above ~1000 $W/m^{2/}K$ suggesting that heat transfer becomes limited by heat conduction through the refractory specimen for these conditions.

Table 4.1: Thermophysical material properties used in the 2-D thermal model

		Material		
Property	Units	Copper	Stainless Steel	Refractory
Thermal Conductivity, k	W/m/K	385	14.7+0.0127T	1.9
Density, ρ	kg/m^3	9860	7800	2650
Specific heat, C_p	J/kg/K	390	490	960

These results suggest that using stainless steel blocks to heat the refractory specimens will not significantly affect the overall thermal profile in the refractory. This is due to the very low value of the thermal diffusivity of the refractory (~7.5×10^{-7} m^2/s). This model also shows that using stainless steel blocks it is possible to create significant thermal gradients in refractory specimens.

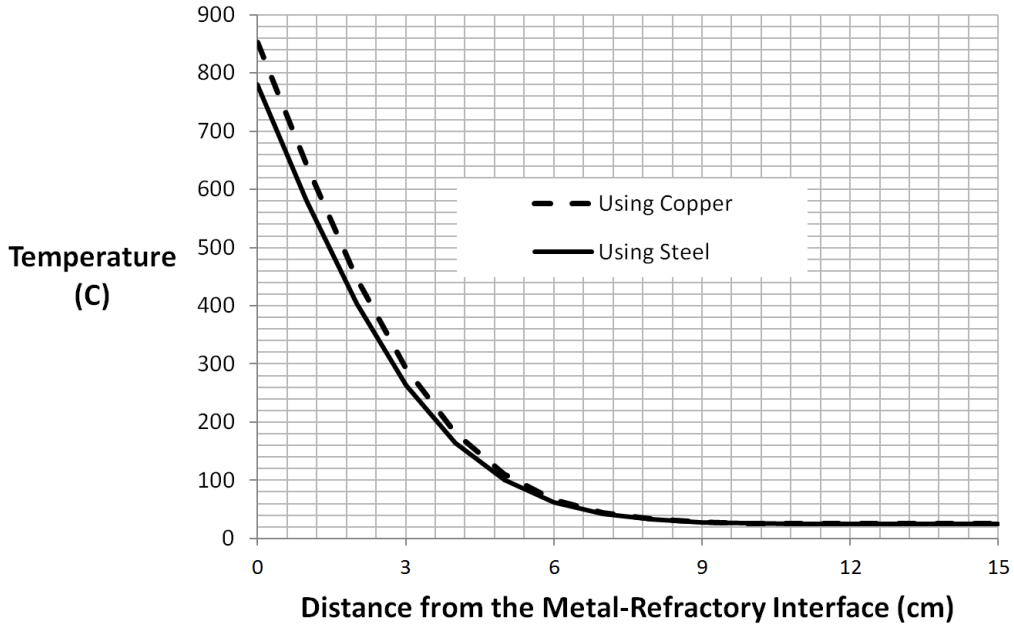

Figure 4.4: Predicted thermal profile of the refractory specimen after 10 min of heating when copper and steel blocks were used.

4.1.4 Design of the Thermal Cycling Experiments

In order to finalize the design of the thermal cycling experiments, the dimensions of refractory specimen and steel block as well as the duration of the heating / cooling cycles need to be defined. These parameters were defined by considering the instrumentation factors as well as the thermal response of the refractory and steel blocks.

Ultrasonic testing can be used to determine velocity of sound in a material and a reduction in the velocity of sound indicates cracking or damage in the material. The refractory specimens used in this work were characterized both before and after thermal cycling in an effort to measure the damage development. To carry out these tests, two transducers, acting as a transmitter and a receiver, are used. A 54kHz ultrasonic transducer (manufactured by TICO),

which is ~5cm in diameter, was used for these measurements. Considering the size of the transducer, the width of the refractory sample and that of the steel block was fixed to 6cm.

The 2-D thermal model presented in Section 4.1.2 was used to assess the effect of the refractory specimen and the steel block lengths. Initially, the model was run with steel blocks of various lengths. The temperature distributions in the refractory block were analyzed after 10min of heating time for each block length. The results showed that the thermal profile of the refractory did not change appreciably when the length of the steel block was changed. Additionally, when various lengths of the refractory specimen (within 10 - 20cm) were implemented in the model, the thermal profile of refractory specimen did not change significantly.

The heat loss from the steel blocks was used as a criterion to choose their size. Small heat loss would ensure that the steel block could be reheated in the furnace in a short period of time and be used for multiple heating-cooling cycles. To estimate the cumulative heat loss from the steel block, the change in the average temperature was used as an indicator. The nodal temperatures along the longitudinal direction of the steel block were averaged and the resultant average temperatures were plotted against time in Figure 4.5 for four different lengths of steel block.

The results show that the average temperature change from the initial condition (1000°C) at 600s decreases with increasing length of the steel block. The temperature drop is significantly for the lengths smaller than 15cm. For instance, the temperature drop for a 10cm steel block is ~170°C compared to ~90°C for the 15cm steel block. Increasing the length of the steel block more than 15cm does not reduce the average temperature drop significantly. In the experiments,

which involve manually manipulating these hot steel blocks, it was desirable to have a smaller block size due to the difficulties in handling heavy and hot steel blocks. Based on the above-mentioned factors, the length of the steel block was chosen 15cm.

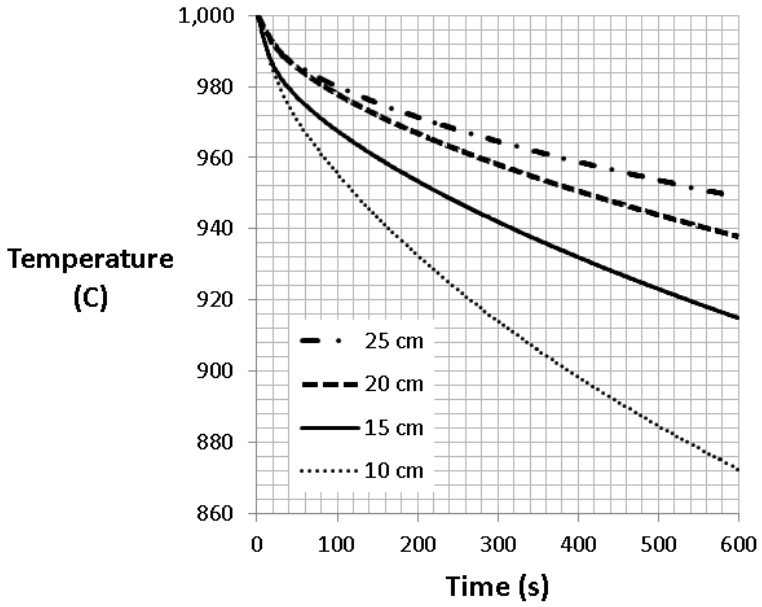

Figure 4.5: Predicted average temperature history of steel blocks with various lengths.

In the thermal cycling experiments, the refractory specimens will go through multiple heating-cooling cycles. The 2-D thermal model was used to determine an acceptable cycle time. Ideally, smaller cycle times were desired to ensure high heat flux across the interface throughout the experimentation. However, the experimental procedure involves replacing the steel blocks with others (either hot or cold depending on the stage in the experiment) and this could consume time. Considering this time lapse, a minimum cycle time of 10 min (5 min for both the cooling and heating stages) was proposed. The thermal model was run with various cycle times to determine the effect on the refractory thermal profile. The lengths of the steel block and the

refractory specimen were 15cm. The simulation was run for five heating-cooling cycles with total (heating and cooling) cycle times of 10, 20 and 30min. The results, shown in Figure 4.6, indicate that the location of the peak temperature moves away from the interface with increasing cycle time but the magnitude of the peak temperature increases only slightly. Therefore, a cycle time of 10min was selected due to the expected small increase in the corresponding thermal stress with the higher cycle times.

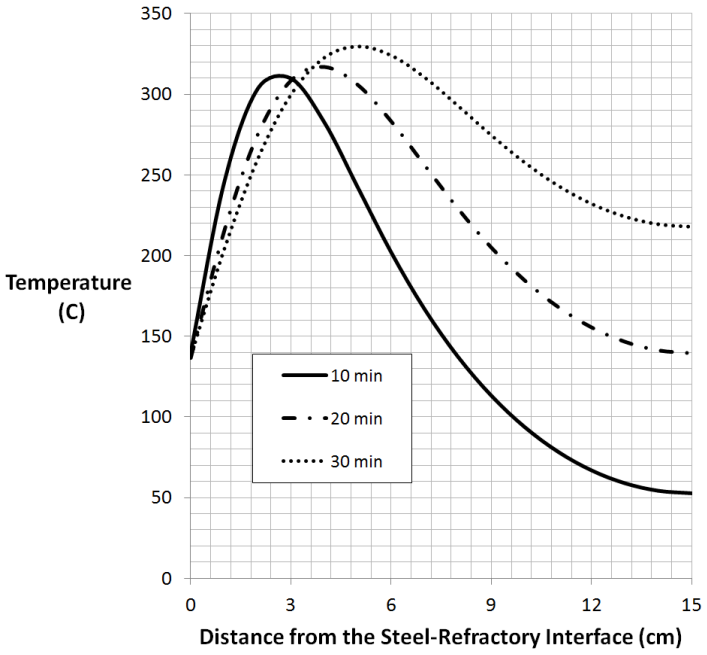

Figure 4.6: Predicted thermal profiles of refractory specimen after 5 cycles with various heating (or cooling) times.

4.2 Instrumentation

An instrumentation plan was developed to collect data before, during, and after the each experiment. The goals for the instrumentation plan were to monitor the temperature changes in

refractory specimen and the steel block during the experiments and measure the damage accumulation in the refractory specimens due to thermal cycling.

4.2.1 Thermocouples

During the experiments, the temperature of the steel block was measured. A type-K thermocouple was spot welded at a location 1cm from the steel-refractory interface at the geometric center of the steel block cross-section. Similarly, a thermocouple was inserted in the refractory specimen 1cm from contact interface on the centerline. The thermocouples from the refractory specimen and the steel blocks were connected to a DAQ system (a National Instruments cDAQ-9171). Temperatures were recorded every 0.2s or 0.5s. The temperature data from the steel block was used in inverse heat conduction (IHC) analysis to calculate the heat flux conditions at the contact interface. The temperature data from the refractory was used to validate the thermal model of the refractory specimen.

4.2.2 Ultrasonic Testing

As discussed earlier, an ultrasonic testing device can be used to measure the velocity of sound in a material. The direct transmission technique was used in this work. An ultrasonic pulse is produced by the transducer to generate a longitudinal sound wave in the material. The sound wave is transmitted through the refractory material to the other side of the specimen where it is measured by another transducer. Based on the time of travel and the distance between the transducers, the velocity of the sound wave is calculated. When a material is damaged, the velocity of sound in the material will be less than when the material is undamaged. The velocity

of longitudinal sound wave in a material can be used to determine the modulus of elasticity using the following equation [68]:

$$E = \frac{\rho v^2(1+\nu)(1-2\nu)}{(1-\nu)} \tag{4.1}$$

where E is the modulus of elasticity, ρ is the density, v is the velocity of sound in the material, and ν is the Poisson's ratio. Employing this equation, the percent reduction in the modulus of elasticity (or percentage damage, "D") can be calculated using the following equation:

$$D = \frac{E_0 - E}{E_0} \times 100 \tag{4.2}$$

The speed of sound in the refractory specimens was measured using two ultrasonic transducers (model TICO operating at 54kHz) placed opposite to each other on either side of the specimen being measured as shown in Figure 4.7. An effort was made to ensure that the transducers were exactly opposite each other while testing to make sure the distance between them is the width of the refractory specimen (6cm). As mentioned earlier, the transducers were circular shaped with a diameter of 5cm. The system was calibrated using a steel sample for which the value of the velocity is known. Measurements were performed at room temperature before and after the thermal cycling experiments. Since the elastic modulus is directly proportional to the square of velocity, the percentage damage is calculated directly from the velocity values. Three readings were performed at each location and the average value was reported. The variation in the measurement at one location on a refractory sample was within $\pm$75m/s of the average value.

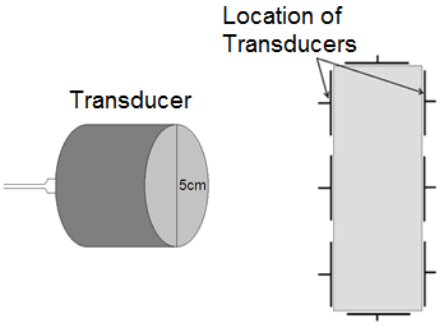

Figure 4.7**:** Locations of the ultrasonic measurements on refractory specimen.

4.3 Experimental Set-up

Considering the experimental parameters and the instrumentation discussed above, a set-up for the experiments was developed. The components used in thermal cycling experiments are shown in Figure 4.8.

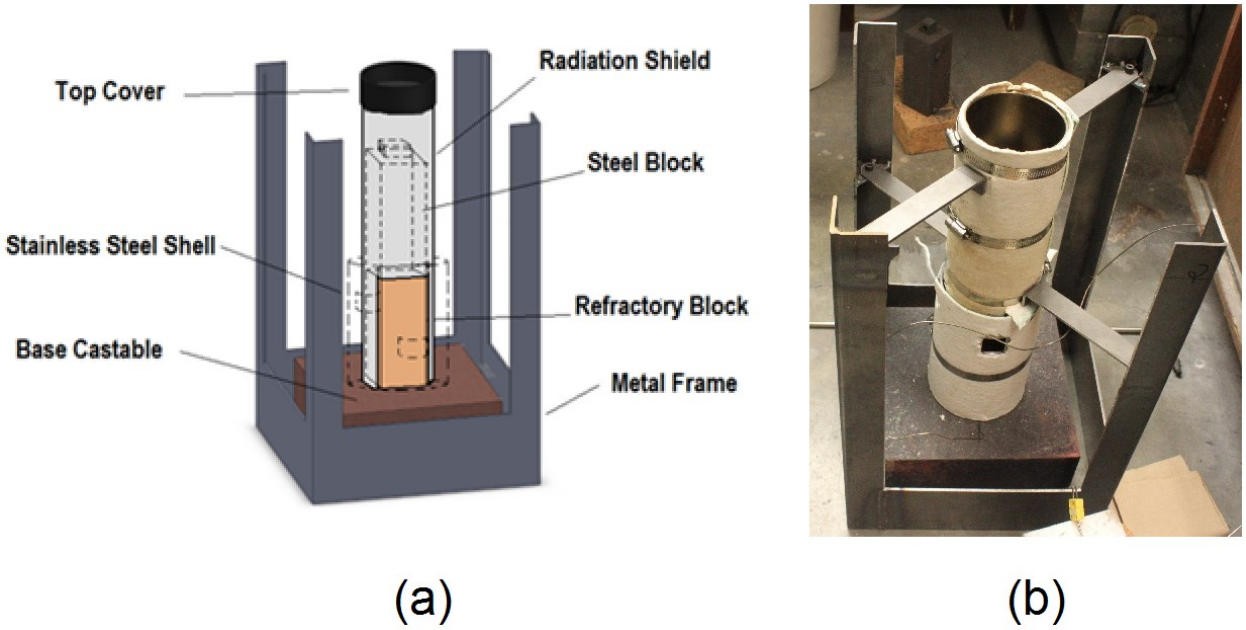

Figure 4.8: Set-up for the thermal cycling experimentation: (a) Schematic representation (b) Photo of the set-up.

During the thermal cycling tests, the refractory test specimen was placed on a base made from a castable refractory material to minimize thermal losses from the bottom end of the refractory specimen. In order to achieve one-dimensional heat flow, the refractory specimen and the steel block were enclosed in a cylindrical cover made from stainless steel with a polished inner surface to minimize the heat loss through the radiation. A cap, also made from stainless steel, was used to cover the top of the steel block. To support the cylindrical cover, a stand was fabricated from steel.

5. Methodology of Thermal Modeling

The design of the experimental apparatus assumes that the stainless steel blocks contacting the refractory specimen are initially isothermal. By alternating contact with hot (~1000°C) and ambient temperature blocks, the refractory specimen will experience thermal, and consequently thermal-stress, cycling. In designing experimental set-up, it was assumed that all of the heat that is transferred from or to the steel block is equal to the heat gained (or lost) by the refractory specimen. Considering the experimental design for this study and the potential for deviation from the assumptions on heat flow, it was crucial to quantify the heat flux from the steel block to the refractory specimen. Two types of thermal models were developed to do this: an inverse heat conduction (IHC) model and a 3-D thermal model in ABAQUS. The IHC model was developed to calculate the interfacial heat flux using the temperature data measured in the steel block. The 3-D thermal model was developed with predicted flux values from the IHC model as a boundary condition and was needed to provide the input temperature field for a 3-D thermal stress model.

5.1 Inverse Heat Conduction Analysis

An IHC analysis was performed to predict the heat loss from the steel block during the experiments based on the measured steel block temperatures. The predicted heat flux from the IHC analysis (interfacial heat flux) was then used to in a forward heat conduction (FHC) model of the refractory specimen to predict the temperature distribution for comparison with measurements. The IHC analysis could not be performed directly on the measured temperature data from the refractory specimen of the very low thermal diffusivity (of the order of $10^{-7}m^2/s$) of the refractory materials, which causes numerical conversion issues. Instead, it was applied to the

steel block temperature data and then a FHC model was used to check the results in the refractory specimen.

IHC analysis can be used to quantify the transient heat flux variation at locations where the temperature data is available. The IHC method employs a heat conduction model to numerically calculate a sensitivity matrix with respect to time by perturbing the heat flux boundary conditions. The measured temperature data and the sensitivity values together are then used to estimate the heat flux value for a time increment. In the current analysis, an FEM based heat conduction model was developed in FORTRAN to predict the temperature changes in the steel block. This section describes the development of the inverse heat conduction analysis, its validation, and the application to the current experimentation.

5.1.1 Forward Heat Conduction Analysis

To predict the temperature evolution in the steel block, a FHC model was developed. This model predicts the temperatures in the steel block based on the input heat flux (hence the term "forward") as opposed to the IHC analysis where the heat flux that is driving the model is predicted based on the temperatures at a known location. The governing equation for transient heat conduction that is solved in this model is:

$$\frac{1}{\alpha}\frac{\delta T}{\delta t} = \frac{\delta^2 T}{\delta x^2} + \frac{\delta^2 T}{\delta y^2} + \frac{\delta^2 T}{\delta z^2} \tag{5.1}$$

where T is temperature, x, y and z are the spatial variables in the Cartesian co-ordinate system and α is the thermal diffusivity of the material given by:

$$\alpha = \frac{k}{\rho C_p} \tag{5.2}$$

where ρ, C_p, k are the density, specific heat and thermal conductivity of the material. The left hand side of equation (5.1) describes the rate of increase in the internal energy per unit volume and the right hand side relates to the heat conducted in the material per unit volume.

In order to solve this transient heat transfer problem numerically, an FORTRAN code was developed using a Finite Element Method (FEM) formulation. Even though the heat transfer in the current experimental design is one-dimensional, the analysis was performed with 2-D elements, as the code was readily available. The size of both the steel block and the refractory specimen used in the experiments was 15cm x 6cm x 6cm. Due to one-dimensional heat transfer conditions that were assumed to prevail, a temperature gradient was expected to develop in the longitudinal direction (along the length of the specimen) only and with no gradient in the transverse directions (along the width of the specimen). To reduce the computational load (number of elements), the model domain was reduced to 15cm x 1cm. The domain was divided into 10 elements of varying sizes in the longitudinal direction as shown in Figure 5.1. For this model, changing the number of elements within the range of 6-20 did not alter the results. The material properties used in the model for the steel block are given in Table 5.1. In model, a constant heat flux boundary condition has been to the edge of the domain consistent with the location where heating or cooling occurs.

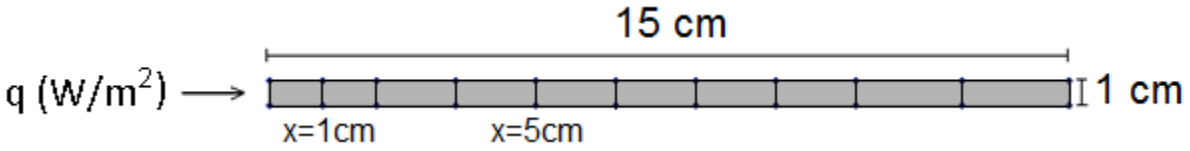

Figure 5.1: Boundary condition and the computation domain for the forward heat conduction model.

Table 5.1: Material properties used in the forward heat conduction model for the steel block [69, 70]

Material Property	**Unit**	**Value**
Thermal conductivity (k)	W/m/K	14.7 + 0.012T
Density (ρ)	kg/m^3	7800
Specific heat (C_p)	J/kg/K	490

5.1.2 Validation of the Forward Heat Conduction Model

The forward heat conduction model used in the IHC analysis was validated by comparing the temperature predictions from the model to an analytical solution for a simple 1-D problem. The 1-D problem selected was the transient heating of a semi-infinite solid via a constant surface heat flux. The analytical solution for this problem is given by [71]:

$$T(x,t) = T_i + \frac{2q(\alpha t/\pi)^{1/2}}{k}\exp\left(\frac{-x^2}{4\alpha t}\right) - \frac{qx}{k}erfc\left(\frac{x}{2\sqrt{\alpha t}}\right) \tag{5.3}$$

where $\alpha = \left(k/\rho C_p\right)$ is the thermal diffusivity of the material, $T(x,t)$ is the temperature at location x at time t after applying a heat flux of q and T_i is the initial temperature of the material. An initial temperature of 900^{o}C was selected for the model. The thermo-physical properties for steel, summarized in Table 5.1, were employed except for k which is assumed to be constant for this

analysis with a value of 25W/m/K. Since, the interfacial heat flux values for the current experimental work are unknown, a range of values from 0.1 - 1 MW/m^2 were considered to test the model with the expectation that this will cover the possible heat flux values experienced in this study. The results for the heat flux value of ~150kW/m^2 are discussed here.

The forward heat conduction model was run for 1500s. The predicted temperatures at nodal locations corresponding to x = 1, 5, 10 and 15cm were selected for comparison with the analytical solution. The temperatures calculated with the analytical solutions at these locations for 1500s, using Eq. (5.3) are compared with the model predictions in Figure 5.2. It can be seen that for each location, the agreement is excellent in the initial period (~400s) and then the predictions diverge from the analytical solution where the semi-infinite solution is not valid. The model was also tested for other material properties that are consistent with the refractory materials. Overall, the model predictions are in a good agreement with the analytical solution when semi-infinite conditions exist in the model domain. This exercise shows that the forward heat conduction model is capable of accurately predicting temperature for conditions relevant to the current study.

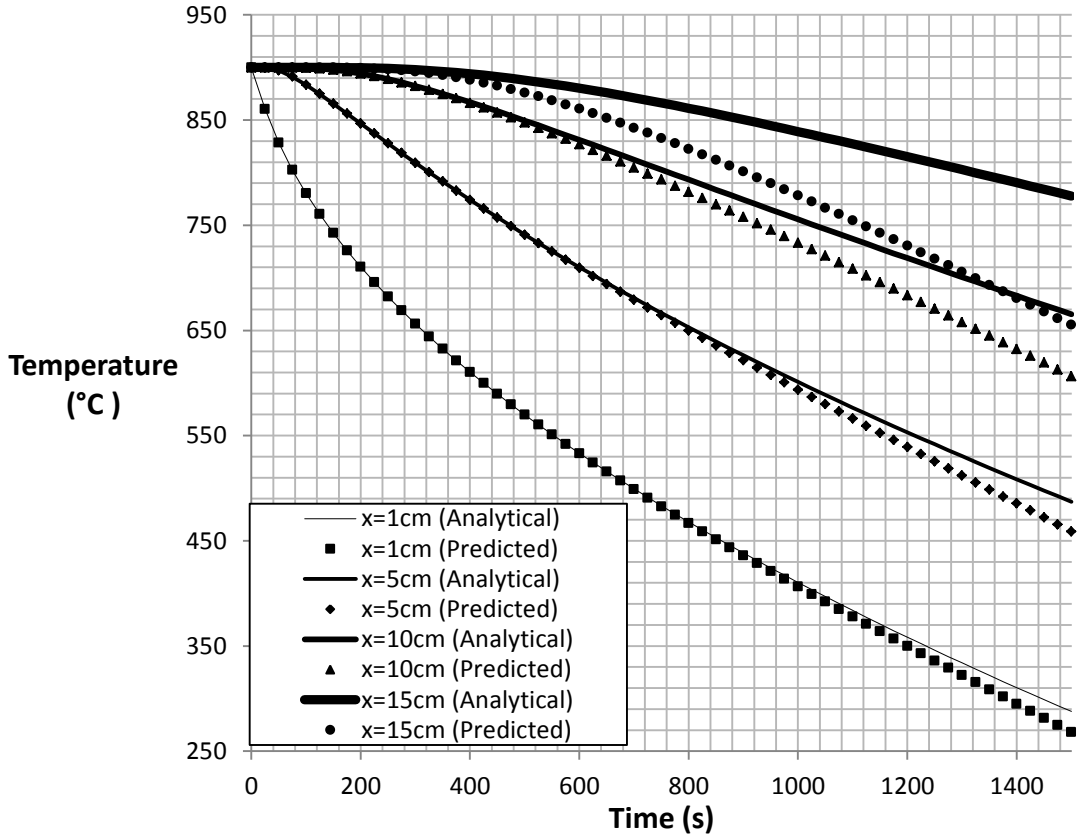

Figure 5.2**:** Comparison between the model prediction and the analytical solution for a semi-infinite geometry with the constant surface heat flux boundary condition.

5.1.3 Inverse Heat Conduction Analysis

In the forward heat conduction analysis (FHC), the temperature distribution within the model domain is predicted using a known boundary condition. By applying an IHC analysis, an unknown boundary condition can be determined using measured temperatures. In an IHC analysis, the temperature distribution within the domain is NOT known *a priori*, rather the IHC analysis determines a boundary condition that replicates the (measured) temperatures at locations in the domain (or at a single point if the problem is 1-D). As part of this analysis procedure, a

FHC model is used to predict the temperature distribution in the domain. The schematic representation of these two problems is shown in Figure 5.3 [72].

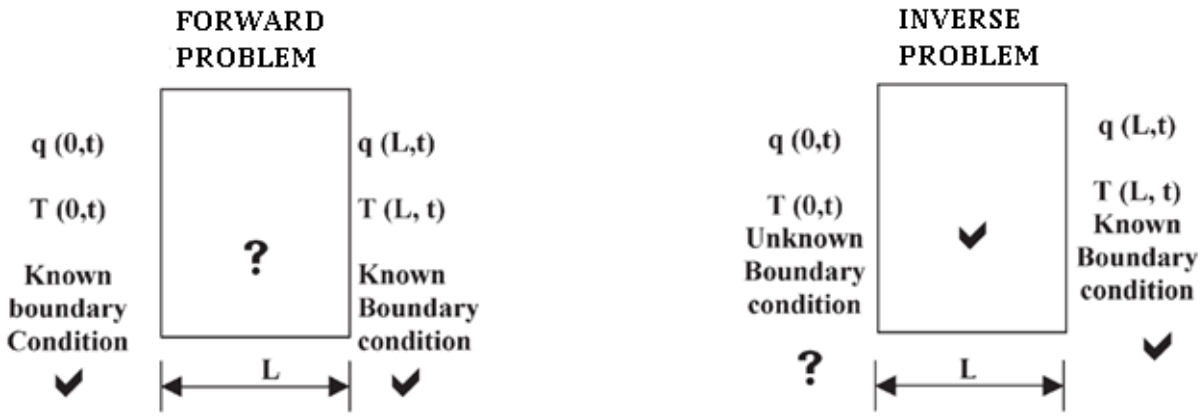

Figure 5.3: Schematics of the forward and the inverse heat conduction problems [71].

In order to understand the algorithm for the inverse analysis, consider a 2-D representation of the computation domain used for the current work shown in Figure 5.3. The thermocouple location and the boundary conditions are also shown in Figure 5.4. This domain represents the steel block in contact with the refractory material. The refractory specimen is assumed to be on the right hand side of the steel block and $q(t)$ is the transient heat flux occurring across the interface with the refractory specimen. Since the steel block is enclosed in a radiation shield, the heat loss to the surrounding from all surfaces except the one in contact with the refractory specimen was assumed to be zero.

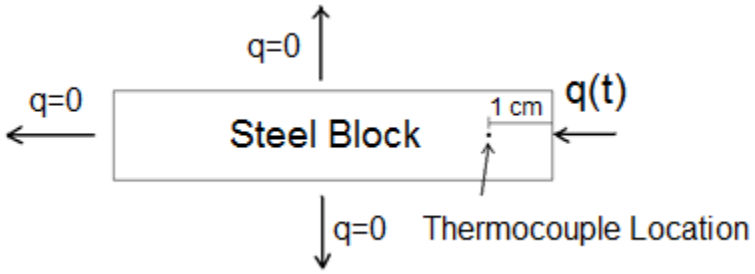

Figure 5.4: Schematic representation of the computation domain and the boundary conditions for the inverse analysis.

As shown in Figure 5.4, a time dependent heat flux, $q(t)$, is applied to the steel block at $x = 0$. The temperature data is available at location 1cm from the interface at time intervals of $\Delta\theta$. The aim of the problem is to calculate the unknown heat flux $q(t)$ based on the knowledge of temperature history at $x = 1\,\text{cm}$ and the thermo-physical properties of the material.

In order to solve the problem, the unknown heat flux $q(t)$ is discretized into a series of heat fluxes, q_i, using the time intervals of $\Delta\theta$. Note that the time interval $\Delta\theta$ is based on the available temperature data being used with the inverse analysis and is different than Δt, the "time step" used in the forward heat conduction analysis. The heat fluxes are calculated to minimize the differences between the calculated (T_i) and measured (T_i^m) temperature values at each time interval.

For any time, i.e. $t = t_i$, an initial value of the heat flux, q^{base}, is applied and the baseline temperature, T_i^{base}, is calculated after the time interval of $\Delta\theta$ using the FHC model. q^{base} is then increased by a small amount Δq ($q_i^{modified} = q_i^{base} + \Delta q$) and the FHC model is re-run from

t = i to predict a modified temperature, $T_i^{modified}$. A sensitivity parameter can then be calculated according to:

$$S_i = \frac{\partial q}{\partial T} = \frac{q_i^{modified} - q_i^{base}}{T_i^{modified} - T_i^{base}} \tag{5.4}$$

Using the sensitivity parameter, the heat flux, q_i, corresponding to the measured temperature, T_i^m, can be calculated as:

$$q_i = q^{base} + xS_i(T_i^m - T_i^{base}) \tag{5.5}$$

The numerical solution of the IHC analysis can have difficulty converging because of the non-linear heat transfer conditions resulting from the temperature dependent materials properties. To avoid or limit solution instability, a relaxation factor x is introduced. The value of the relaxation factor lies between 0 and 1. Suitable values of x are chosen based on the convergence behaviour of the problem being investigated. For the current analysis, 0.2 was found to be a suitable relaxation factor value. The calculated heat flux, q_i, is then applied in a forward model step and the temperature T_i is calculated. If the temperature difference ($T_i^m - T_i$) is smaller than a specified tolerance limit ($T_i^m - T_i \le Tolerance$), then the calculation has converged. Ideally, the tolerance limit should be small in order to approach the exact solution. However, if too small a value is used, convergence issues or a physically unrealistic solution occur. In this analysis, the tolerance limit was chosen to be 5°C.

In this instance, the nodal temperatures of the domain are updated and the calculations are carried out for the next time interval t_{i+1} ($t_{i+1} = t_i + \Delta\theta$). If the condition $T_i^m - T_i \le Tolerance$ is

not satisfied, then the calculations are repeated with $q^{base} = q_i$ until the condition is satisfied. The temperatures are then updated and the calculations are carried out for the next time interval t_{i+1}. The flow chart for the inverse analysis is shown in Figure 5.5.

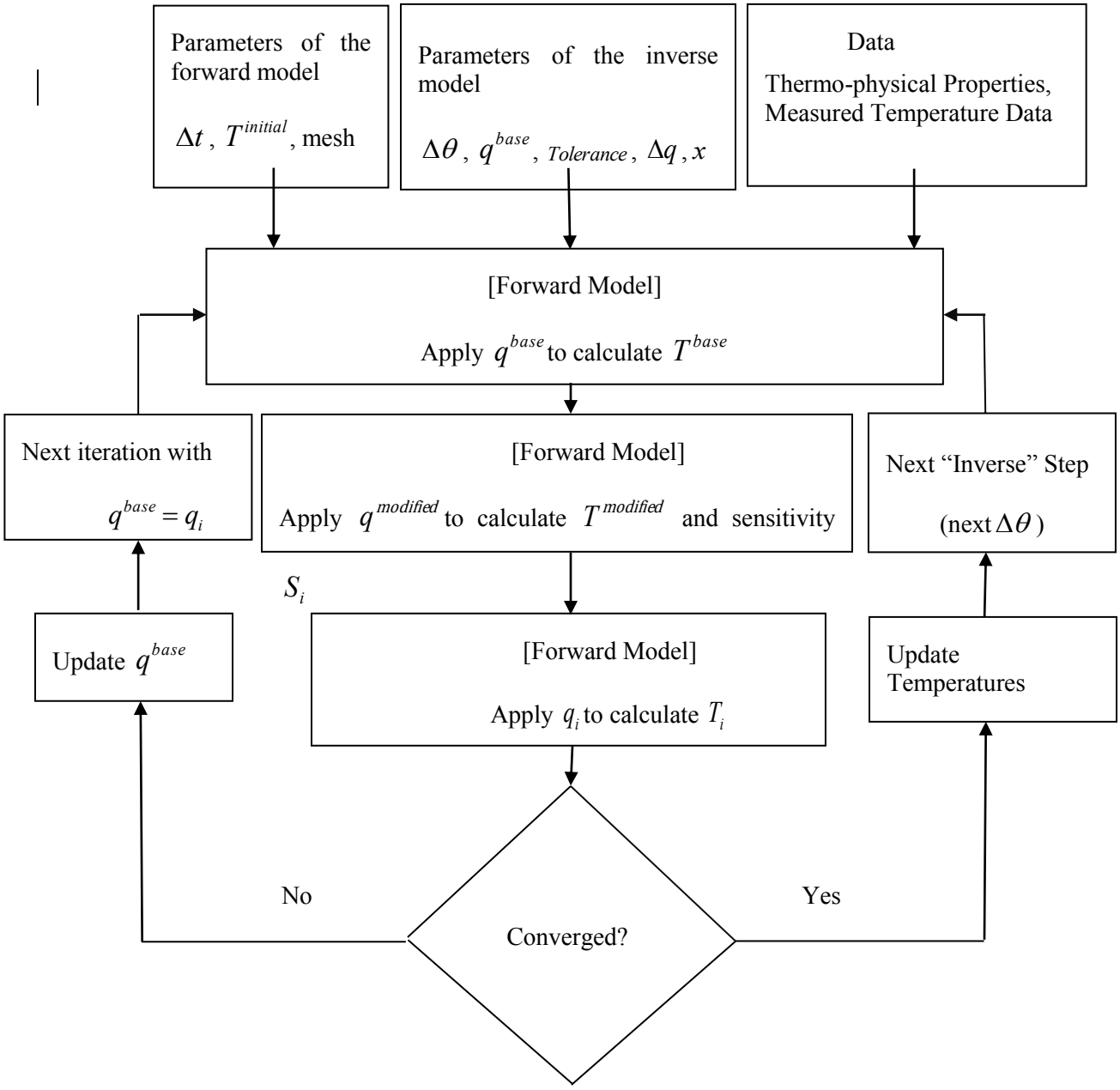

Figure 5.5: Flowchart for the inverse heat conduction analysis

5.1.4 Validation of the Inverse Heat Conduction Model

In the current work, the temperature data from the steel block will be used to calculate the heat flux experienced by the steel block at the contact interface. The heat flux at the interface is expected to vary with time as the steel block cools and the refractory heats up. Thus, the ability of the IHC model to calculate a time varying heat flux was used as a test problem to validate the IHC analysis methodology.

As a first step in this validation process, the transient temperature variation in a steel block subjected to a time varying heat flux was predicted with the forward conduction model. The predicted temperature data was then input to the IHC model to back-calculate the heat flux.

A known heat flux, $q(t)$, based on a sinusoidal curve given by Eq. (5.6), was applied to the forward model.

$$q(t) = 50 + \left[10^3 \sin\left(\frac{\pi t}{250} \right) \right] \tag{5.6}$$

where t is the time in seconds and $q(t)$ is in kW/m^2. A time step of 0.2s was used for both the FHC and IHC models. The initial temperature of the domain was 25°C. The 10-element mesh, shown in Figure 5.1, with varying element size was employed.

The forward model was run for 250s. The temperature data at a node, located 1 cm from the hot end, with a constant interval of 5s was extracted. This data was used as an input to the IHC model and the heat flux values were back-calculated. Consistent with the temperature date, a 5s time interval was used in the IHC analysis. The input and predicted values of the flux are compared in Figure 5.6.

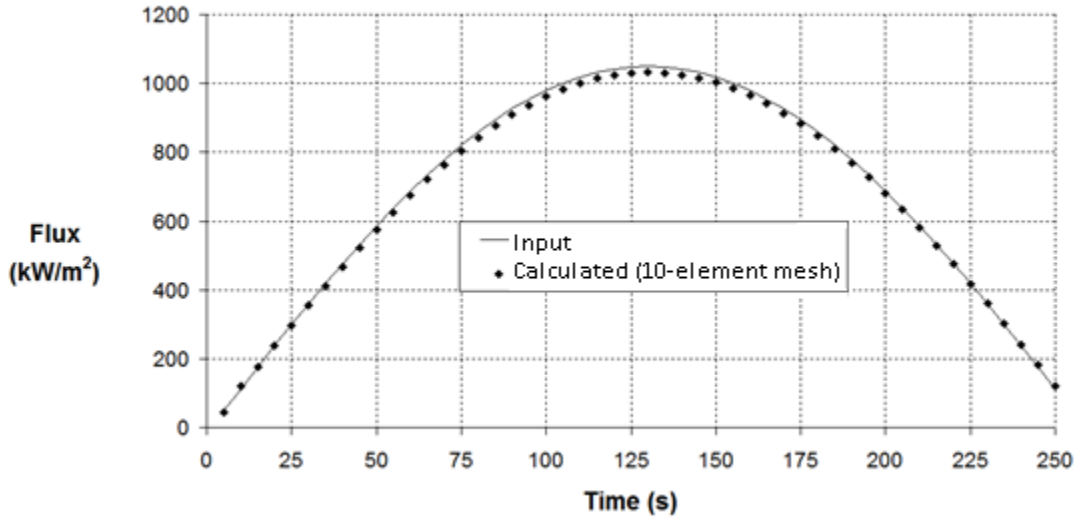

Figure 5.6: Comparison between the input and the predicted values of the heat flux using a 10-element mesh.

Overall, Figure 5.6 shows good agreement between the input and the predicted values of the heat flux. However, at the center of the curve, at about 125s, the calculated heat flux deviates from the input. This was attributed to the coarse mesh used for the simulation. The domain was refined to 100 elements with a gradually increasing mesh size. The results with the refined mesh show a very good agreement as shown in Figure 5.7.

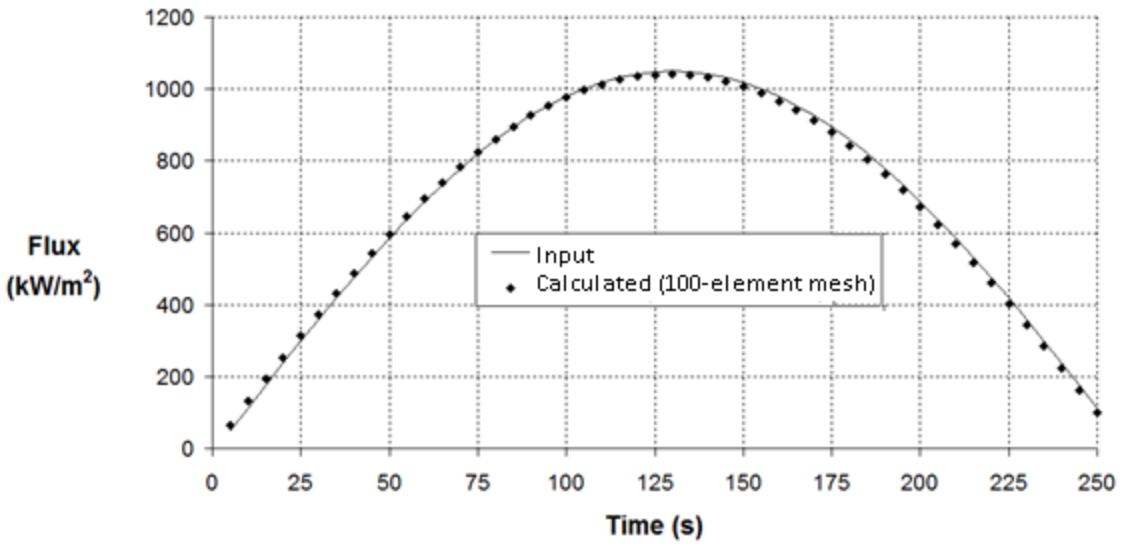

Figure 5.7: Comparison between the input and the predicted values of the heat flux using a 100-element mesh

This exercise shows that the IHC model is capable of predicting the heat flux entering into the refractory specimen using the temperature data from the steel block.

5.2 3-D Thermal Model

The heat fluxes calculated using the IHC analysis were used as input to a 3-D thermal stress model developed with ABAQUS. The thermal stress model was developed as a sequentially coupled simulation where a thermal model is run first and used as input to a stress model. The 3-D thermal model was developed using the interfacial heat flux values as a boundary condition. The predicted temperature data from the thermal model was used as an input to a 3-D stress model developed separately using the same mesh as the thermal model. The computational domain, shown in Figure 5.8, was based on the refractory specimen geometry. Due to symmetry only a quarter section of the geometry (15cm x 3cm x 3cm) was simulated. The domain was divided into elements (ABAQUS heat transfer element designation is DC3D8) of

varying sizes as shown in Figure 5.8. The thermal properties of the Andalusite-based refractories used in this study are summarized in Table 5.2.

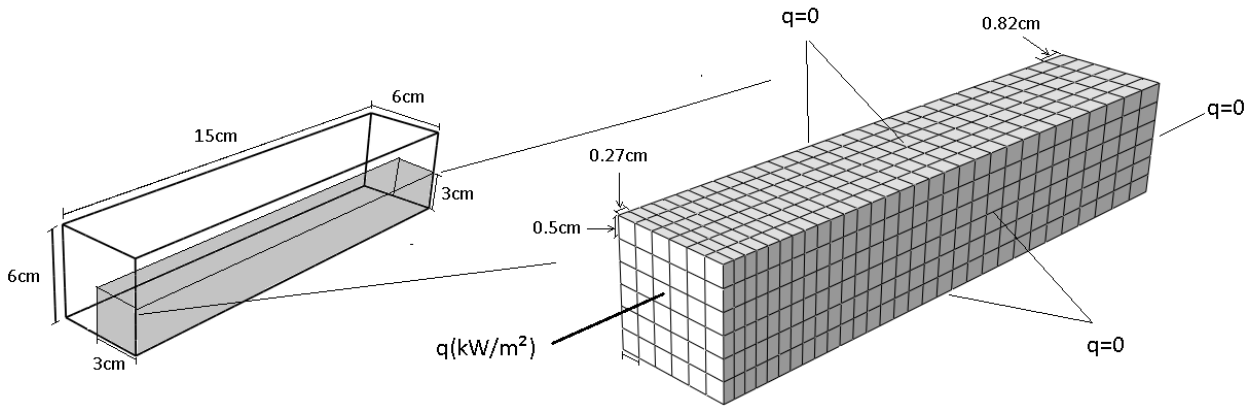

Figure 5.8: Boundary conditions and the computation domain for the 3-D thermal model.

Table 5.2: Thermal properties of refractory used in this study [73,75].

Material Property	**Unit**	**Value**
Thermal conductivity (k)	W/m/K	1.9 (573 K)
		1.8 (873 K)
		1.7 (1273 K)
Density (ρ)	kg/m^3	2600
Specific heat (C_p)	J/kg/K	980

It should be noted that refractories are heterogeneous materials with two or more phases and porosity. Furthermore, the properties change with direction as well as the temperature. The values of the thermal conductivity at various temperatures is available however, the data for density and specific heat at elevated temperatures are not available. Therefore, these properties were assumed to remain constant at

elevated temperatures. It was also assumed that the material under consideration is homogeneous and isotropic. The effect of damage on the value of conductivity and density was assumed negligible.

5.2.1 Model Validation

A heat flux of 150 kW/m^2 was applied to the refractory specimen, which started at an initial temperature of 20°C. The simulation was run for 300s and a contour plot of the temperature predictions is shown as Figure 5.9. The results show that a sharp thermal gradient is developed initially near the surface and that the gradient gradually decreases moving away from the surface. At ~5cm from the surface, there is no change in the temperature. The FHC model discussed in section 5.1.1 was used to simulate the same thermal conditions in this refractory material. The predicted temperature distributions as a function of depth into the refractory specimen from the FHC model and the 3-D thermal model were compared at various times. The results are shown in Figure 5.10. The results show that the results from the FHC model and 3-D thermal model predict the same temperature distributions at each time. Hence, the 3-D model is reliable and its temperature predictions can be used to carry out the 3-D thermal stress analysis. The methodology of thermal-stress modeling is discussed in the next chapter.

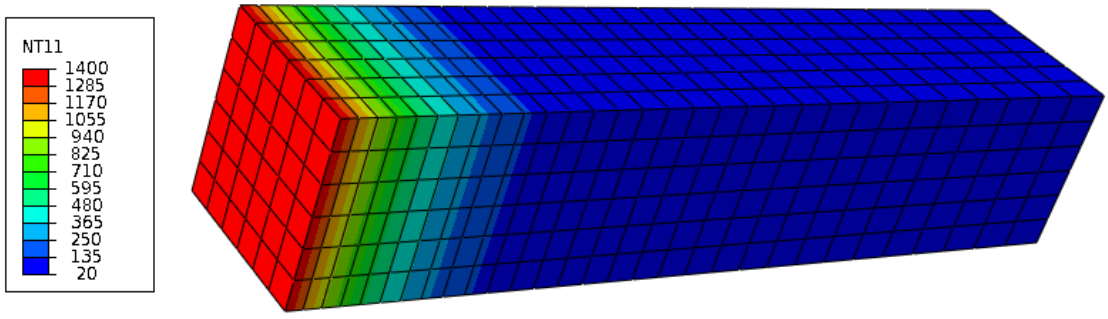

Figure 5.9: Contour plot of temperature after 300s from the 3-D thermal model.

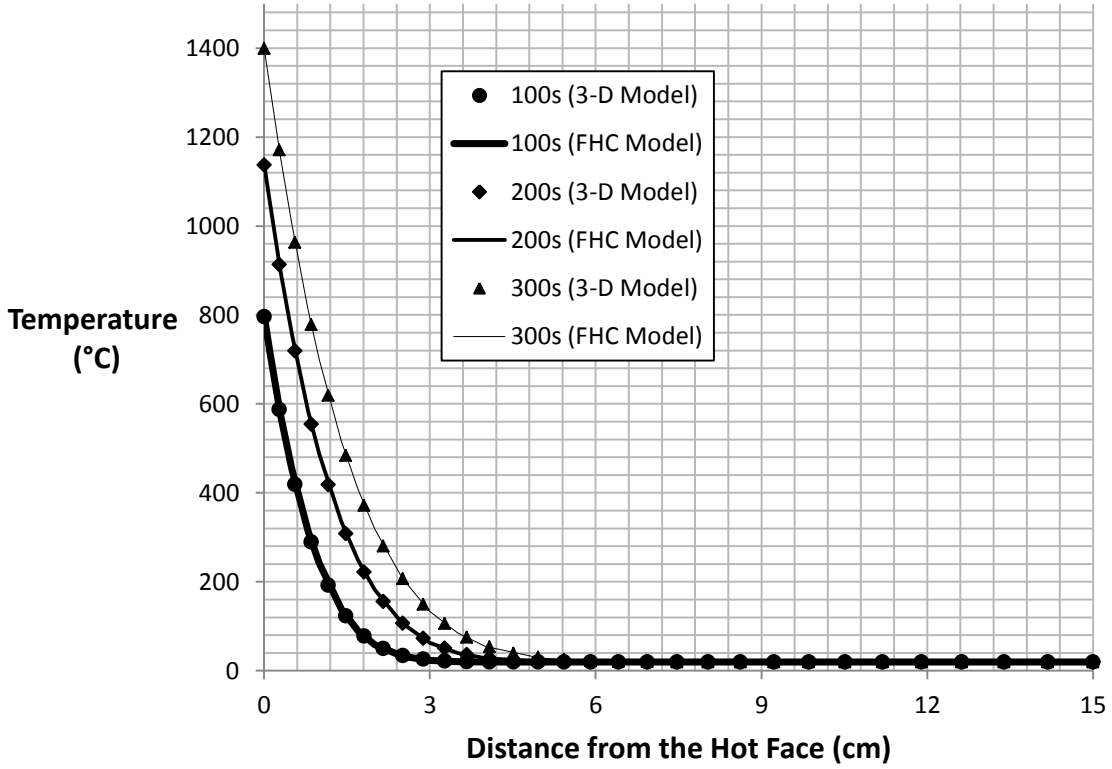

Figure 5.10: Comparison of the prediction temperature distributions from the FHC model and the 3-D thermal model.

6. Thermal-Stress Model Development

A thermal-stress model has been developed to predict the stress development in the refractory specimens during thermal cycling. Since, the stress in the refractory is dependent on thermal field but not vice-versa, a "sequentially coupled" model has been developed with ABAQUS, where a standalone thermal analysis is first conducted followed by the thermal-stress analysis. The predicted temperature data from the 3-D thermal model discussed in chapter 5 was employed as input to the thermal-stress model for the refractory specimen.

6.1 Computational Domain and Boundary Conditions

Taking advantage of symmetry in the refractory specimen, only a quarter section of the geometry was considered in the thermal stress simulation. The mechanical boundary conditions and computation domain applied to achieve symmetry and to constrain the specimen are shown in Figure 6.1. The same mesh that is used in the thermal analysis (Figure 5.8) is used for the stress analysis.

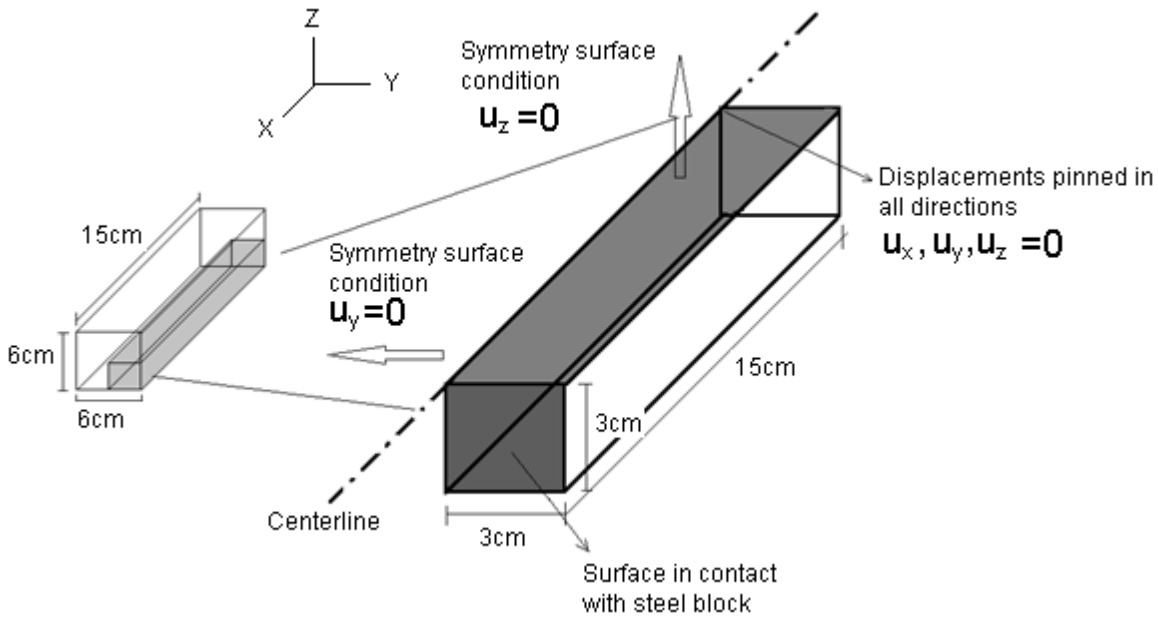

Figure 6.1: Schematic representation of the computational domain and the boundary conditions of the thermal-stress model.

The temperature of the refractory measured before the start of the thermal cycling experiments was specified as an initial condition for the model. The temperatures throughout the refractory block, calculated with the 3-D thermal model, were used as input to the thermal-stress model. The mechanical behaviour of the refractory specimen in the thermal-stress model was based on the 'concrete damaged plasticity (CDP)' model available in ABAQUS for describing , quasi-brittle materials. Details of CDP material property formulation for describing the refractory material used in this work are discussed in the next section.

6.2 Theory of the 'Concrete Damaged Plasticity' (CDP) Formulation

The CDP model was originally developed to describe the effects of alternating stress on concrete, but it can be readily applied for other quasi-brittle materials such as refractories. To

describe the behaviour of the quasi-brittle materials, isotropic damaged plasticity was employed. To predict the irreversible damage associated with cracking, non-associated hardening plasticity and isotropic damaged elasticity were combined. The model also allows the user to describe the elastic modulus recovery during the change of the state of stress and can be defined to be sensitive to the strain rate. Since refractories behave differently in tension and in compression, the stress-strain relationship must be described both in tension and in compression along with the damage. More specifically, the material properties related to the elastic response and damage behaviour need to be specified. The elastic behaviour of the material is defined by specifying the Young's modulus and the Poisson's ratio. In the presence of a tensile force, the model assumes a linear elastic behaviour for the material followed by softening due to damage accumulation. Within ABAQUS, the damage behaviour is defined by specifying the stress, cracking strain, and damage parameter at various points along the stress-strain softening curve in tension, like Point 'X' in Figure 6.2. In Figure 6.2, σ_{t0} indicates the peak tensile stress, ε_t^{ck} and ε_{ot}^{el} represent the cracking strain and the elastic strain of an undamaged material, respectively. E_0 represents the Young's modulus of the undamaged material and E represent the Young's modulus of damaged material that has been loaded to point 'X'. When the material is unloaded to point 'A' and loaded again, it follows the path 'AX'. By calculating the slope of 'AX', the Young's modulus of the damaged material, E is determined. The elastic strain ε_{ot}^{el} of the undamaged material ('BC') is calculated by knowing the stress at point 'X' and the elastic modulus of the undamaged material, E_0. The cracking strain ε_t^{ck} ('OB') is calculated by subtracting the elastic strain ('BC') from the total strain at point 'X' ('OC'). The damage parameter in tension, represented by d_t, is a

fractional change in the elastic modulus of the undamaged material. It is calculated based on the undamaged and damaged Young's moduli as shown in the following figure.

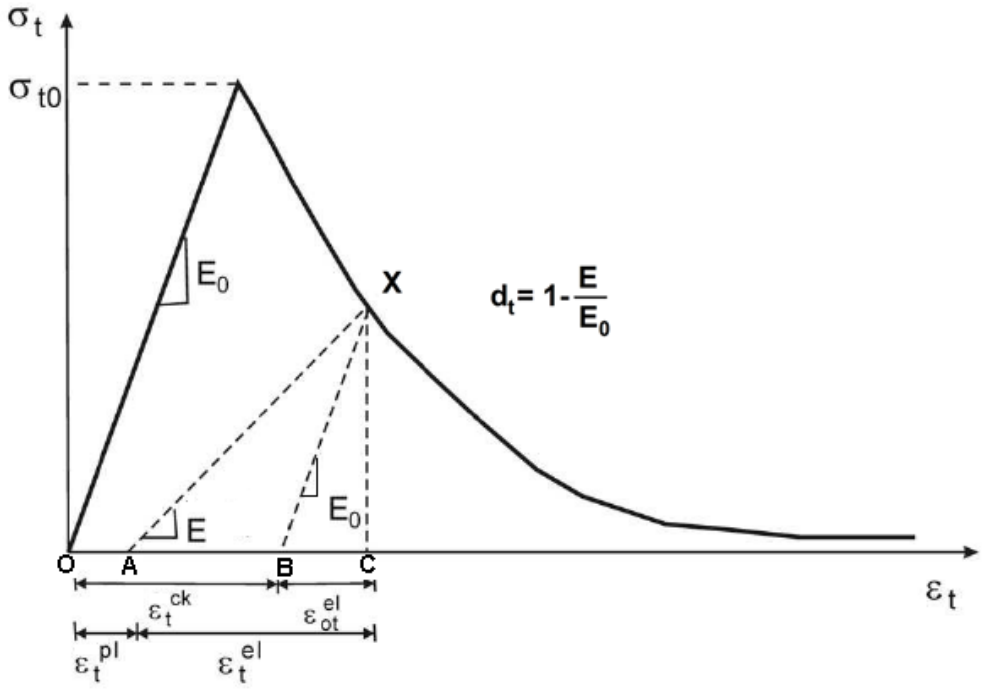

Figure 6.2: Parameters defining the tensile damage behaviour in the concrete damaged plasticity (CDP) model [74].

The thermo-mechanical properties of the refractory material employed in this work have been extracted from the stress-strain curves reported in the literature [75,76] from experimental loading-unloading tests of the same material. The necessary parameters for this material in tension were calculated based on the curves shown in Figure 6.3 at various temperatures.

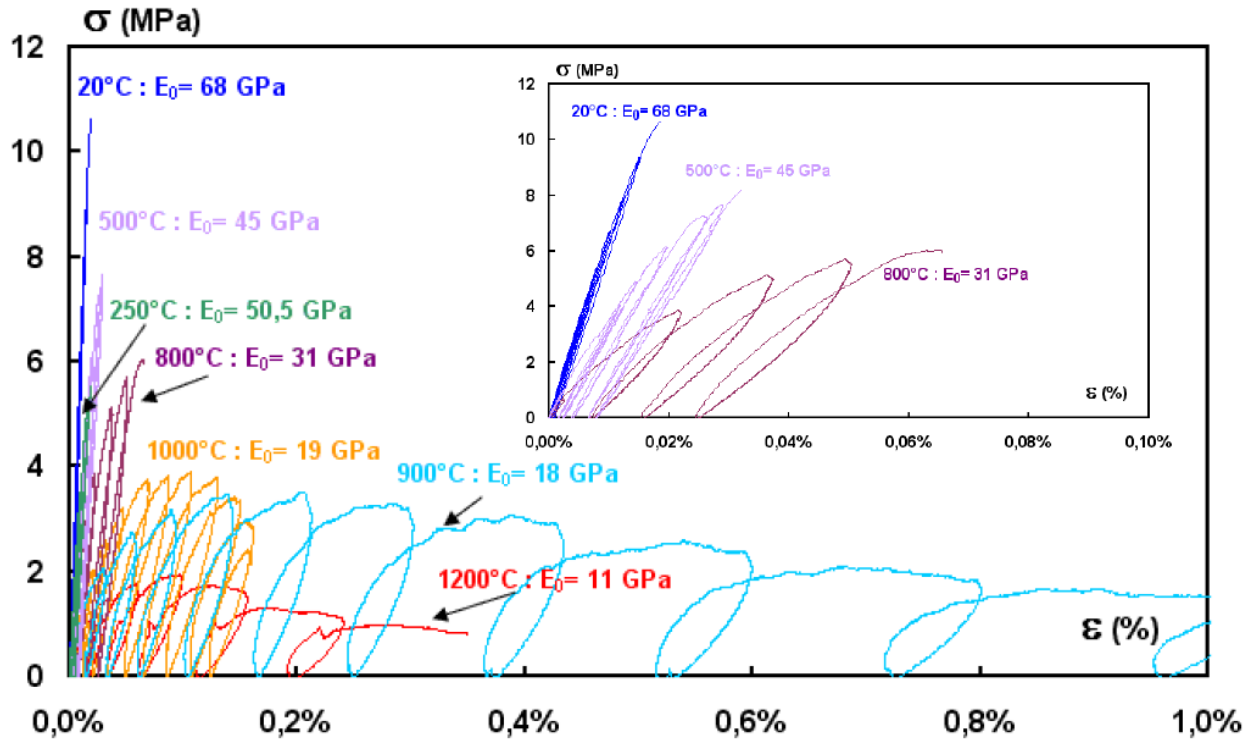

Figure 6.3: Tensile loading-unloading curves of the refractory material used for the current study at various temperatures [75]

It can be seen from the Figure 6.3 that the material exhibits non-linear behaviour with increasing temperature. It can also be seen that the strength (peak stress) and the Young's modulus decrease at elevated temperatures and that the material shows elastic-viscoplastic behaviour above 800°C.

Similar to the tensile loading conditions, the elastic response of the material is defined by the Young's modulus and the Poisson's ratio for compressive loading conditions. In the presence of a compressive force, the material will respond in a linear-elastic manner initially, followed by a behaviour that resembles hardening in ductile materials due to the consolidation of

micro-porosity and finally the damage due to crushing as shown in Figure 6.4. In Figure 6.4, σ_{c0} and σ_{cu} represent the elastic limit and the peak stress in compression, respectively. When the material is unloaded from point 'X', ε_c^{in} and ε_{oc}^{el} represent the inelastic strain and the elastic strain of an undamaged material, respectively, and d_c is the damage parameter in compression.

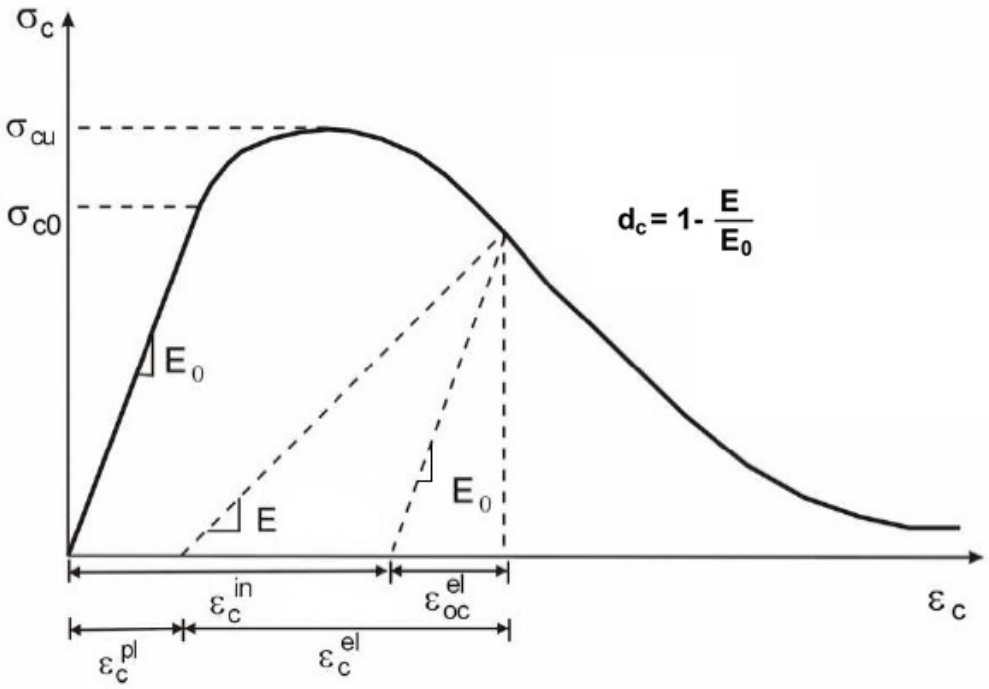

Figure 6.4: Parameters defining the compressive damage behaviour in the concrete damaged plasticity (CDP) model [74]

The necessary parameters were extracted from the experimental loading-unloading curves in compression that are published in the literature [76]. The data is only available for room temperature conditions. Figure 6.5 shows the loading-unloading curve of the two samples tested. Compared to the tensile loading-unloading curves (Figure 6.3) it can be seen that the peak stress in compression (Figure 6.5) is about an order of magnitude more than that of in tension.

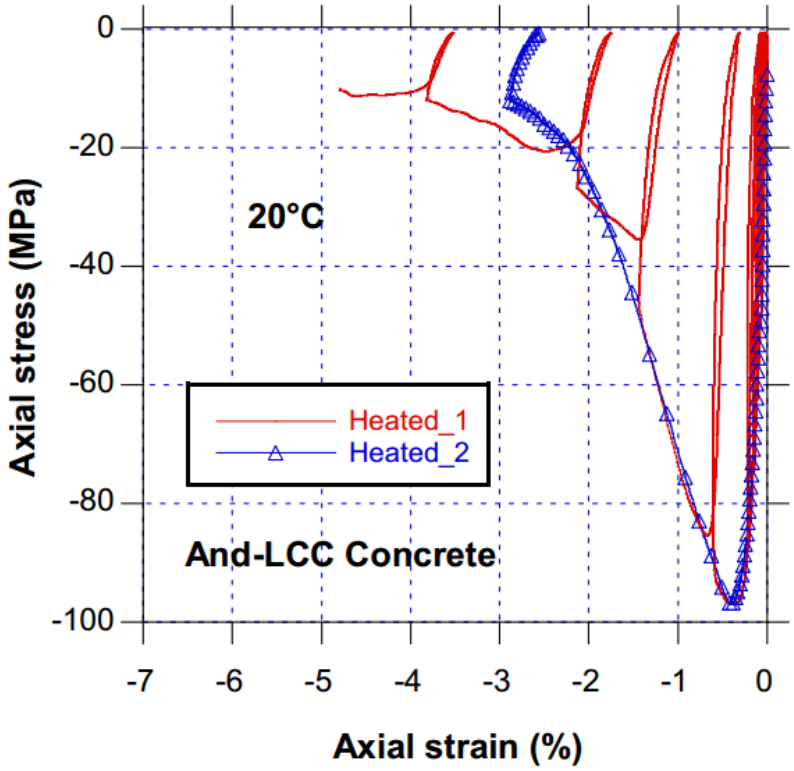

Figure 6.5: Compressive loading-unloading curves of the two samples of the refractory material used for the current study at room temperature [76].

The CDP model implementation in ABAQUS is capable of incorporating the phenomenon of strain hardening in compression. It can also accommodate the variation in material properties due to variation in the strain rates and temperature and considers recovery in the Young's modulus when the state of stress changes from tensile to compression.

The accuracy of a model employing this material description critically depends upon the availability of material testing data that can be used to tune the various material parameters employed in the model. The algorithm used by ABAQUS for the 'concrete damaged plasticity model (CDP)' is not accessible to the user, therefore, a series of simple example problems were

used to verify the material parameter selection and material model implementation prior to applying the model to the simulate the thermal cycling experiments.

6.3 Implementation of the 'Concrete Damaged Plasticity' (CDP) Material Model

In this section, the complexity and capability of the thermal-stress model will be developed gradually using a series of cases. The CDP model was employed to simulate the deformation of a block of concrete material. Initially, the case of a concrete material undergoing uniaxial tensile and compressive loading has been simulated. The boundary condition complexity has then been gradually increased to simulate the case of cantilever bending of the block and finally the case of a material experiencing an alternating state of thermal-stress has been considered.

The main differences between the cases that will be examined are the changes in loading conditions. In each case, the material being considered is damageable and the data related to damage evolution must be specified as an input. In ABAQUS, this refers to discrete points specifying stress, the corresponding cracking or inelastic strain (or the displacement) and the damage parameter. The values of material parameter between the two discrete points, is linearly interpolated during the analysis. The specific details of the material parameters will be discussed in the next sections. Thermo-mechanical properties employed for the thermal-stress model are given in Table 6.1-6.3 based on the Figures 6.3 and Figure 6.5. It should be noted that since, the raw data for the loading-unloading tests represented by Figure 6.3 and Figure 6.5 is not available in the literature; the data was graphically extracted from the figures and was prone to small errors associated with the measurements.

Since, the temperature dependence of damage variation during the compressive loads has not been studied for any refractories, the room temperature data was employed. It should be noted that due to porosity, various phases, and the presence of aggregates, refractories are very inhomogeneous materials. In order to employ these material properties in the CDP model, it has been implicitly assumed that the material is homogeneous and these properties do not vary spatially within the material. It was also assumed that the properties do not change with the thermal history of the material. The thermo-physical property data for the current refractory material is presented in Tables 6.1-6.3.

Table 6.1: Modulus of elasticity values employed in the thermal-stress model [74].

Temperature (°C)	Elastic Modulus (GPa)
15	68.0
250	50.5
500	45.0
800	31.0
900	18.0
1000	19.0

Table 6.2: Compressive damage properties employed in the thermal-stress model [75].

Compressive Stress (MPa)	Inelastic Strain ($\times 10^{-3}$)	Damage
70.0	0	0
86.0	4.94	0.25
26.0	20.31	0.19
13.0	34.98	0.15

Table 6.3: Tensile damage properties employed in the thermal-stress model [74].

Temperature (°C)	Tensile Stress (MPa)	Cracking Strain ($\times 10^{-5}$)	Damage
15	10.3	0	0
500	6.7	0	0
500	8.6	4.6	0.02
800	1.0	0	0
800	5.0	20.2	0.05
800	5.6	22.1	0.03
900	2.0	0	0
900	3.4	264.8	0.08
900	3.0	406.6	0.12
900	2.5	581.5	0.14
900	1.8	794.7	0.19
1000	3.7	0	0
1000	3.8	82.3	0.14

Table 6.4: Thermophysical material properties used in the thermal-stress model

Property	Units	Refractory
Thermal Conductivity, k	W/m/K	1.9 at 573 K 1.8 at 873 K 1.7 at 1273 K [73]
Density, ρ	kg/m^3	2600 [74]
Specific heat, C_p	J/kg/K	980
Co-efficient of Thermal Expansion (CTE)	m/(mK)	4×10^{-4} at room temperature 6×10^{-6} at 1273 K
Poisson's ratio, ν	-	0.19

6.3.1 Uniaxial Tensile and Compressive Deformation

The CDP model was used to simulate the uniaxial tensile and compressive loading of a concrete block. The computational domain and the boundary conditions used for the simulation are shown in Figure 6.6. It can be seen that the displacements in all the three directions, are pinned (u_x, u_y, $u_z = 0$). Velocity of 0.1cm/s in the x-direction was imposed on the free-end of the specimen.

The values of longitudinal stress and longitudinal strain were examined at a node in the geometric center of the block (See X in Figure 6.6).

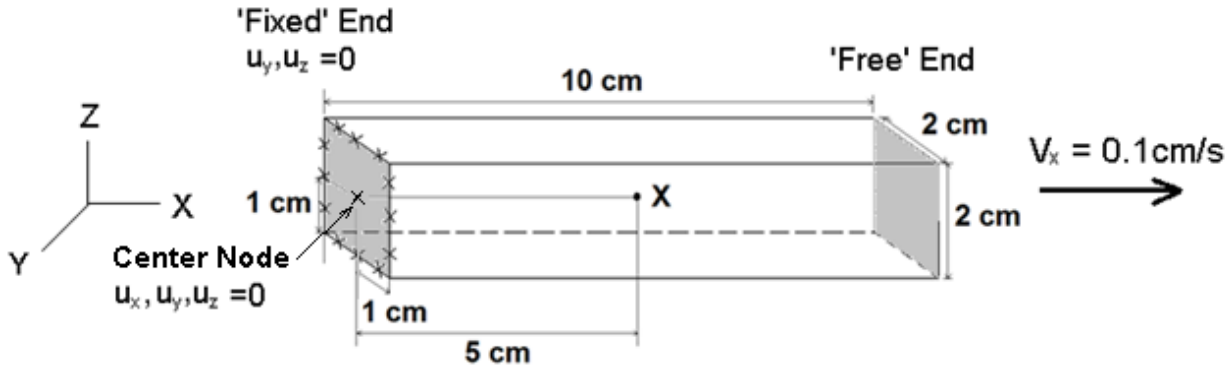

Figure 6.6**:** Schematic representation of the specimen geometry and the corresponding boundary conditions for the uniaxial tension example problem. Point 'X' shows the geometric center of the block where the results were analyzed.

To simplify the problem initially, the strain-damage correlation in tension and in compression was assumed to be linear and material properties consistent with a concrete material [76] were selected. The elastic behaviour was defined by specifying the Young's modulus and

the Poisson's ratio. The inelastic and damage behaviour in tension was defined by specifying the stress, corresponding cracking strain and the damage parameter based on the four discrete points shown in Figure 6.7. The damage parameter used in this model indicates fractional loss in the elastic modulus of the material.

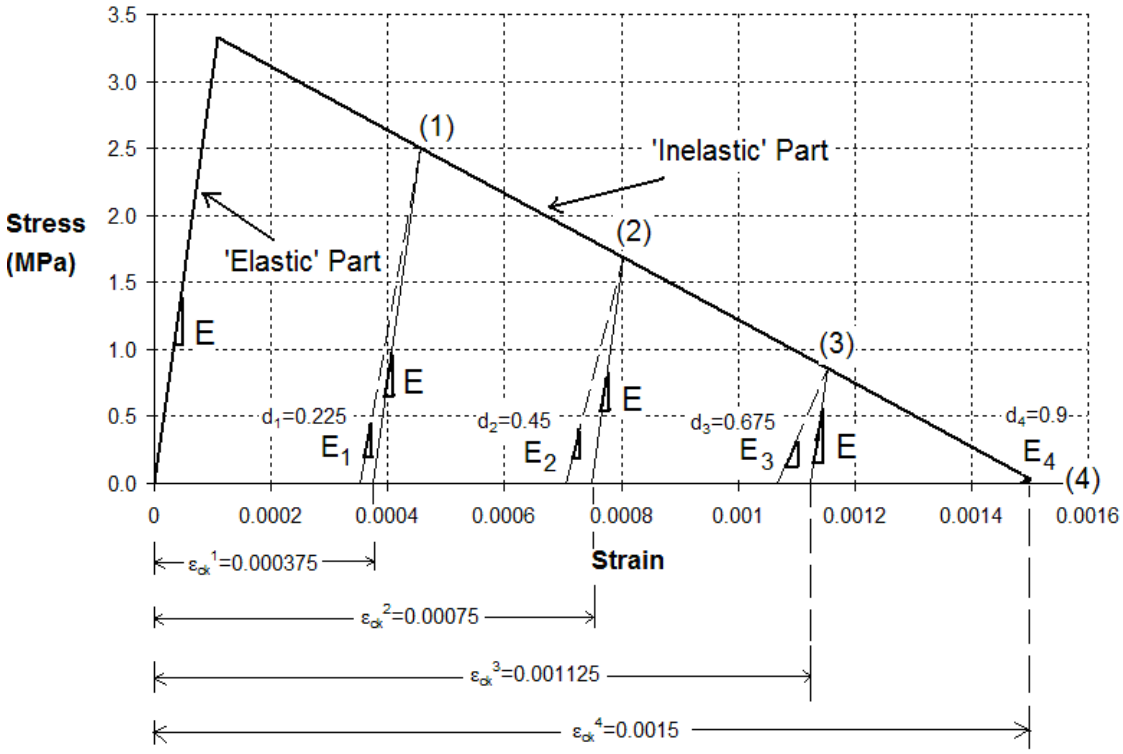

Figure 6.7: Material properties used in the model to simulate the uniaxial tension.

Initially, a boundary condition consistent with uniaxial tensile loading was applied. With the tensile damage behaviour defined, the material should exhibit softening behaviour as damage is accumulated.

To examine the deformation in compression, the direction of the displacement boundary condition was reversed to generate uniaxial compressive loading. The material property data for

compression, which exhibits hardening behaviour, was entered as four discrete points (See Figure 6.8)

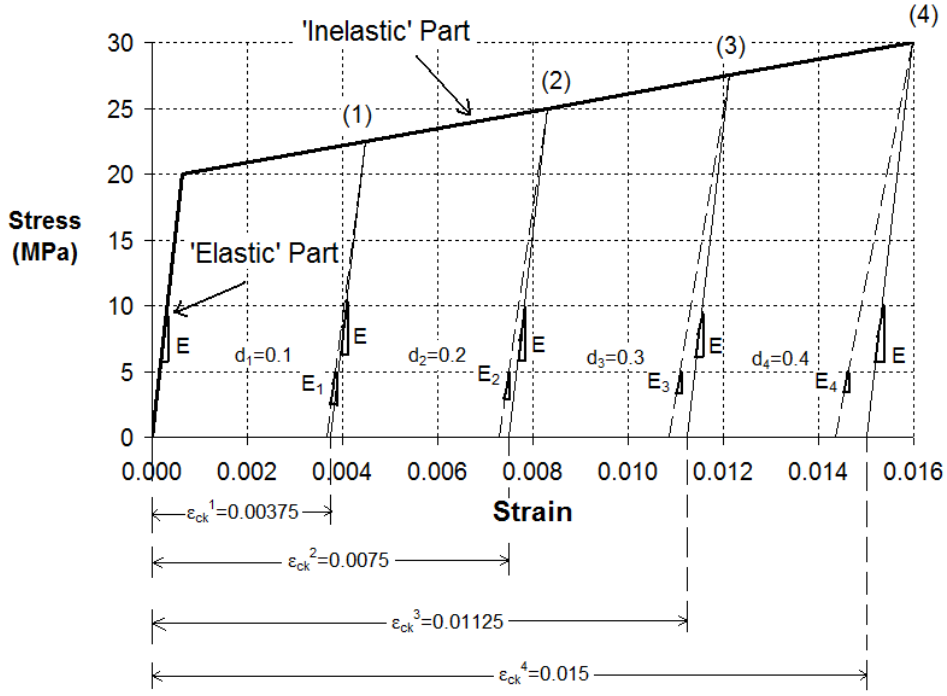

Figure 6.8: Material properties used in the model for the elastic-plastic and damageable material employed to simulate the uniaxial compression.

The predicted variation in the damage parameter with strain was extracted for each loading case and is compared with the calculated variation based on the input data in Figure 6.9. These results show that the model predictions are in a good agreement with the input data. The effects of changing the rate of deformation and magnitude of deformation were considered with the model and the results remain unchanged. This indicates that the model was computationally stable and results were not compromised even at the higher loads.

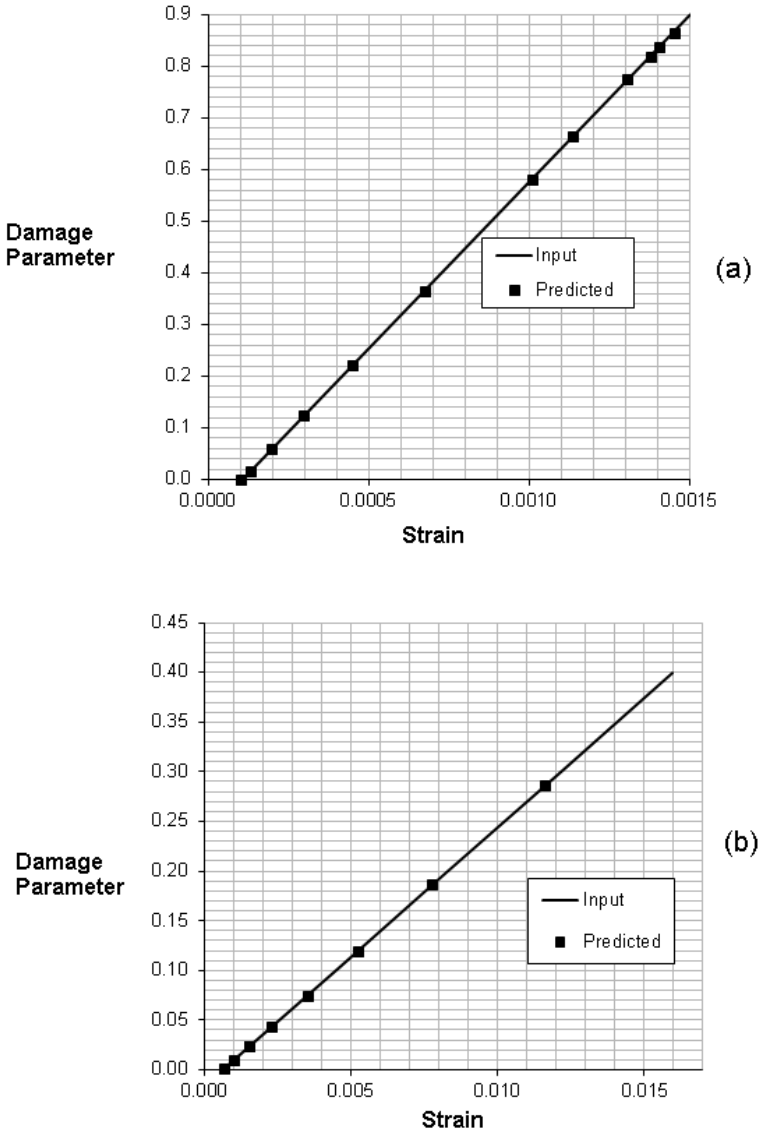

Figure 6.9: Comparison between the input stress-strain data and predictions by the model for the elastic-plastic and damageable material (a) Material behaviour under tension exhibiting softening in inelastic part of the stress-strain curve (b) Material behaviour under compression exhibiting hardening in inelastic part of the stress-strain curve.

It should be noted that the predictions from this model have not been compared against an analytical solution, as one does not exist for this type of material behaviour. This exercise was conducted to build confidence in the material properties implementation in the CDP model.

6.3.2 Cantilever Bending

In this case, a concrete block, subjected to bending, has been simulated in an effort to assess the effect of a more complex stress state than uniaxial tension or compression (discussed in the previous section) on the capability of the CDP model to predict the mechanical response of the material. Same computation domain as shown in Figure 6.6 was employed. The boundary conditions employed in this example are shown in Figure 6.10. The CDP model with the combined tensile and compressive behaviours defined in Section 6.3.1 was employed. Since the load is applied normal to on longitudinal surface near the end of the cantilever, the stresses on that surface are expected to be tensile and the stresses on the opposite surface are expected to be compressive.

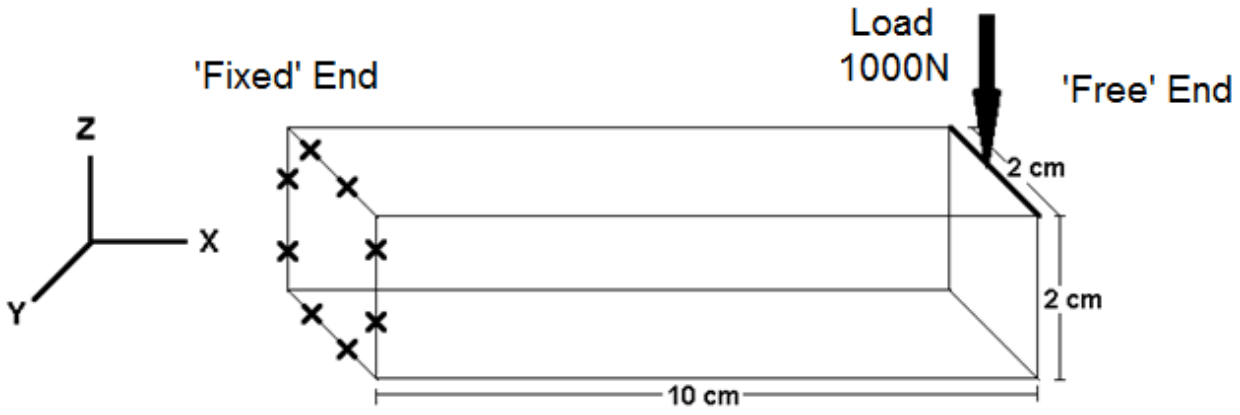

Figure 6.10: Schematic representations of the cantilever deflection and the boundary conditions.

The results of this model were compared with the model that assumes the material to be purely linear-elastic (and non-damageable). The same elastic modulus, 68GPa and Poisson's ratio, 0.16 as the CDP model were used to define the linear-elastic material. The longitudinal

stress for both cases are compared in Figure 6.11, along with the damage prediction from the CDP model. It can be seen from the figure that the stresses predicted by the linear-elastic material model (Figure 6.11 (a)) are higher than those predicted by the CDP model (Figure 6.11(b)). This is due to the fact that when the material is damaged due to cracking, the stresses are relieved. The effects of damage are not captured by simple material models such as the linear-elastic model. The CDP model considers damage due to tensile and compressive stresses hence, the predicted stresses are lower in Figure 6.11(b) than in Figure 6.11(a).

It can also be seen from Figure 6.11(b) that the magnitude of the peak tensile stress (red) is lower than that of the peak compressive stress (blue). Since, refractories are more susceptible to damage in tension than in compression, the red area in the figure must have experienced damage that resulted into lowering the stresses. Figure 6.11(c) shows the damaged prediction. The maximum value of the damage variable is 0.47 indicating a 47% loss in the Young's modulus.

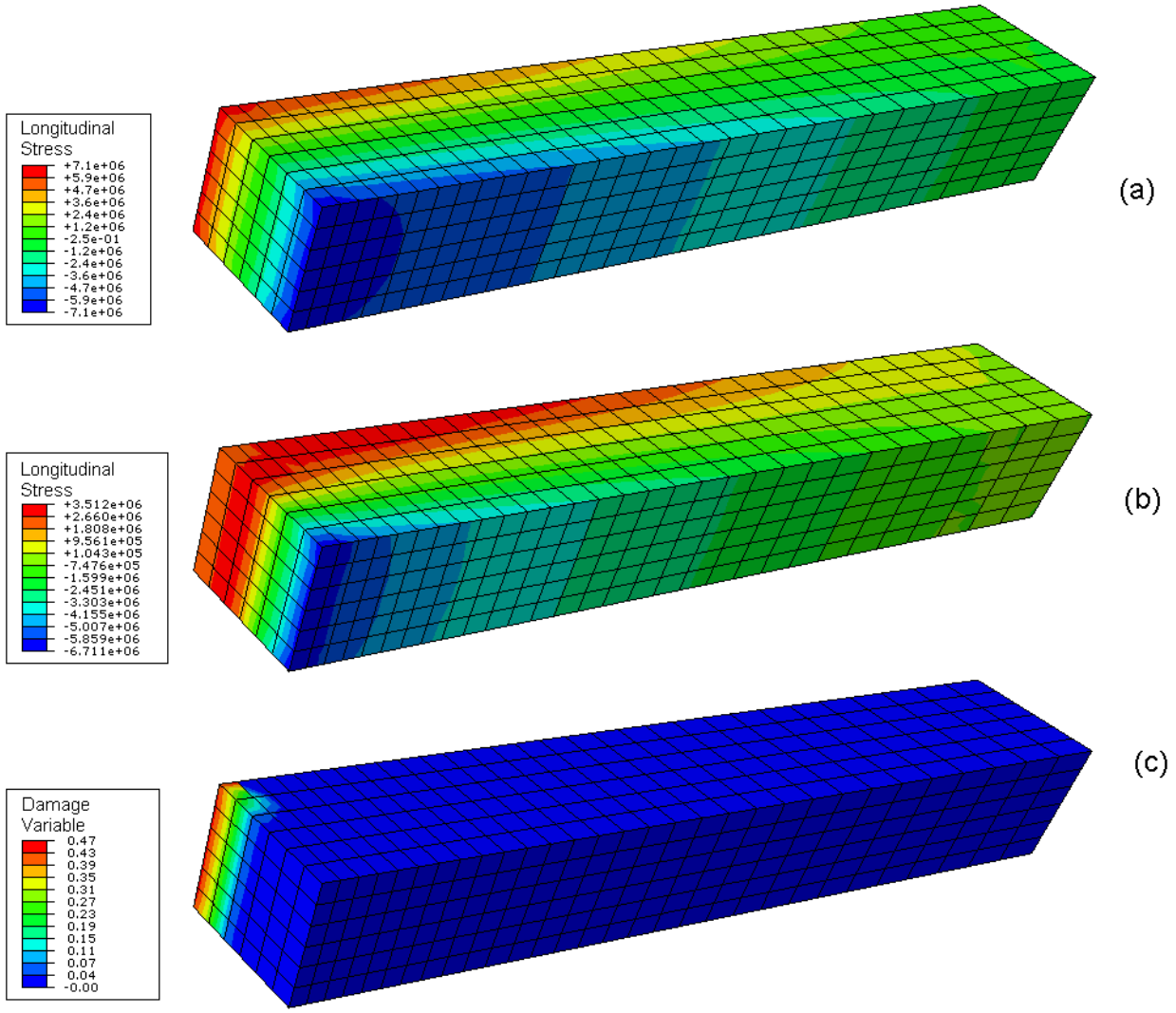

Figure 6.11: Contour plots for the cantilever bending problem (a) longitudinal stress distribution predicted by the linear-elastic material model, and (b) longitudinal stress distribution predicted by the CDP model, and (c) variation of damage variable predicted by the CDP model.

This example shows the difference between predictions by the simple models such as linear-elastic model and the CDP model. It also shows that the CDP model is capable of predicting more complex stress states such as those observed in a cantilever.

6.3.3 Thermal-Stress

As the final step in developing the thermal-stress model for this study, the model has been modified to calculate the stresses generated when a refractory material is subjected to alternating heating and cooling cycles. The thermal gradients resulting from the heating and cooling cycles cause thermal stress in the material. It is important to examine the mechanical response of the material in the presence of thermal gradients to assess the behaviour of the CDP model.

In this case, a model was developed for the situation in which a block of refractory material is subjected to a 1-D heat flow. The predicted temperature data from a thermal-only model was used as input to a thermal-stress model. The boundary conditions and computational domain used in this case are the same as those implemented in the current study (Figure 6.1). Two material models were considered; linear-elastic and CDP model. The thermo-mechanical property data used in the CDP model were based on the refractory material used in the current study (refer to Table 5.2 and Table 6.1). The linear-elastic material model does not consider damage in the material and the material behaviour was defined with a temperature dependent modulus of elasticity (given in Table 6.1) and a Poisson's ratio equal to 0.19. The same input thermal data was used to examine the thermal-stress response with linear-elastic and CDP material behaviour.

The heat transfer conditions employed in this case assumed a flux of 150kW/m^2 was applied to one end of the specimen for 100s. The temperature distribution and stress in the longitudinal direction after 100s for both the CDP and the linear-elastic models are shown in

Figure 6.12. The temperature plot (Figure 6.12(b)) shows that the heat has penetrated only up to ~1/4 of the length specimen however, the associated thermal stress is experienced further into the specimen (Figure 6.12 (c-d)). The stresses experienced by material vary depending upon the choice of the material behaviour. In the case of linear-elastic material (Figure 6.12(c)) the stress accumulates in the absence of any damage. As mentioned in Chap. 2, refractories do not behave in a linear-elastic manner especially, at elevated temperatures. They undergo damage in the form of cracking and as a result, the stresses are reduced. The CDP model accounts for this behaviour, hence the magnitude of stress observed in the case of CDP model (Figure 6.12(d)) is lower than in the case of linear-elastic model (Figure 6.12(c)).

By observing the magnitude of the stresses in Figure 6.12(c), it is apparent that, in the absence of any damage mechanism, stresses are well above the strength of the refractory material (See Figure 6.3 and Figure 6.5). This indicates that damage due to the mechanical fatigue which results from an alternating stress that is well below the strength of the material must be negligible. Due to this reason, fatigue was not considered as a failure mechanism in the current model.

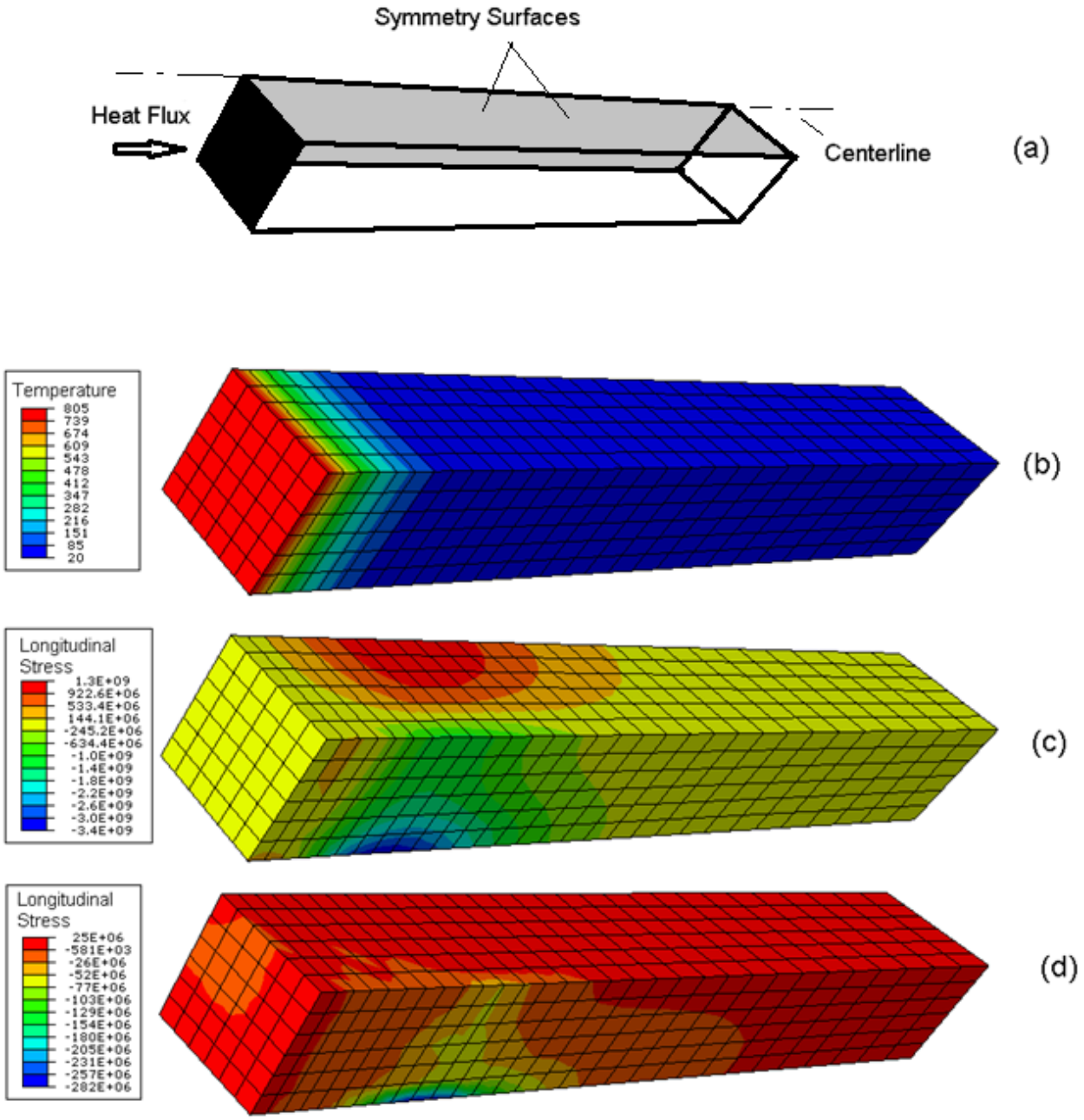

Figure 6.12: (a) Schematic of the computation domain, and (b) the temperature distribution, (c) longitudinal stress distribution predicted by the linear-elastic material model, and (d) longitudinal stress distribution predicted by the CDP model.

The damage predicted by the CDP model at the end of 100s is shown in Figure 6.13. The damage has accumulated in areas that experienced both compressive and tensile stresses. The

maximum value of the damage variable is about 0.37, indicating 37% reduction in the stiffness value due to cracking.

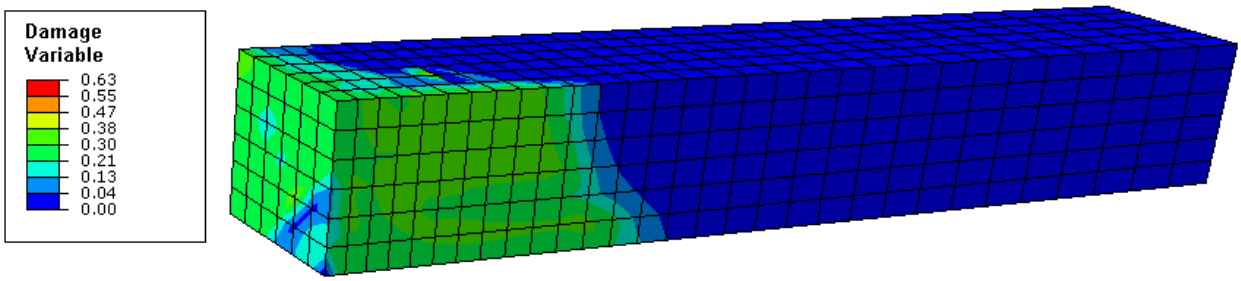

Figure 6.13: Damage distribution predicted by the CDP model.

As mentioned in the literature review, a state of alternating compressive and tensile stresses is introduced in the material in the transverse direction during heating and cooling stages of the cycle. However, when the material is damageable with temperature dependent Young's modulus, the state of stress is complex. To illustrate this, the transverse stress distribution at the centerline of the refractory specimen has been plotted for the linear-elastic and CDP models at various times during heating.

Figure 6.14 shows that the stress distribution for the linear-elastic model at 50s and at 300s is in a state of compression at the surface changing to tension in the interior of the sample. The CDP model predicts that with damage, the magnitude of stress is smaller than that of the linear-elastic model. It shows that the surface is in compression at 50s, however, at 300s, the surface stress has become tensile. This is due to the fact that as the surface temperature increases significantly, the elastic modulus of the material at the surface decreases whereas the subsurface material that is at lower temperatures has higher moduli. As the "sub-surface" material tries to expand, the rest of the material resists the expansion causing the surface material to change the

state of stress from compressive to tensile. In the absence of temperature-dependency of the Young's modulus (i.e. the case of linear-elastic material considered in this particular example), the resultant stress on the surface (due to expansion of the "sub-surface" material) is relatively small. Hence, the surface stress is compressive in nature.

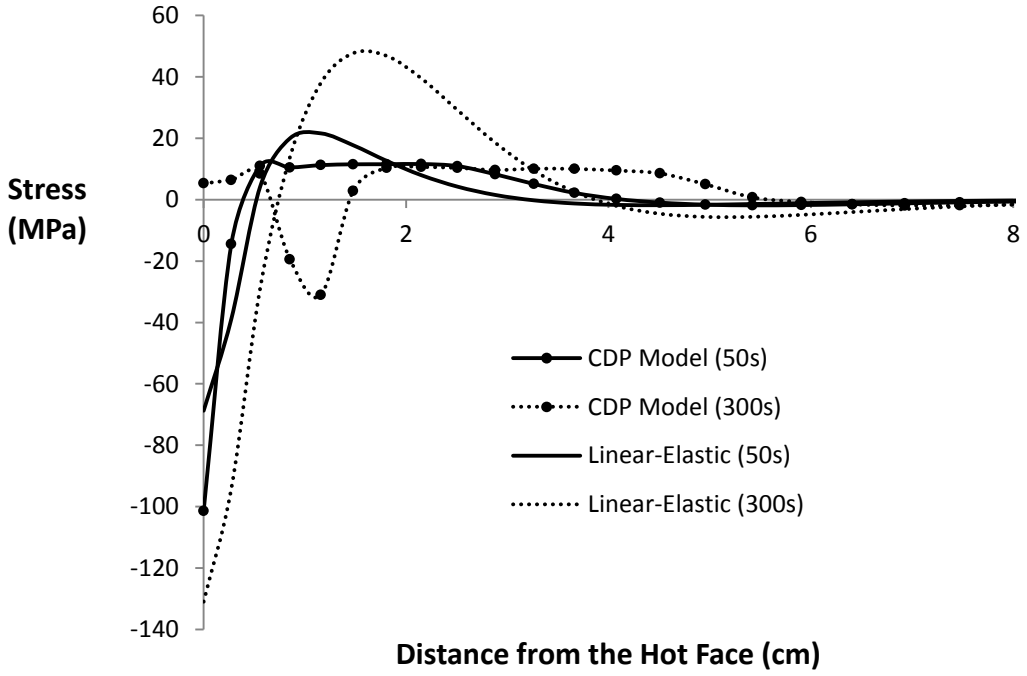

Figure 6.14: Transverse stress distribution along the centerline of refractory specimen for the linear-elastic and CDP models at various times.

The cases presented in this chapter indicate that the CDP model is capable of reproducing the stress-strain response and the accumulation of damage for refractory materials for both simple or more complex stress states. Although, the models could not be validated against any analytical solutions, this exercise proves that the model implementation for refractory blocks experiencing mechanical and thermo-mechanical loading is reliable. This model can now be used

to analyze the complex states of stress and evolution of damage that develops in the thermal cycling experiments.

7. Thermal Cycling Modeling and Experimental Results

Two types of thermal cycling experiments were conducted. In the first type of experiment (referred to as a "cold-refractory" experiment), refractory specimens, initially at room temperature, were subjected to thermal cycling by alternating contact with steel blocks heated to 1000°C and room temperature. In the second type (referred to as a "hot-refractory" experiment), refractory specimens were heated to ~1000°C before thermal cycling with cold and hot steel blocks. In this chapter, the results from both types of experiments are discussed.

7.1 Material Preparation and Instrumentation Set-up

Prior to testing, each refractory sample was dried in a furnace held at 110°C for a period of 24 hrs. A hole was drilled into the refractory specimen at the mid length and 1 cm from one of the ends along the centerline of the specimen to insert the thermocouple. The surface which would be in contact with the steel block was polished with SiC abrasive of grit size 1200 to reduce the roughness and enhance the contact heat conduction. The refractory specimen was then characterized using the ultrasonic testing method described in section 4.2.2.

After the ultrasonic tests, Inconel sheathed, K-type thermocouple (OMEGA, INC-K-MO-062) was inserted into the refractory specimen. The location of the thermocouple mounted in each specimen is shown in Figure 7.1

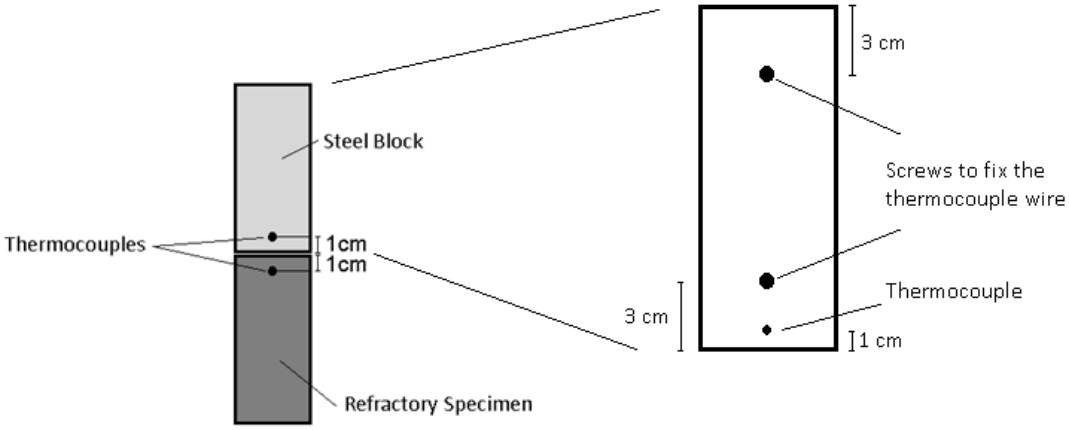

Figure 7.1: Thermocouple locations on steel block and refractory specimen.

As seen from Figure 7.1, every steel block was also instrumented with a thermocouple. A K-type thermocouple was spot welded at the base of a 3 cm hole on the centerline located at 1cm from the steel-refractory interface as shown in the figure. To spot weld the thermocouple, the thermocouple sheathing was removed to expose approximately 4 cm of thermocouple wire. The thermocouple wires were passed through a ceramic insulating sheath and then were spot-welded to the bottom of the hole. To ensure that movement of the block on and off the refractory sample does not dislodge the thermocouple during the experiments, the thermocouple wire was held in place on the steel block with the help of screws (locations shown in Figure 7.1).

Prior to testing, the hot steel blocks were soaked in a resistance furnace with a target temperature of 1000°C. Three sets of experiments distinguished by the number of heating-cooling cycles (i.e. 1, 2 or 3) were conducted with different refractory blocks. The surfaces of the steel blocks were polished after each experiment to remove any surface oxidation.

It should be noted that more than one attempt was required to successfully perform each experiment due to unexpected experimental issues. The issues that occurred were:

1) Occasionally, the spot-weld connecting the thermocouples to the steel block would fail while in the furnace or during the transfer operation from the furnace to the specimen (or vice versa). The thermocouple wires were spot-welded at the base of 3-cm hole and attempts to improve the reliability of this weld were unsuccessful.
2) As mentioned previously, thermocouple wires were fixed by the screws on the steel block. Due to high temperatures, these screws, as well as the threads in the holes where screws fit in, oxidized during the experiments and the screws had to be replaced after each experiment. The threads were sharpened after every 3-4 heating cycles. In addition, the thermocouple wires were compressed under the screws, which occasionally led to failure during the handling of the hot steel block.

7.2 Experimental Results

7.2.1 Cold-Refractory Experiments

Experimentation commenced with a single heating-cooling cycle starting with a room temperature refractory specimen. The steel block was soaked for a minimum of 20min in the furnace heated to 1000°C. Once the centerline thermocouples reached a steady-state temperature, the steel block was taken out and placed on top of the refractory specimen. During the time required to remove the steel block and transfer it to the testing apparatus, the temperature of the block decreased (~40°C based on the thermocouple measurement) due to the heat loss to the

surrounding environment. After 5min of contact with the refractory specimen, the hot steel block was removed and replaced with a room temperature steel block. The refractory specimen was then cooled for 5 min. After 5 min of contact cooling, the steel block was removed and the specimen was allowed to cool to room temperature in air.

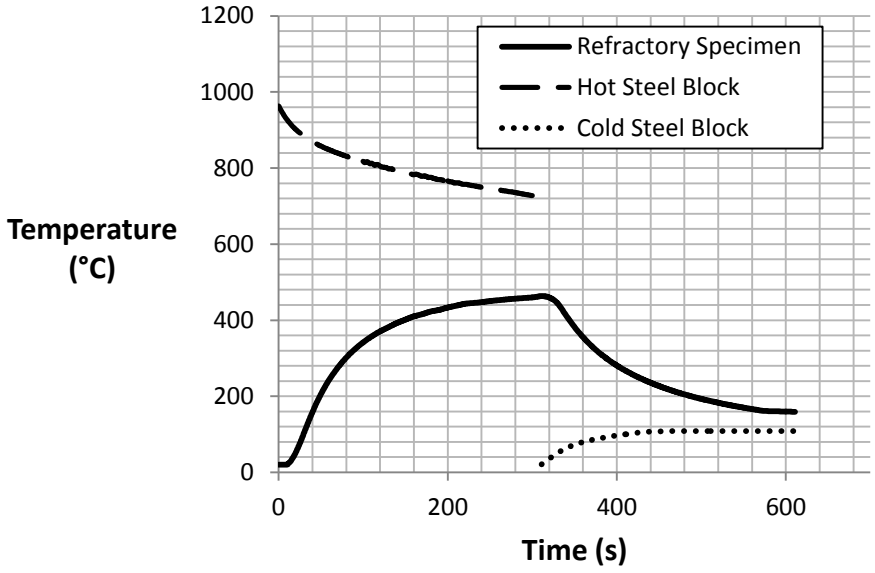

Figure 7.2: Measured temperatures in the hot and cold steel blocks and refractory specimen during a single heating and cooling cycle during a cold-refractory experiment.

The temperature history measured in the refractory specimen and in the hot and cold steel blocks during one heating-cooling cycle are shown in Figure 7.2. During the heating portion of the cycle, the temperature of the refractory specimen increased from ~20°C to ~460°C in 300s. The idle time between the heating and cooling stage was ~11s. During contact cooling, the temperature of the refractory specimen decreased to ~160°C. The temperature of the hot steel block decreased by ~240°C whereas the temperature of the cold steel block increased by only

~90°C indicating higher interfacial heat flux during refractory heating than during refractory cooling.

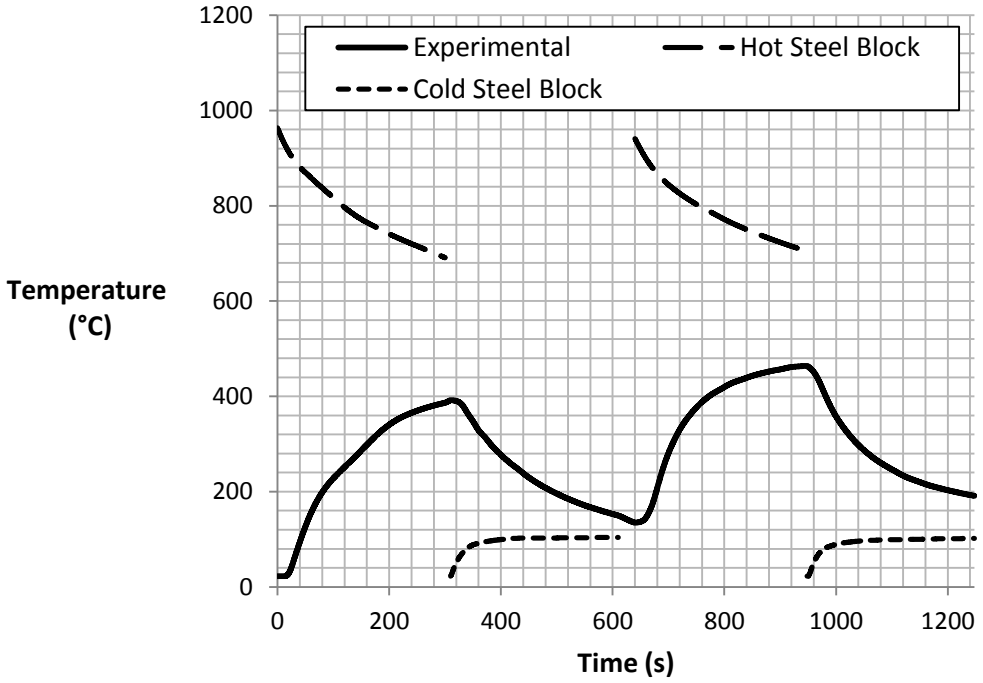

Figure 7.3: Measured temperature history in the hot and cold steel blocks and the refractory specimen during two cycles of heating and cooling during a cold-refractory experiment.

The temperature variation during the 2-cycle cold-refractory experiment is shown in Figure 7.3. The refractory temperature profile shows that after 2 heating and cooling cycles the overall refractory temperature has increased. The temperature at the end of the second heating cycle is ~65°C higher than the temperature at the end of the first heating cycle. It can also be seen that there is a time delay between the end of first cooling cycle and the start of second heating cycle. This is due to the time taken to replace the cold steel block with the hot one. It is

also noted that the temperature change in the steel block during the first refractory-heating cycle is higher in this experiment than in the 1-cycle cold-refractory experiment (see Figure 7.2). In addition, the temperature increase in refractory is lower than in 1-cycle experiment. This indicates that the heat transfer during this experiment was not as efficient as during 1-cycle experiment.

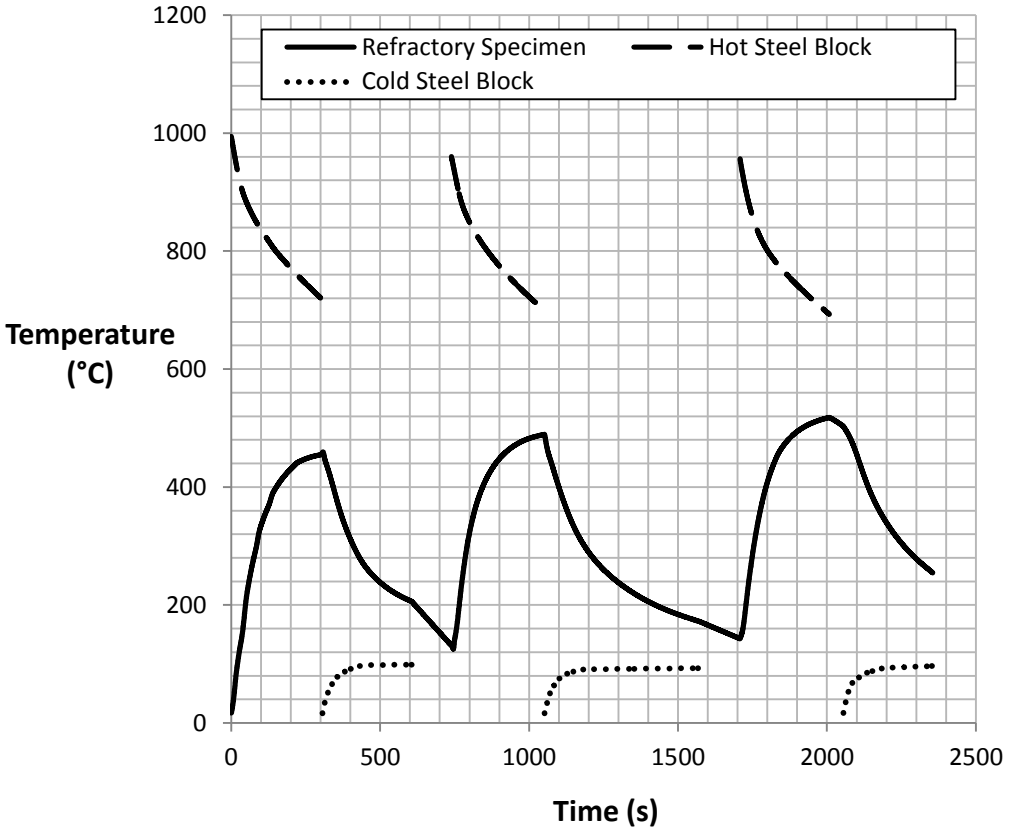

Figure 7.4: Measured temperature history in the hot and cold steel blocks and the refractory specimen during three cycles of heating and cooling during a cold-refractory experiment.

The temperature changes for a 3-cycle cold-refractory experiment, shown in Figure 7.4, exhibits similar trends to that of the 1 and 2-cycle experiments where the temperature of refractory at the end of heating cycle increases with each cycle. It should be noted that due to an

experimental error the second cooling cycle was extended to 520s resulting in extended cooling of the refractory. Additionally, due to the significant delay in changing the cold steel block with the hot one after 2nd cooling event, there is a significant temperature loss from the refractory.

7.2.2 Hot-Refractory Experiments

Hot refractory experiments were carried out with refractory specimens that were heated to ~1000°C prior to thermal cycling. Initially, a hot refractory specimen was cooled with a steel block starting at room temperature and then heated with a hot steel block at ~1000°C. Three experiments were carried out with 1, 2, and 3 cooling-heating cycles.

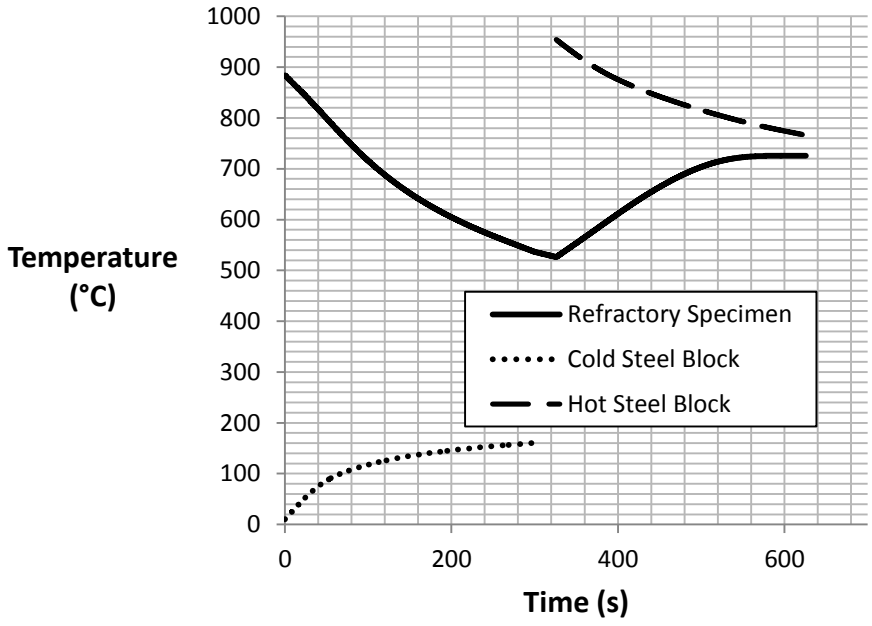

Figure 7.5: Measured temperature history in the cold and hot steel blocks and the refractory specimen during a single cooling and heating cycle during a hot-refractory experiment.

The temperature variation in the cold and hot steel blocks and the refractory specimen for a 1-cycle hot refractory experiment are shown in Figure 7.5. During the cooling stage, the

refractory temperature decreases ~350°C and the cold steel block is heated by ~150°C. During the heating stage, the refractory is heated by ~200°C and the steel block cools by ~190°C. This experiment indicates that the cooling stage is more effective in achieving significant thermal cycling than the heating stage.

The results for 2-cycle and 3-cycle experiments are shown in Figure 7.6. It can be seen (from Figure 7.6(a)) that during the second cooling stage of the 2-cycle experiment, there was a small perturbation in the temperature. This is attributed to a small adjustment of the steel block needed during the experiment.

It can also be seen from Figure 7.6 that the first cooling stage is the most severe, showing the largest change in temperature among all subsequent stages. Therefore, high thermal stresses are expected during the first cooling event. It is also observed that with increasing number of cycles the refractory temperature drops, this trend is opposite to the temperature changes in the cold-refractory experiments where the refractory temperature is increasing. The temperature change from start-to-finish of the experiment is about 575°C for the 3-cycle hot refractory experiment whereas it is about 500°C for the 3-cycle cold-refractory experiment. Due to the increased temperature difference, higher thermal stresses are expected in the 3-cycle hot-refractory experiments. In addition, refractories have a higher susceptibility to accumulate damage at elevated temperatures suggesting that the overall damage should be higher in the case of hot-refractory experiments.

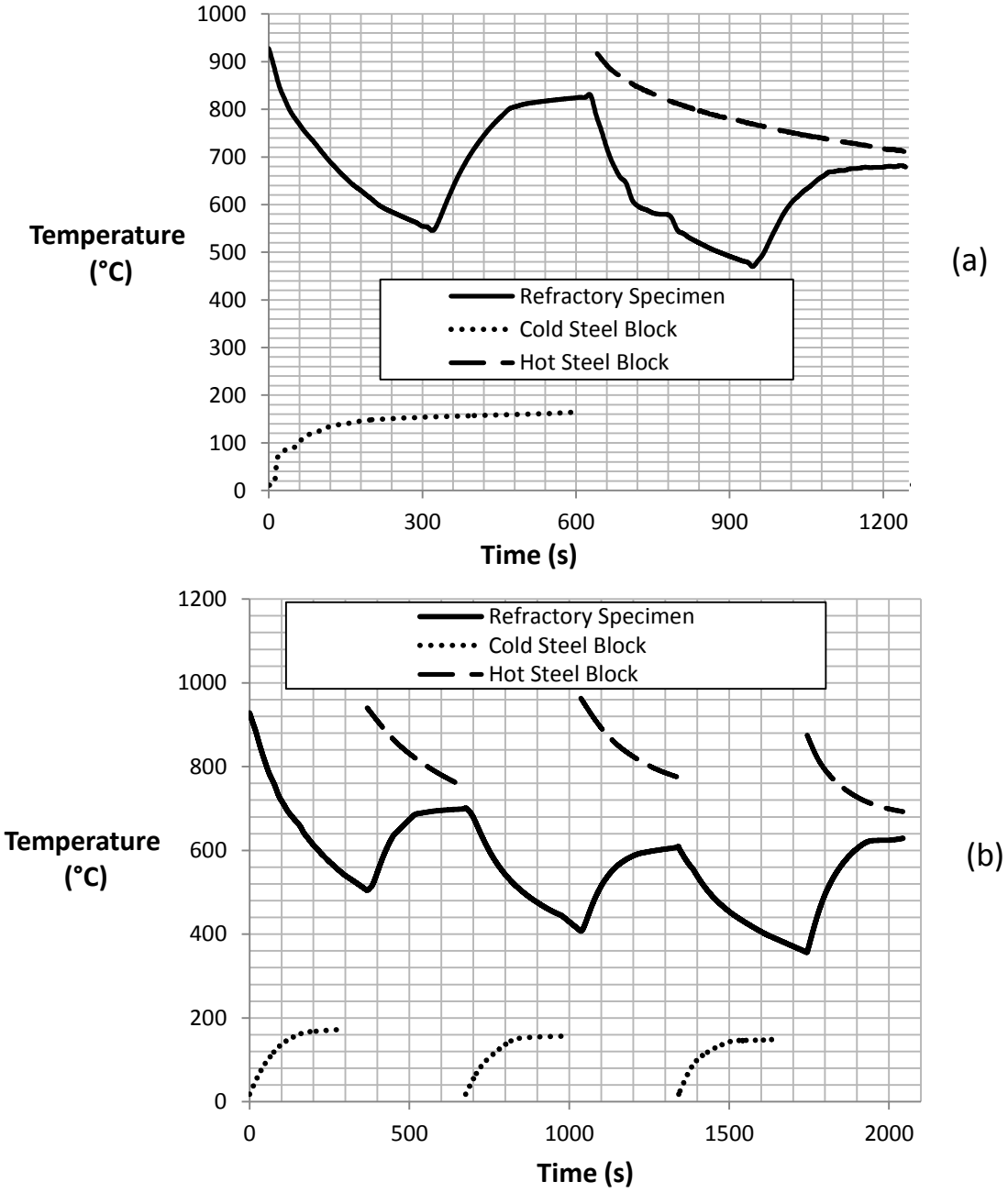

Figure 7.6: Measured temperature history in the cold and hot steel blocks and the refractory specimen during a) 2-cycle and b) 3-cycle hot-refractory experiments.

The experimental results discussed in this section are consistent with expectations. The temperature variations during the 1-cycle experiments are similar to the variation in the first cycle for the 2- and 3-cycle experiments during both the hot- and cold-refractory experiments. The results also show that the experimental set-up was capable of inducing significant thermal cycling in the refractory specimen. The thermal modeling results are discussed in the next section.

7.3 Thermal Modeling Results

The IHC model was run using the temperature data from the steel blocks. The techniques required to complete this analysis and the results are discussed in this section.

7.3.1 Cold-Refractory Experiments

The temperature variation in the hot steel block during the heating stage of the single cycle cold refractory experiment are shown in Figure 7.7. The heat fluxes predicted by the IHC analysis of the raw thermal data (refer to Figure 7.7) are shown in Figure 7.8. The calculated heat fluxes exhibit significant instability, ranging from high positive to low negative values (350 to -50 kW/m^2), starting at ~90s. The instability coincides with low-level noise observed in the thermal data.

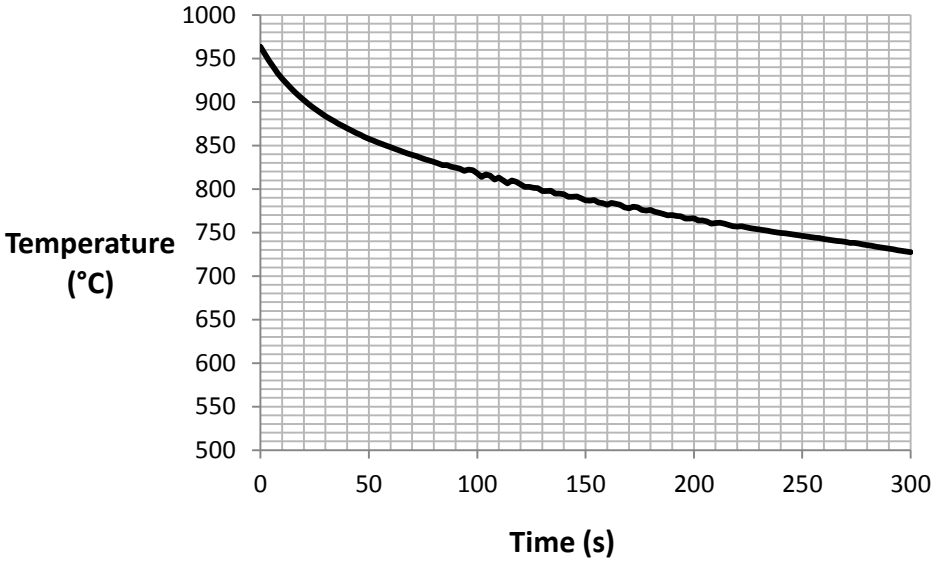

Figure 7.7: Measured temperatures in the steel block during refractory heating for the single cycle cold-refractory experiment.

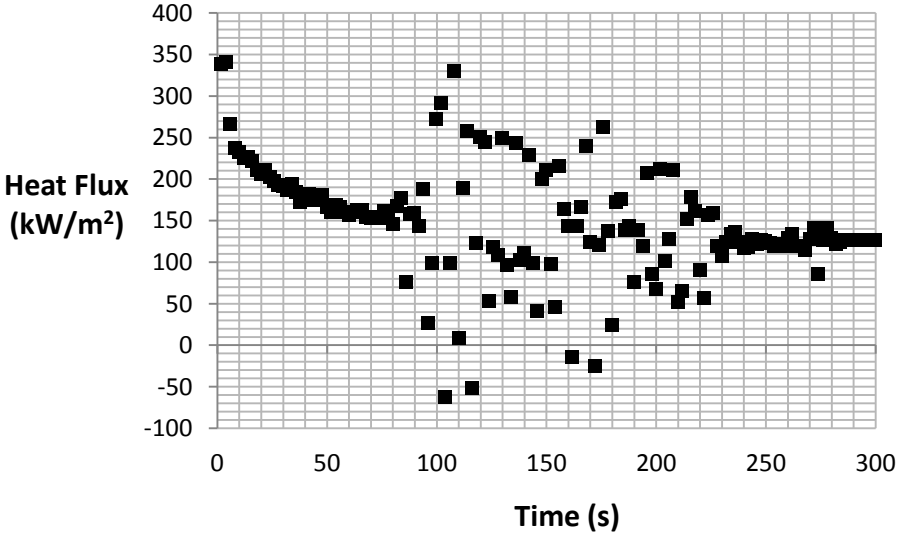

Figure 7.8: Heat fluxes calculated using IHC analysis with the raw input steel block temperature data for the refractory heating stage of the single cycle cold-refractory experiment.

To reduce the noise in the input temperature data, a spline function was used in MATLAB to smooth the data. The smoothed temperature data is compared with the raw measured data in Figure 7.9 over the range of 90s-200s where the noise is significant. The smoothing process has reduced the short-range noise in the data but has not altered long-range temperature variation.

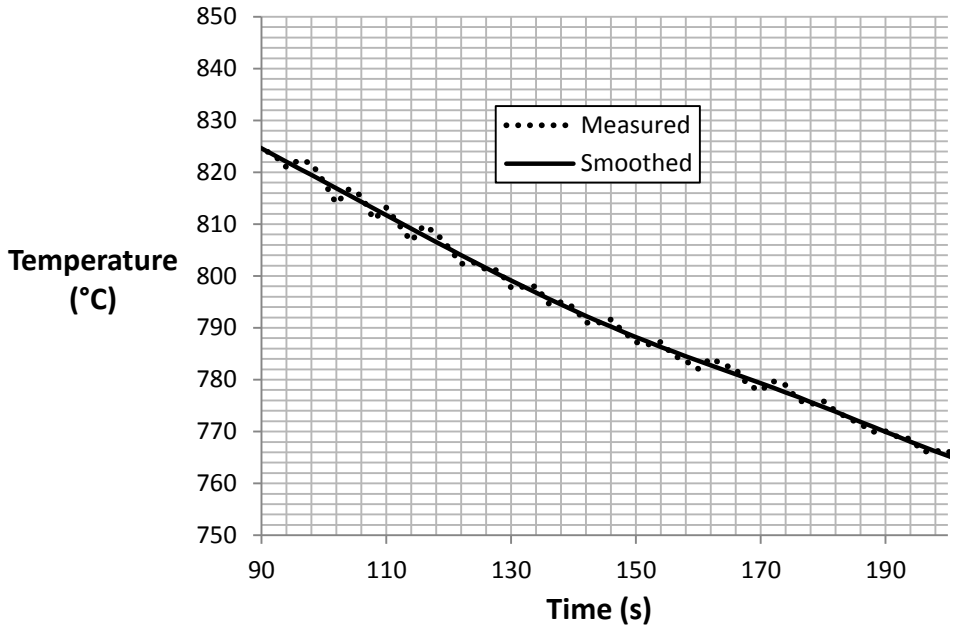

Figure 7.9: Comparison of the smoothed and raw measured temperature data of the steel block for the heating stage of a single cycle cold-refractory experiment.

The smoothed temperature data was then used to calculate the heat flux values. As seen from Figure 7.10, there is a significant reduction in the noise in the calculated heat flux values. Compared to Figure 7.8, Figure 7.10 shows that noise prevalent in the 90–200s has been eliminated. It can be seen that the heat flux values at the start of the heating process are higher than that at the end. The maximum heat flux value observed is about 250kW/m^2 which reduces

to about 120kW/m^2. This observation is consistent with expectations where the maximum heat flux should occur when there is the largest temperature difference between the steel and the refractory (i.e. upon initial contact).

Based on the improvements observed in the calculated heat fluxes, the smoothing procedure was applied to the measured steel block temperature data set from the heating and cooling stages of each experiment.

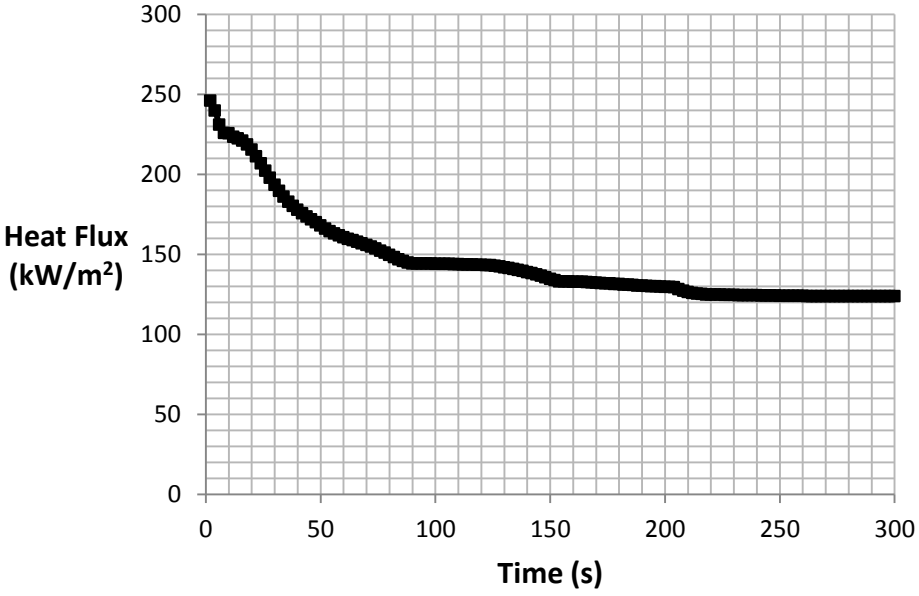

Figure 7.10: Heat fluxes calculated by IHC analysis using smoothed input steel block temperature data for the refractory heating stage of the 1-cycle cold-refractory experiment.

The calculated heat fluxes during refractory-heating based on the smoothed steel block temperature data were then employed in a 3-D forward heat transfer analysis (discussed previously in section 5.2) to predict the temperature of the refractory specimen at 1 cm from the

steel-refractory interface. The predicted temperature history in the refractory specimen was then compared with the measured refractory specimen temperature at the same location. The results for the heating stage of the single cycle cold-refractory experiment, shown in Figure 7.11, indicate a substantial difference between the predicted and measured behaviour, especially after 150s.

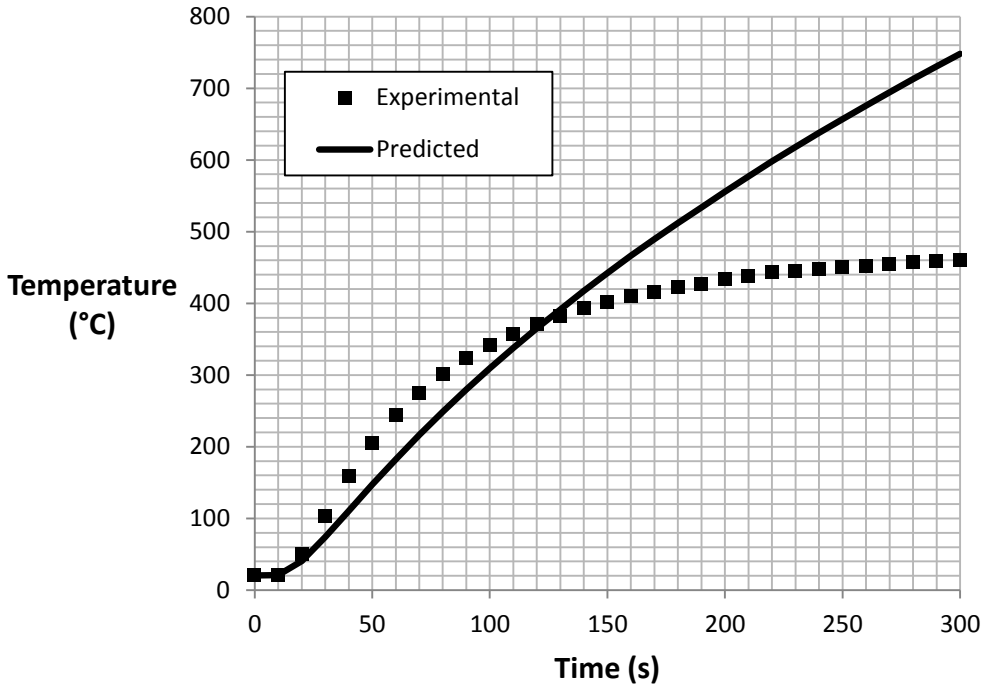

Figure 7.11: Comparison of the measured and predicted temperature profiles in the refractory specimen during the refractory heating stage of the 1-cycle cold-refractory experiment.

The differences between the measured and predicted temperatures may be due to one or both of the following two factors:

1) The experiment is designed to ensure that the heat flow in the steel block as well as the refractory specimen is 1-D by minimizing the heat loss from them to the surrounding. However, the heat loss from the steel block to the surrounding could be significant because of its higher conductivity compared to the refractory. Since this heat loss is not accounted for in the inverse analysis, the resultant heat flux values could be different from the actual ones.
2) The heat loss through the sides of the refractory specimen could be significant causing deviation from the 1-D heat flow. In that case, the measured temperature would be lower than the expected assuming a purely 1-D heat flow.

To check whether the heat flow in the refractory specimen is 1-D or not, an experiment was carried out by inserting two thermocouples in a new refractory specimen. Thermocouples were placed 1 cm from the end on the centerline and 2.5 cm from the centerline of the specimen, as shown in Figure 7.12. The temperatures measured at both locations during a single cycle cold-refractory experiment are plotted in Figure 7.13. The temperature difference between the two locations is less than 10°C during the test. This suggests that the heat loss from the refractory specimen to the surrounding is not significant and the heat flow in refractory specimen is 1-D.

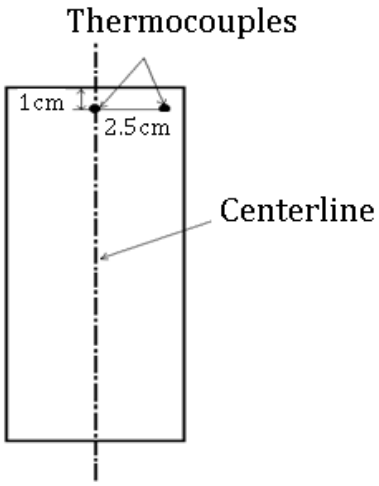

Figure 7.12: Locations of thermocouples inserted into a refractory specimen to check the heat loss to the surrounding. The thermocouples are 3cm deep into the specimen.

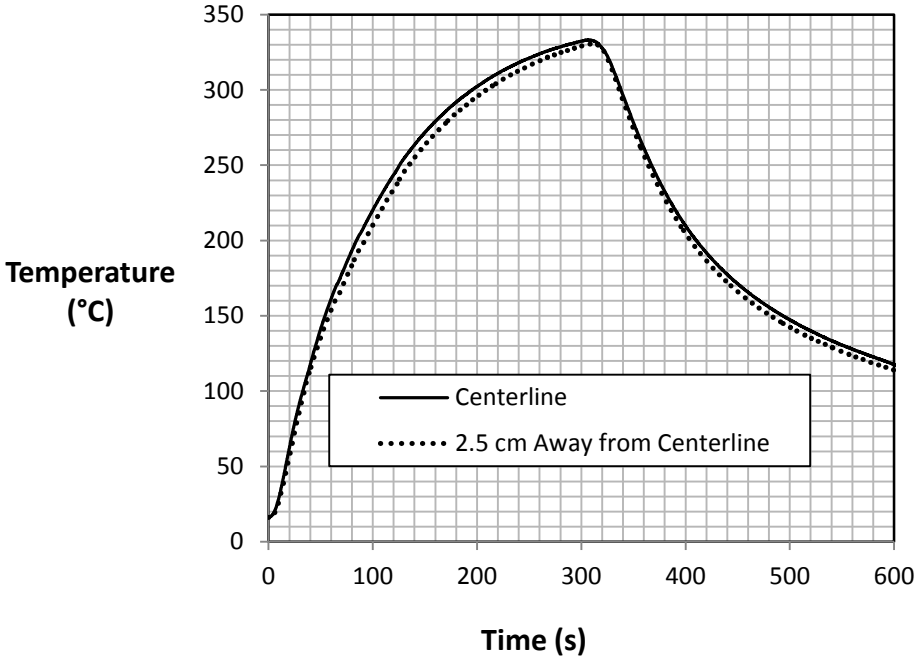

Figure 7.13: Temperature profiles at two different locations on refractory specimen for 1-cycle cold-refractory experiment.

Based on this result, it was deduced that there must be significant heat loss from the steel block to the surrounding environment. The output of the IHC model (i.e. the heat flux calculated from the temperature data gathered at 1 cm from the steel-refractory interface) is based on the assumption that 1-D heat flow conditions were achieved in the steel block. If heat flow conditions are not 1-D, the heat flux, and corresponding temperature change 1 cm from the interface, would be different than that expected with the 1-D heat flow. In this case, the heat flux experienced by the steel block during the experiment (q_{exp}) consists of two components: 1) heat flux due to the heat loss to the surrounding (q_{loss}) from all the surfaces of the steel block except the one in contact with the refractory specimen and 2) heat flux to the refractory specimen ($q_{refract}$). i.e.

$$q_{exp} = q_{loss} + q_{refract} \tag{7.1}$$

Assuming these fluxes result in differences in temperature at the thermocouple location and cool from an initial temperature, an equation describing the different contributions is:

$$\left(T_{init} - T_{exp}\right) = \left(T_{init} - T_{loss}\right) + \left(T_{init} - T_{refract}\right) \tag{7.2}$$

where T_{init} is the initial temperature of the steel block and T_{exp} is the experimentally measured temperature of the steel block during the experiment. T_{init} and T_{exp} are known temperatures measured by the thermocouple in the steel block. $T_{refract}$ represents the temperature that would be measured by a thermocouple if there were no heat loss to the surrounding. This is temperature that needs to be known in order to calculate the correct heat flux entering into the refractory specimen and can be thought of as a "correction" to the experimentally measured temperature.

For the sake of simplicity $T_{refract}$ will be referred as the "corrected" temperature (T_{cor}). T_{loss} is the temperature of the steel block due to heat loss to the surrounding environment when there is no heat transfer between the steel block and the refractory specimen. Rearranging the above equation yields:

$$T_{cor} = T_{init} + (T_{exp} - T_{loss}) \tag{7.3}$$

As seen from the equation, only T_{loss} is unknown. To calculate this, a 3-D heat transfer model of the steel block was developed in ABAQUS. In this "heat loss" model, convective and radiative boundary conditions were applied to all the surfaces of the steel block except the one in contact with the refractory specimen as shown in Figure 7.14. Boundary conditions were selected based on those used in the 3-D refractory model. A convection heat transfer coefficient consistent with natural convection conditions equal to 10 W/m^{2}K was assumed. An emissivity of 0.08 was assumed for the polished steel surface to define the radiative boundary condition. A room temperature reading at the time of experimentation was used as the ambient temperature.

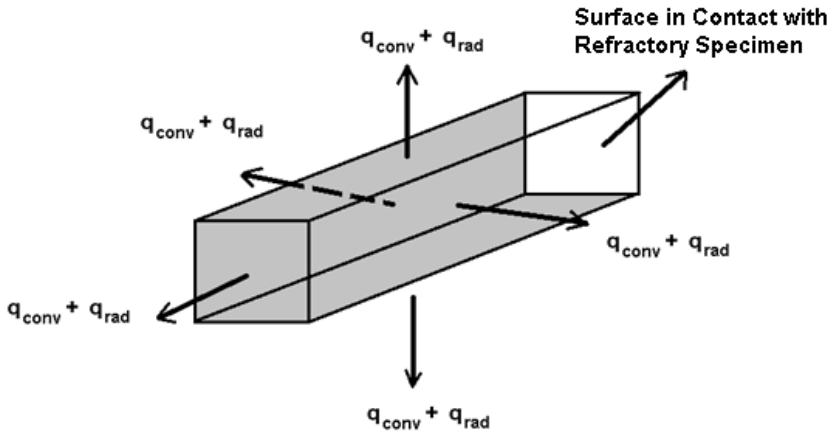

Figure 7.14: Computation domain and the boundary conditions of the "heat loss" model for steel block.

The simulation started with a uniform temperature in the steel block equal to T_{init} and was run for 300s (i.e. for the refractory-heating period). The temperature at the thermocouple location (i.e. 1cm from the interface at the centerline) is equal to T_{loss}. T_{cor} is then calculated using Equation (7.3). Figure 7.15 shows the variation of T_{exp}, T_{loss}, and T_{cor} during a refractory-heating experiment. It can be seen from the figure that T_{cor} is higher than the T_{exp}. The difference between T_{cor} and T_{exp} increases with time and at the end of 300s, it is about 90°C. Based on T_{cor}, the IHC model was run again to calculate corrected heat flux values that taken into account the heat loss from the steel block and represents the actual heat flux entering into the refractory specimen from the steel block (for the heating stage). The comparison of the two heat fluxes; the corrected heat flux and the heat flux based on thermocouple temperature data is shown in Figure 7.16. As heat is lost to the surrounding environment with time, the corrected heat flux values deviate from the heat flux values based on the thermocouple temperature data.

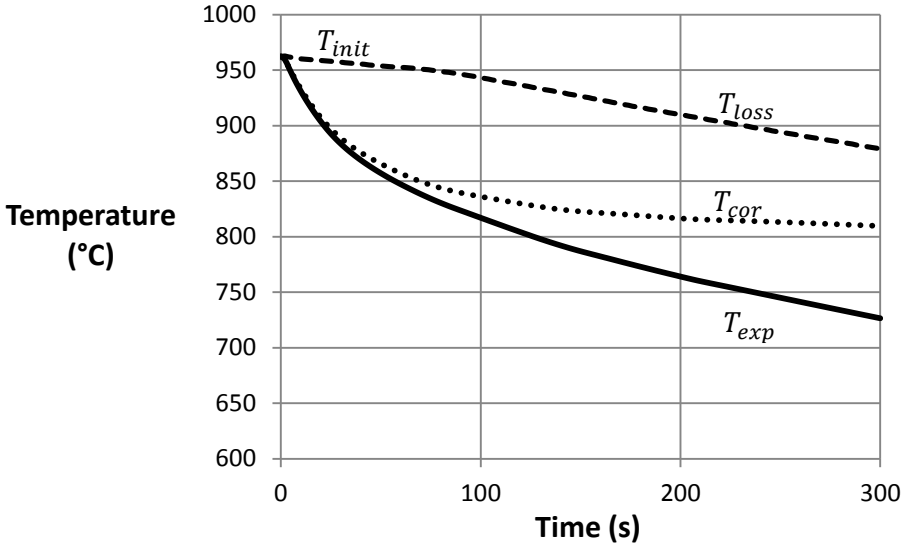

Figure 7.15: Variation of experimental and corrected temperature values during refractory-heating of 1-cycle experiment.

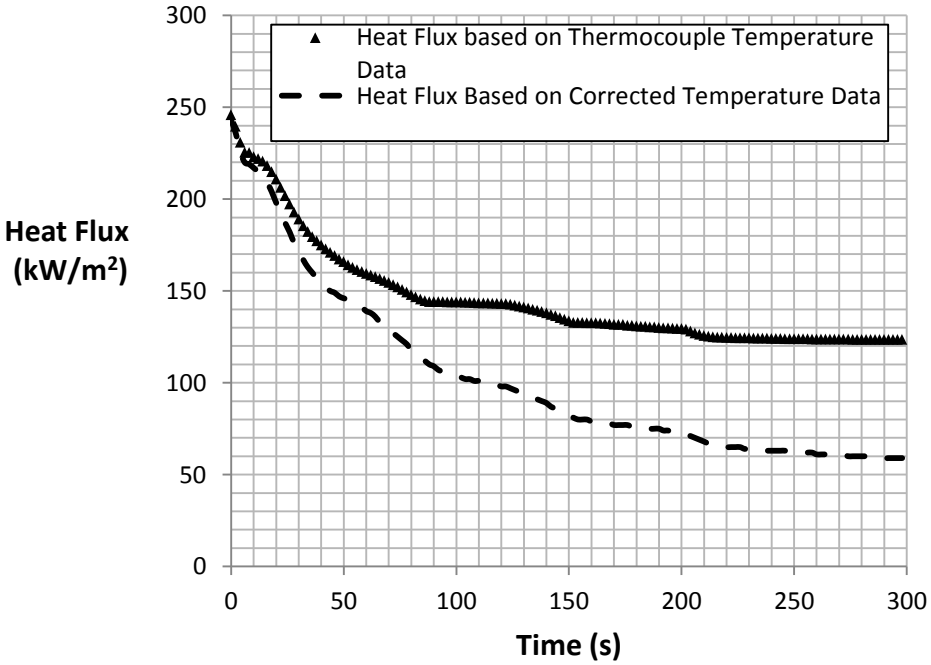

Figure 7.16: Comparison of the original and corrected heat fluxes, calculated using IHC analysis, for the heating state based on the original and corrected temperature values of the steel block for a single cycle cold-refractory experiment.

Based on the corrected heat flux values the forward model for refractory specimen was run again to predict the temperature history in the refractory. Figure 7.17 compares the predicted and measured values, revealing that the predicted temperature variation follows the same trend as the measured values and the maximum temperature difference between the two values is ~60°C.

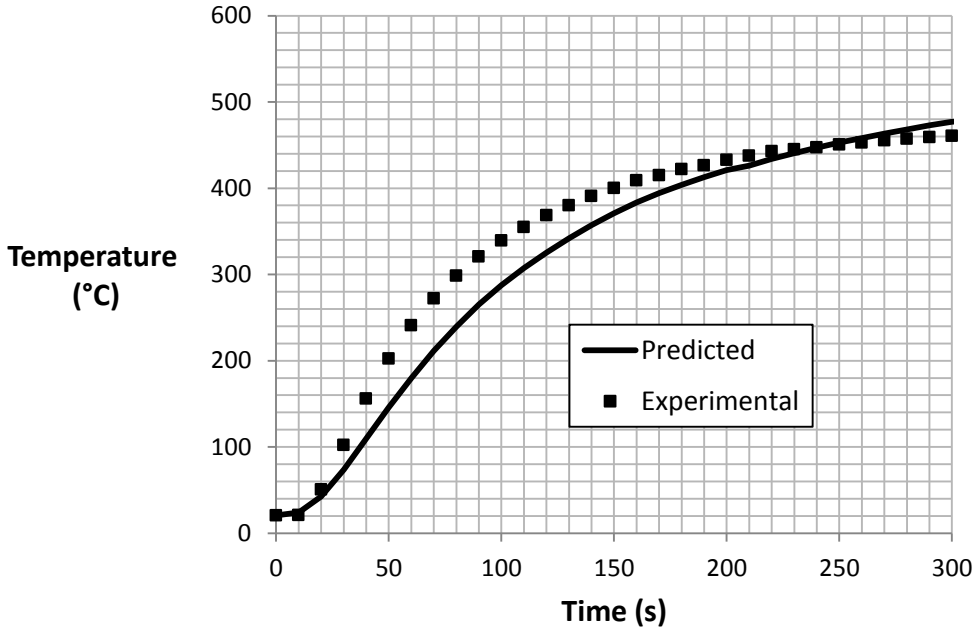

Figure 7.17: Comparison of the experimental temperature variation and the predicted temperature variation that accounts for the heat loss from the steel block to the surrounding during the refractory-heating event.

It should be noted that at the end of each refractory-cooling or refractory-heating event, there is a delay when the steel block is being replaced. During this idle time, the refractory specimen loses heat to the surrounding. The idle time at the end of the heating stage is small and hence the heat loss is not significant. However, the idle time and the associated heat loss at the end of cooling stage is significant. Due to the absence of thermocouple data during the idle time,

quantifying heat flux to the refractory specimen was based on assumed boundary conditions. The boundary conditions employed during the idle time are shown in Figure 7.18.

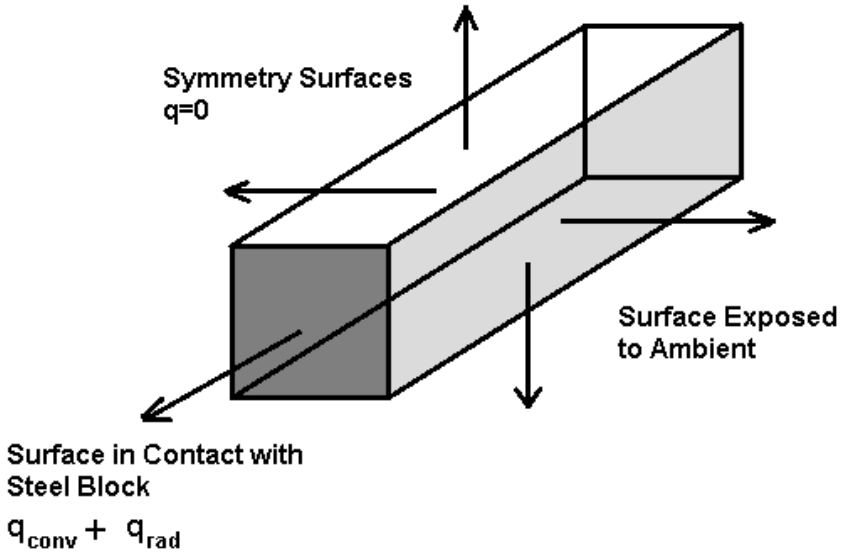

Figure 7.18: Thermal boundary conditions for the idle times during cold-refractory experiments.

As discussed previously, the heat flow in the refractory specimen during the cold-refractory experiments is 1-D and the heat loss from the "side" faces is not significant. Therefore, during the idle time, heat loss is expected only from the surface that is in contact with the steel block. Therefore, the boundary conditions are applied only on this surface. The choice of the parameters of the boundary conditions was based on assuming natural convection and values of thermal emissivity of refractory brick materials. A heat transfer coefficient of 15W/m^{2}K was assumed. Since, the emissivity of refractory materials varies from 0.4 to 0.95[78], the simulation was run with the emissivity value of 0.9.

Turning now to the cooling stage of the single cycle cold-refractory experiment, Figure 7.19 and Figure 7.20 show the measured temperatures in the steel block and the calculated heat fluxes occurring during the refractory cooling stage of the experiment. It can be seen that the heat fluxes during the cooling stage of the experiment are lower than the ones observed during heating. The heat loss from the steel block to the surrounding environment is expected to be negligible due to the lower temperature of the steel block. For the cooling portion of this analysis, the heat flow in the steel block may be approximated as 1-D and there is no need to correct the steel block temperature.

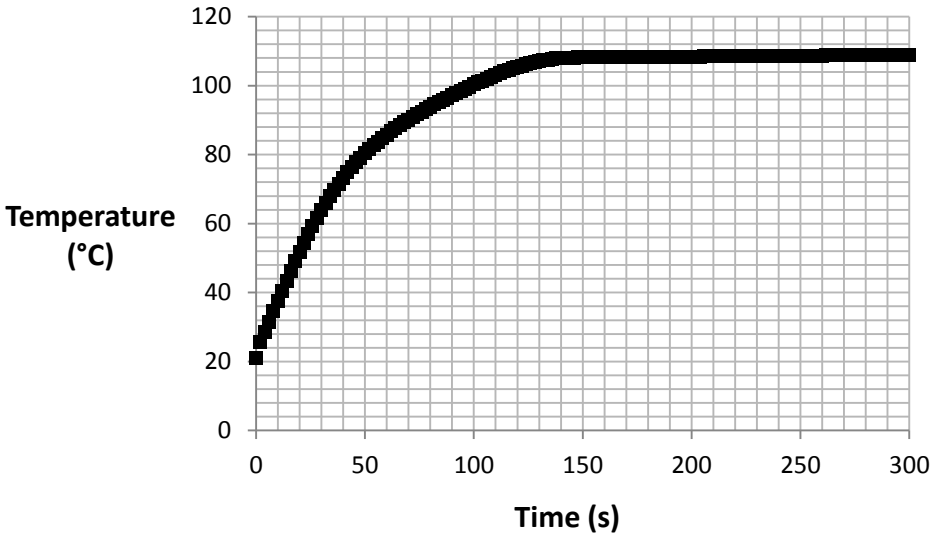

Figure 7.19: (a) Measured temperature in the steel block during the refractory cooling stage of the 1-cycle cold-refractory experiment.

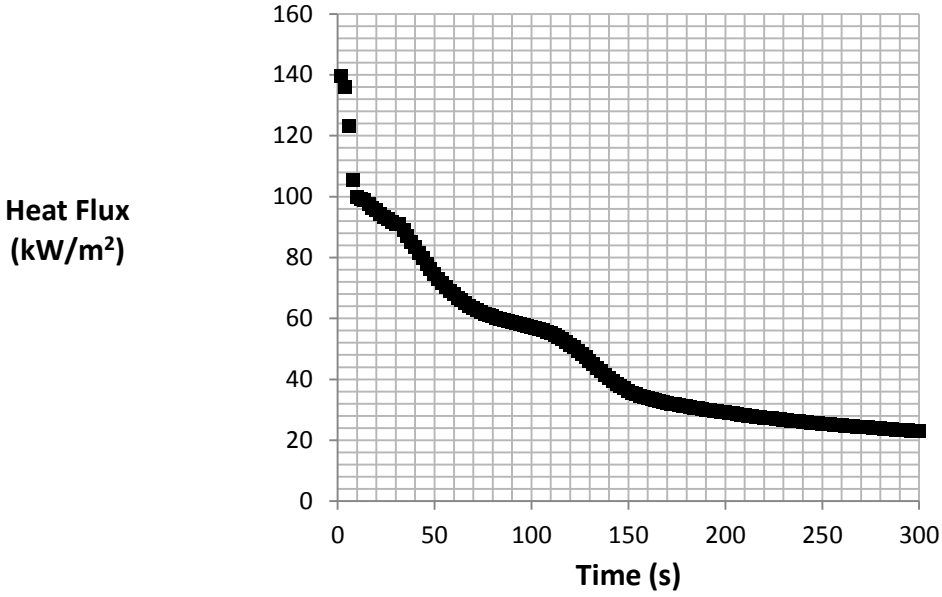

Figure 7.20: calculated heat flux during the refractory cooling stage of the 1-cycle cold-refractory experiment.

The heat flux values calculated from the IHC analysis during the heating and cooling stages were combined to predict the temperature in the refractory specimen for one complete (heating-cooling cycle) of 600s. The corrected heat flux values from the heating stage were applied for the first 300s and the heat flux values from the refractory-cooling stage were applied for the next 300s. The predicted and experimental temperatures of the refractory specimen for the 1-cycle cold-refractory experiment are shown in Figure 7.21. The results indicate that the predicted temperatures are within 60°C.

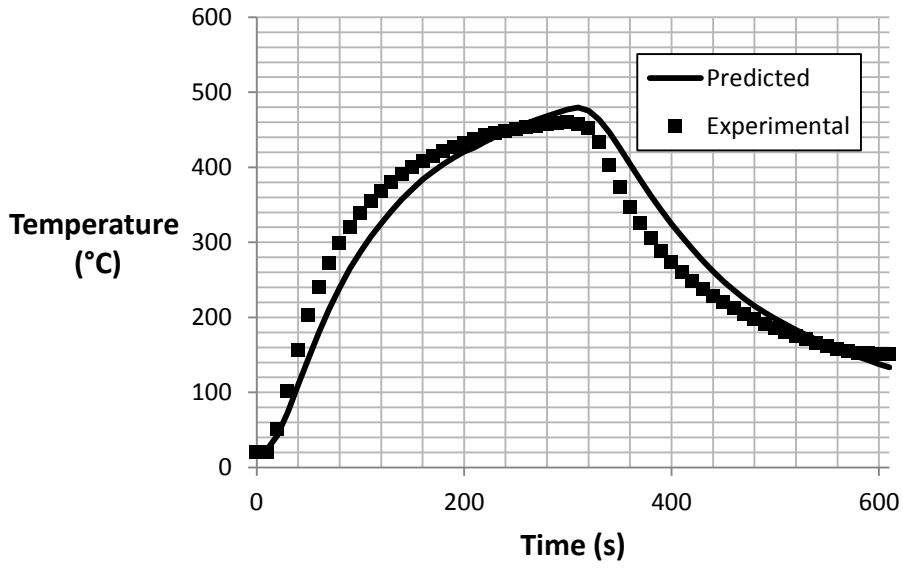

Figure 7.21: Comparison of the measured and predicted refractory specimen temperatures for the 1-cycle cold-refractory experiment.

The analysis procedure was then used to analyze the 2-cycle cold-refractory experiment. The temperature data for the hot steel block was corrected for each cycle. As discussed previously, it was determined that the heat loss from the steel block during the heating stage (in both cycles) was higher than observed in the previous 1-cycle experiment. In order to achieve acceptable agreement (~60°C) between the measured and predicted refractory temperatures, the magnitude of the radiation heat losses were increased. The assumed value of the surface emissivity of the steel block was increased to 0.2. The increase in the value of emissivity is attributed to the fact that even though the oxidized steel surfaces were polished after the first experiment, the surface finish had deteriorated. The process of oxidation causes an increase in the surface emissivity [78].

Figure 7.22 shows the difference in heat flux values calculated with the original boundary conditions (emissivity equal to 0.08) and the modified boundary conditions (emissivity equal to 0.2). During the refractory-cooling stage of the cycle, the heat loss from steel block is not significant owing to the lower temperature of the steel block compared to refractory-heating stage. Therefore, the heat flux correction is not needed. It can be seen that during the refractory-heating stage the heat flux variation with modified boundary conditions shows a lower heat flux magnitude than the one with original boundary conditions due to higher heat losses from the steel block. The figure also shows fluctuations in the calculated heat flux curves during the heating and cooling stages that are associated with the noise in the thermocouple temperature data of the steel block.

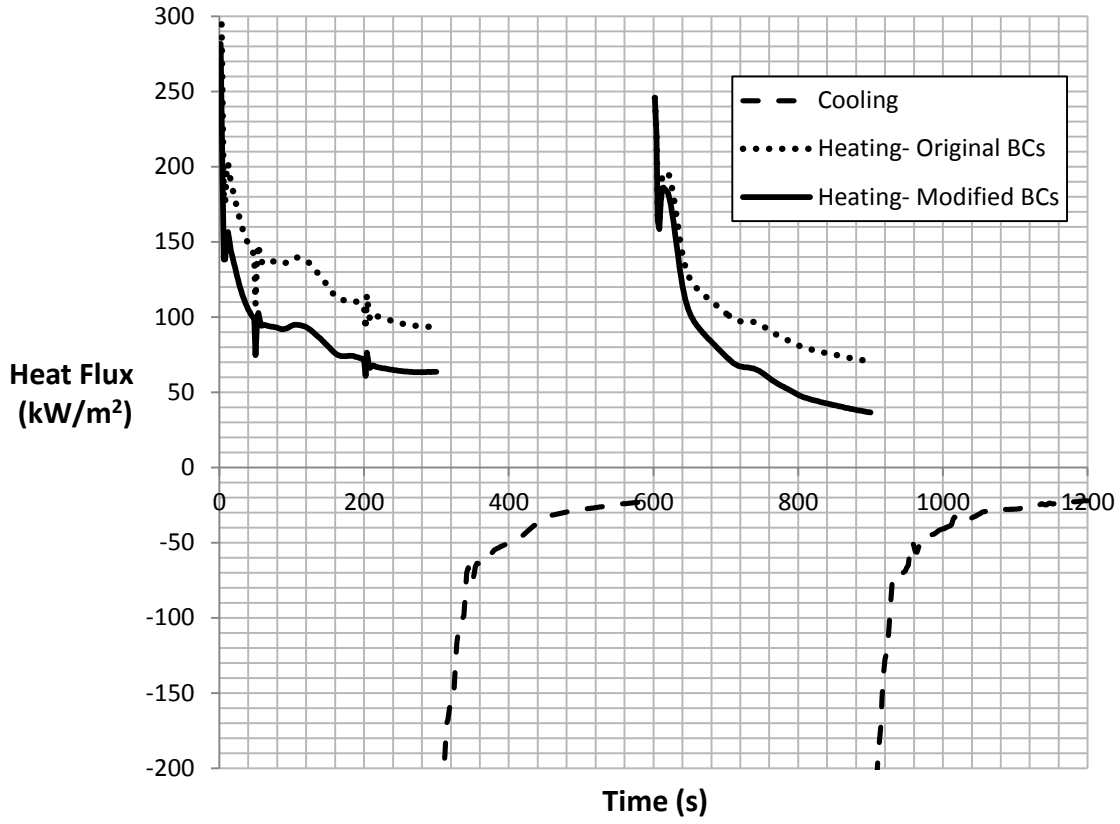

Figure 7.22: Predicted heat flux during the heat stage of 2-cycle cold-refractory experiment. The cases with original BCs and modified BCs are based on different boundary conditions applied to the hot steel block to correct the temperature data. For the case of original BCs, h=10W/m^{2}K, ε=0.08 and for the case of modified BCs, h=10W/m^{2}K, ε=0.2.

The values of the heat transfer coefficient and refractory surface emissivity were assumed to be 10W/m^{2}K and 0.7, respectively, during the idle time of the 2-cycle cold-refractory experiment. Figure 7.23 shows the measured temperature profile and the predicted temperature profile for 2-cycle cold-refractory experiment. It can be seen that the agreement between the measured and predicted temperatures is good, suggesting that the modifications to the boundary

conditions on the steel block during heating were warranted. The refractory-heating during the first cycle is not as severe as that in 1-cycle experiment (Figure 7.21).

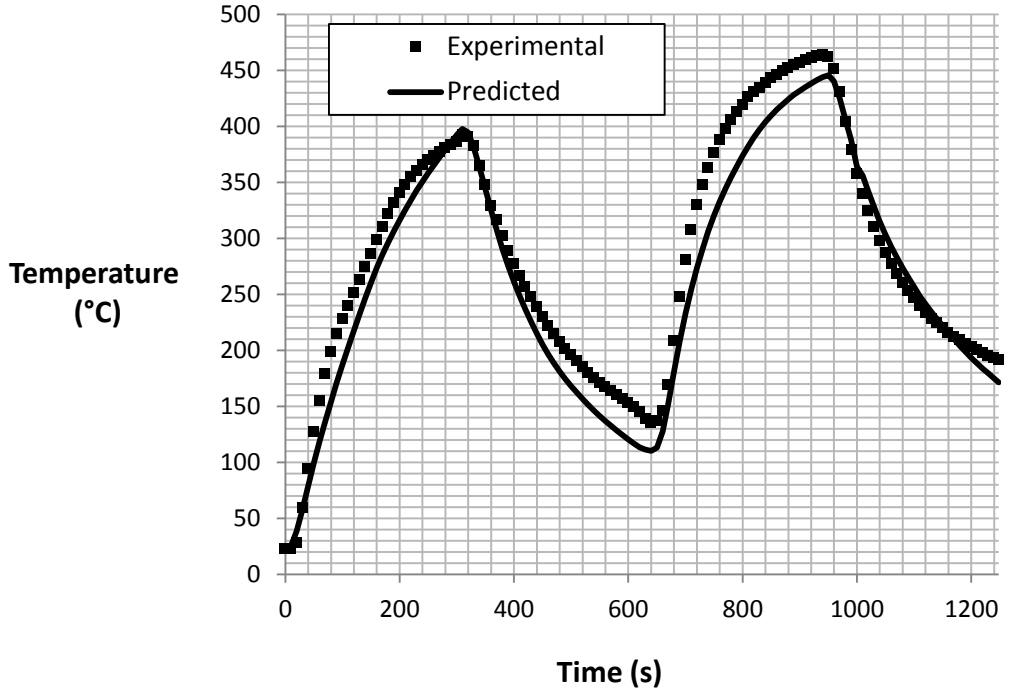

Figure 7.23: Comparison of the measured and predicted temperatures (based on corrected steel block temperatures during heating stage) of the refractory specimen for a 2-cycle cold-refractory experiment.

Next, the 3-cycle cold-refractory experiment was analyzed. In this experiment, due to an experimental error, the second refractory-cooling period was extended to 520s. The values of the heat transfer coefficient and refractory surface emissivity that apply during the idle period were assumed to be 15W/m^{2}K and 0.95, respectively. The predicted refractory temperatures are within 45°C of the measured temperatures, as shown in Figure 7.24.

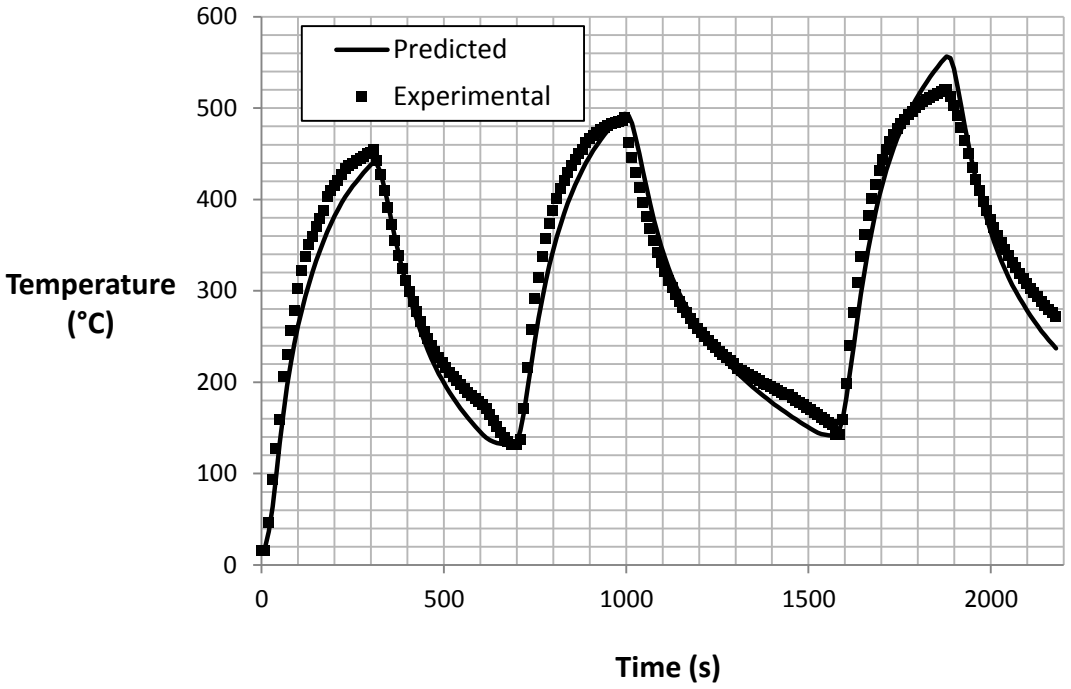

Figure 7.24: Comparison of the measured and predicted temperatures (with corrected steel block temperature during refractory-heating) of the refractory specimen for the 3-cycle cold-refractory experiment.

The temperature variation during each experiment (shown in Figures 7.21, 7.23 and 7.24) show that at a distance of 1 cm from the steel-refractory interface, the refractory material undergoes significant thermal cycling (± 300°C) with time. Figure 7.25 shows the predicted temperature variation in the refractory specimen with distance from the contact interface at the end of each heating and cooling stage for the 3-cycle experiment. It should be noted that due to the longer cooling duration of the second cycle, the temperatures near the interface are lower than expected. The temperature distribution after the heating stages shows that the interfacial surface temperatures of the refractory reach up to ~800°C and that the temperatures drop to ~200°C within 3cm from the interface indicating the presence of a large thermal gradient.

Overall, the thermal modeling results show that a significant thermal gradient is introduced across the length of the specimen during the thermal cycling experimentation.

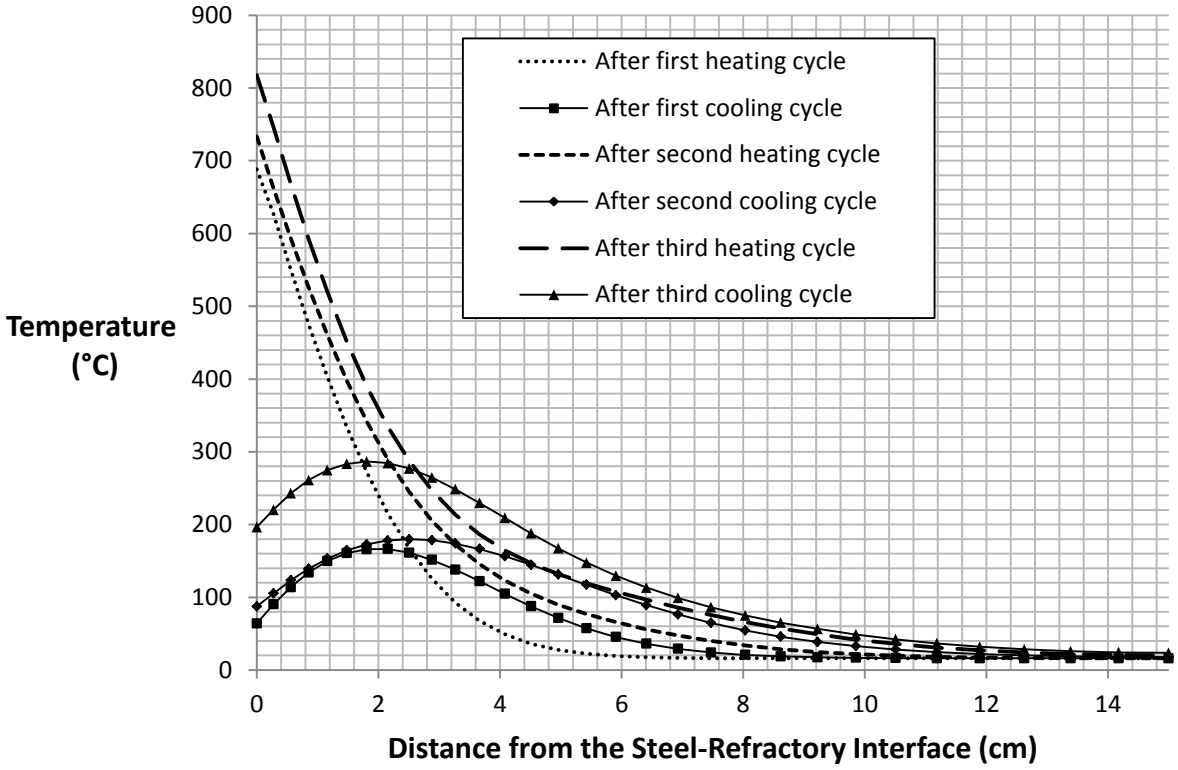

Figure 7.25: Predicted temperature distributions in the refractory specimen at the end of each heating and cooling stage for the 3-cycle cold-refractory experiment.

The results from the thermal cycling experiments on cold-refractory indicate that

1) Despite the heat loss from the steel block to the surrounding, the experiments were capable of inducing 1-D heat flow in the refractory specimen.

2) The modeling methodology was capable of quantifying the heat flux occurring in the refractory specimen. Based on the assumed boundary conditions, the predicted temperatures of the refractory specimen were within ~60°C of the experimental values.
3) The thermal cycling was significant enough to produce large thermal gradients across the length of the specimen.

7.3.2 Hot-Refractory Experiments

In the hot-refractory experiments, the refractory block (at ~1000°C) was taken out of the furnace with a thermocouple attached to it, placed in the apparatus, and then a cold steel block was placed over it. During the cooling stage of the 1-cycle hot refractory experiment, the temperature of the refractory, measured using the thermocouple, decreased by ~116°C and the temperature in the steel block increased from room temperature to ~160°C. As in the previous tests, the noise in the temperature data was reduced using the spline function in MATLAB. This procedure was followed for all the data from the steel blocks during all the experiments starting from the hot-refractory. The temperature variation in the steel block after reducing the noise for the cooling stage of the 1-cycle hot-refractory experiment is shown in Figure 7.26. The IHC analysis was performed with this temperature data and the corresponding heat flux variation is shown in Figure 7.27.

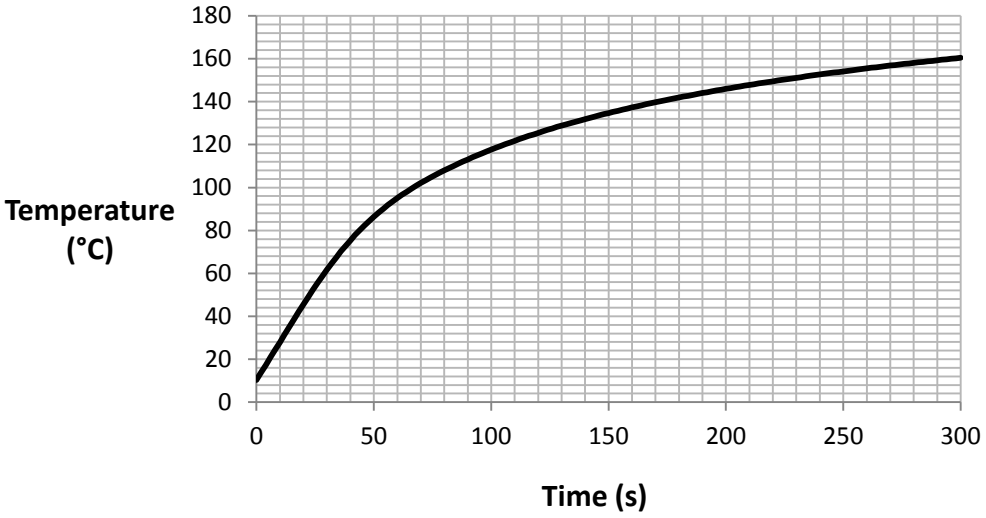

Figure 7.26: Temperature profile of the steel block during the cooling stage of the 1-cycle hot-refractory experiment.

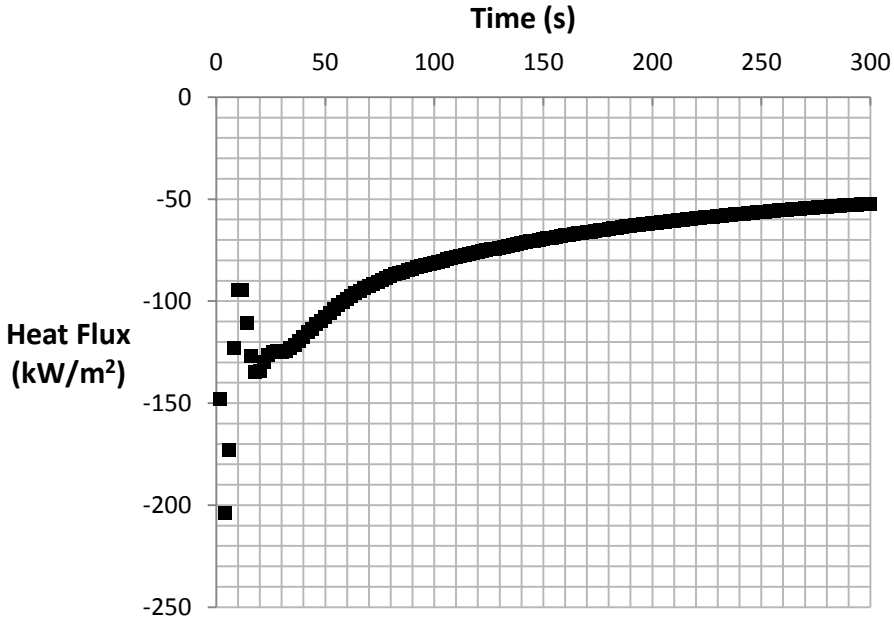

Figure 7.27: Predicted heat flux values during the cooling stage for the 1-cycle hot-refractory experiment.

The heat transfer model was run for the refractory using these heat flux values. The temperature predictions are compared with the measured temperatures in Figure 7.28. The results show a reasonable agreement (within 25°C).

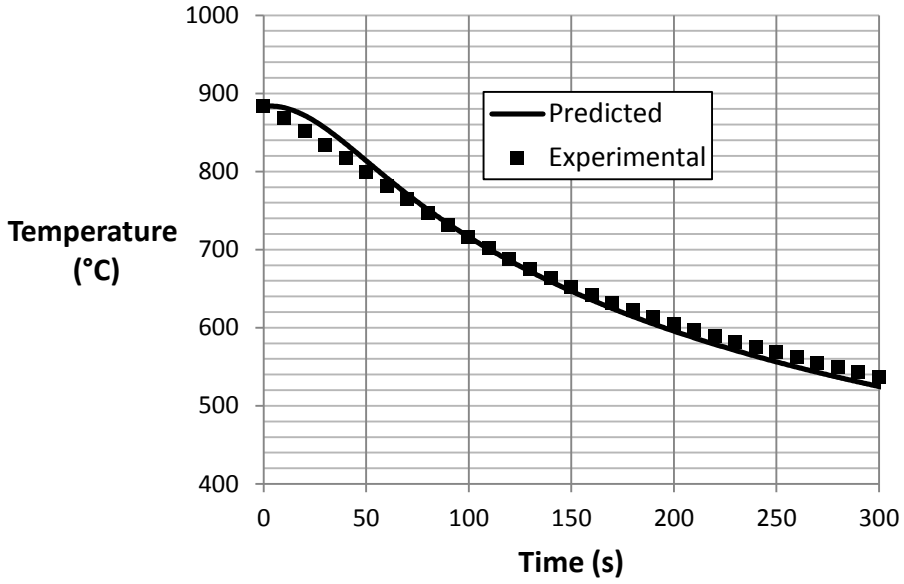

Figure 7.28: Comparison of the experimental and the predicted temperature profiles of the refractory specimen during the refractory cooling for 1-cycle hot-refractory experiment.

After cooling the refractory for 300s, the cold steel block was replaced with a hot one from the furnace. While positioning the steel block, the temperature of the block dropped from ~1000°C (furnace temperature) to ~880°C. With minor modifications in the experiments, this drop in temperature was decreased in the subsequent experiments.

The 3-D heat transfer model was run to correct the heat loss from the hot steel block during the heating stage. To simulate thermal conditions during the idle time of the heating stage of the 1-cycle hot-refractory experiment, the emissivity of the refractory and the heat transfer

coefficient were assumed to be equal to 0.5 and 10W/m^{2}K, respectively. When values for the convective heat transfer coefficient, ambient temperature and the emissivity of steel surface of 10W/m^{2}K, 11°C and 0.15, respectively, were assumed, the agreement between the predicted and the measured temperatures was found to be within ~40°C. The comparison of measured and predicted temperatures during the 1-cycle hot-refractory experiment is shown in Figure 7.29.

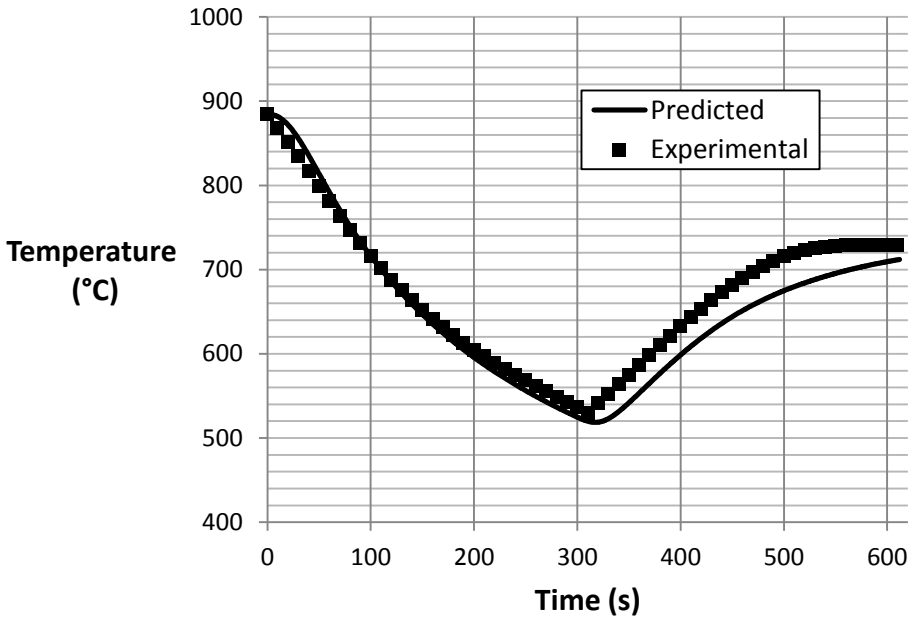

Figure 7.29: Comparison of the measured and predicted temperature profiles in the refractory specimen during a single cycle hot-refractory experiment after correcting for heat loss from the steel block.

In the 1-cycle hot-refractory experiment, the emissivity of the steel block was assumed 0.15 to calculate the heat loss. This value is lower than the assumed emissivity value used in other calculations. This has been attributed to the fact that since, multiple attempts were made to conduct the hot-refractory experiments, the steel blocks accumulated oxide with multiple heating events. Thus, the emissivity of the steel block was expected to vary slightly from block-to-block.

The IHC model was then applied to the remaining sets of data (for 2- and 3-cycle experiments). The result of 3-cycle experiment is representative of the results for each of these experiments. For this experiment, the emissivity of refractory and the heat transfer coefficient were assumed to be 0.6 and 10W/m^{2}K, respectively. The results for three heating-cooling cycles, presented in Figure 7.30, show that the predicted temperatures are in agreement with the measured temperatures. Even though the boundary conditions are assumed during the idle times, the temperatures are still within a reasonable agreement (within ~80°C).

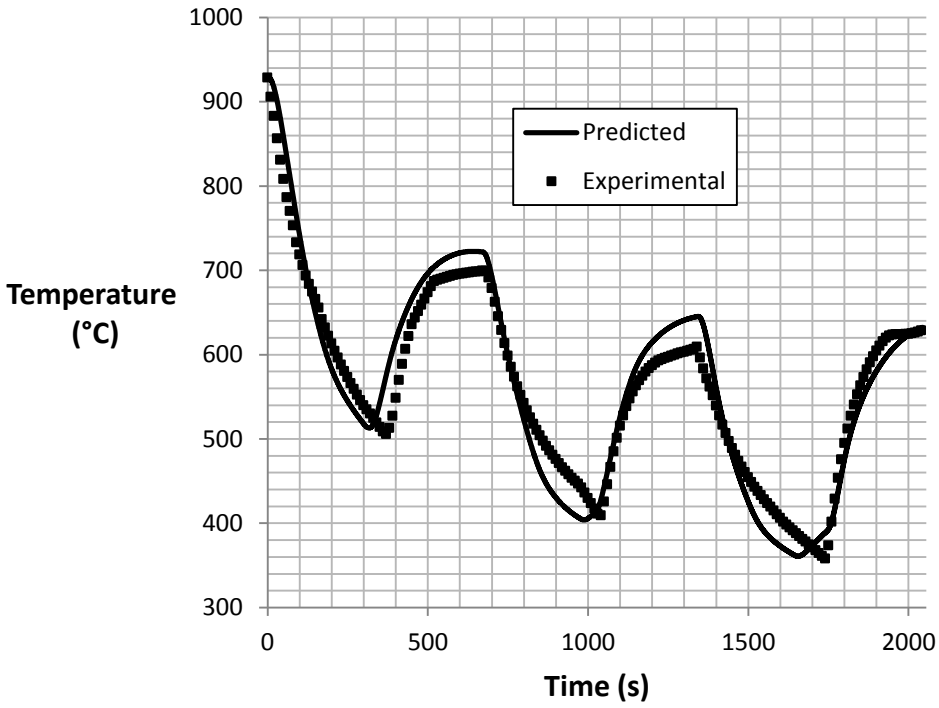

Figure 7.30: Comparison of the measured and predicted temperature profiles for the refractory specimen for a 3-cycle hot-refractory experiment.

Thermal profiles along the length of the specimen at various times indicate that significant thermal gradients develop which may lead to the formation of damage. The thermo-mechanical predictions and their correlation to damage are discussed in the next section.

The experimental issues experienced with the hot-refractory test were similar to those discussed previously for the cold-refractory tests. Additionally, the use of hot refractories posed a problem with loosening of the thermocouple-refractory contact while taking the refractory out of the furnace. As a result, multiple attempts were made to get the temperature data.

The results from the thermal cycling experiments on hot refractories indicate that

1) After considering the heat loss from the steel block the predicted results were in agreement with the experimental data.
2) The thermal cycling was severe enough to produce large thermal gradients across the length of the specimen. The magnitude of the gradients is larger than the ones observed during the cold-refractory experiments indicating larger damage and significant damage is expected.

7.4 Stress Modeling Results

The predicted heat flux values were used as an input to a 3-D thermal model of the refractory blocks in ABAQUS using a FORTRAN based subroutine DFLUX. The temperature predictions from this model were used to run the 3-D thermal-stress model.

7.4.1 Cold-Refractory Experiments

The stress model was run using the data from each cold-refractory experiment (i.e. 1, 2 and 3-cycle) to assess the stress distribution and damage evolution. To describe the evolution of thermal-stress and damage accumulation, a "3-cycle experiment" will be presented in detail, while the results of the 1 and 2 cycle cases will be summarized.

To examine the effect of the heat flux on the refractory with time, contour plots of temperature distribution are plotted for 100s, 200s and 300s into the first heating stage (Figure 7.31).

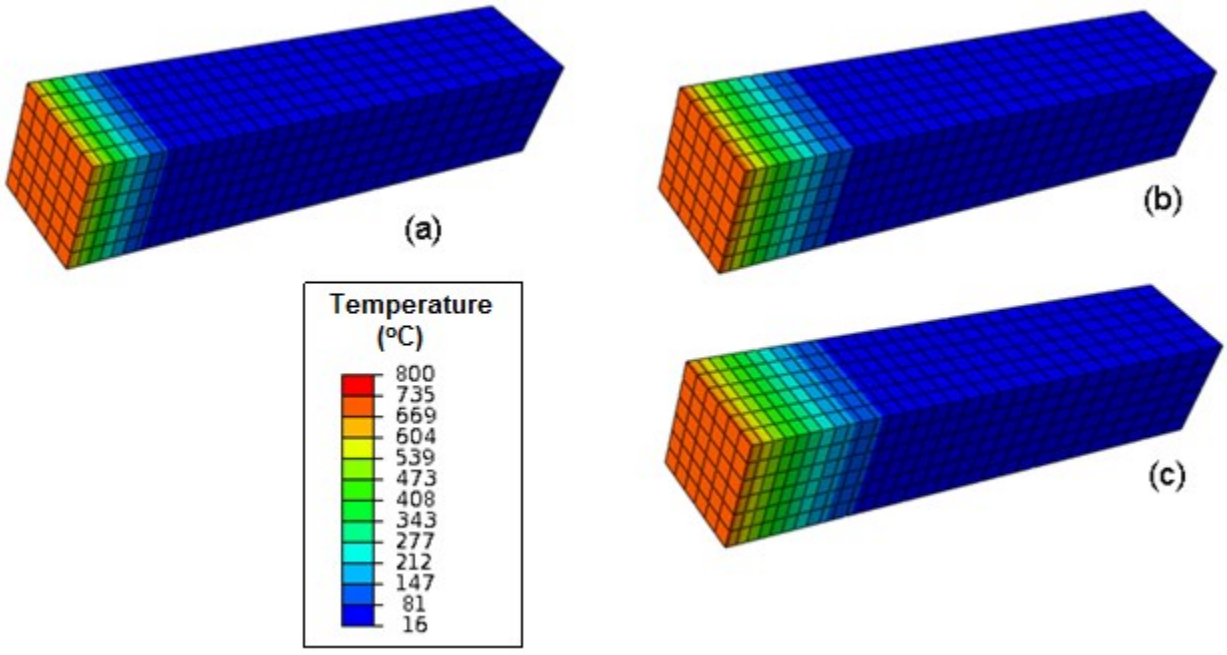

Figure 7.31: Contour plots of predicted temperature distribution during 3-cycle cold-refractory experiment after (a) 100s (b) 200s and (c) 300s into heating.

It can be seen from Figure 7.31 that the effect of surface heat flux penetrates deeper into the refractory with time. At the end of the refractory-heating cycle of 300s, the temperature effects have penetrated up to 1/3rd of the length of the specimen. Even though the heat flow is one-dimensional, the state of stress is three-dimensional. Due to symmetry, the magnitude of the stress in the two transverse directions is the same. The corresponding longitudinal and transverse stress distributions are shown in Figure 7.32. At the start of heating, the surface of the refractory in contact with the hot steel block tries to expand and the sub-surface material, which is lower in temperature, hinders this expansion. As a result, in the transverse direction, compressive stresses are introduced near the heated surface and tensile stresses are introduced in the material next to the surface. The longitudinal stresses near the heated surface are negligible compared to the transverse stresses. The material near the edge of the refractory block is less constrained than the material at the centerline near the symmetry surfaces. Therefore, the transverse stresses are significant at the centerline and not so significant at the edge. Due to the same reason, the stresses near the edge are mainly longitudinal. The figure also shows that the longitudinal stress is spread across a larger section of the material than the transverse stress.

As the effects of heat penetrate further into the specimen the zone of longitudinal compressive stress (blue area) and the zone with longitudinal tensile stress (read area) penetrate further into the specimen (see Figure 7.32). Similar effects are observed in the case of the transverse stresses.

Since refractories exhibit higher strength in compression than in tension, it can be seen that at 300s (Figure 7.32(d)) the highest compressive stress is ~78MPa and the highest tensile stress is ~12MPa.

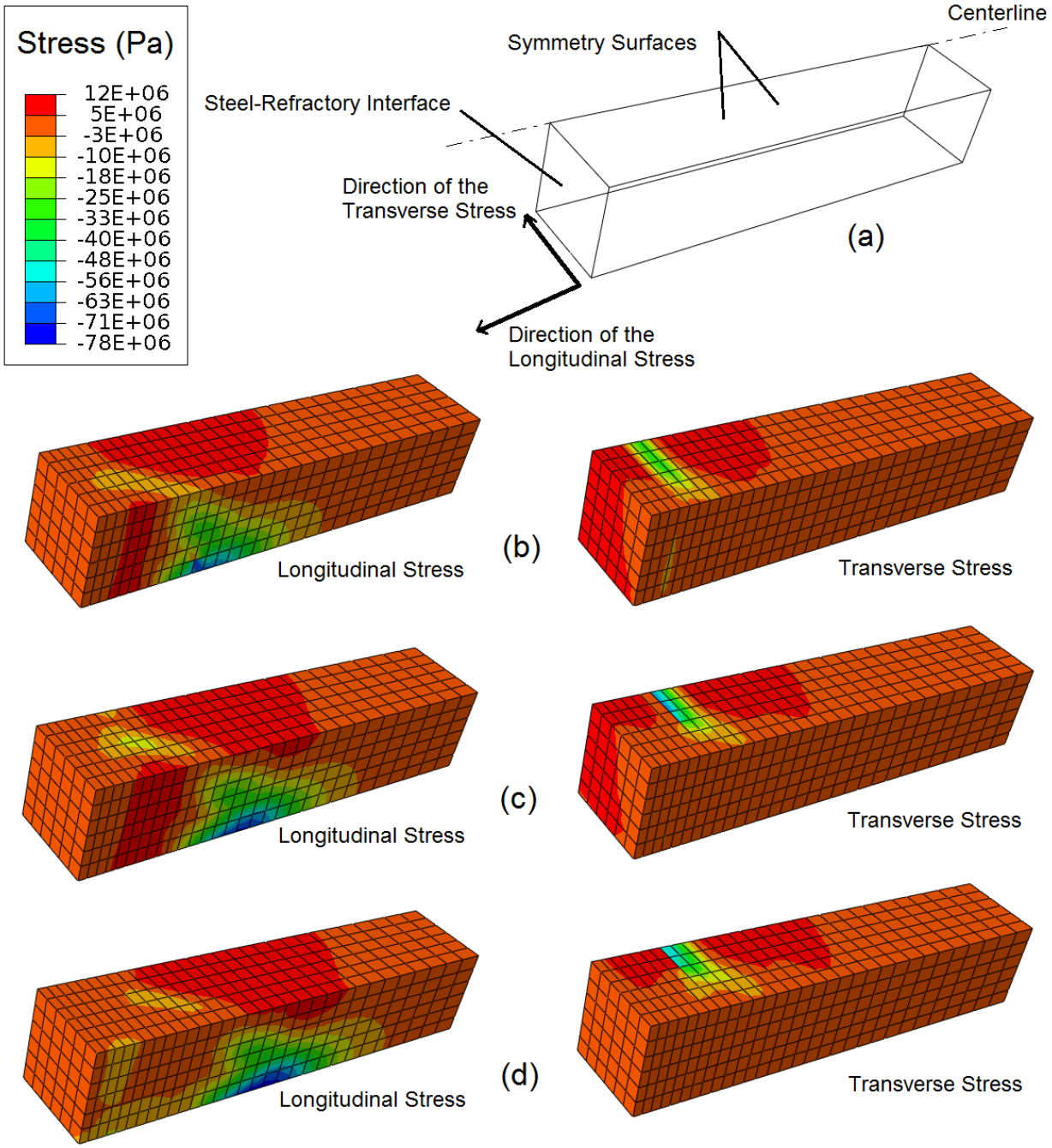

Figure 7.32: (a) Schematic of the computation domain and mechanical boundary conditions. Contour plots of predicted longitudinal and transverse stress distribution during a 3-cycle cold-refractory experiment after (b) 100s (c) 200s and (d) 300s into heating.

The scalar degradation (SDEG) variable indicates the combined damage accumulated due to the tensile and the compressive stress history at each location in the domain. SDEG represents the fractional loss in the elastic modulus. It can be seen from Figure 7.33 that most of the damage has accumulated on the edge of the specimen where the maximum stresses were present in a larger area than at the center indicating the possibility of the visible cracking.

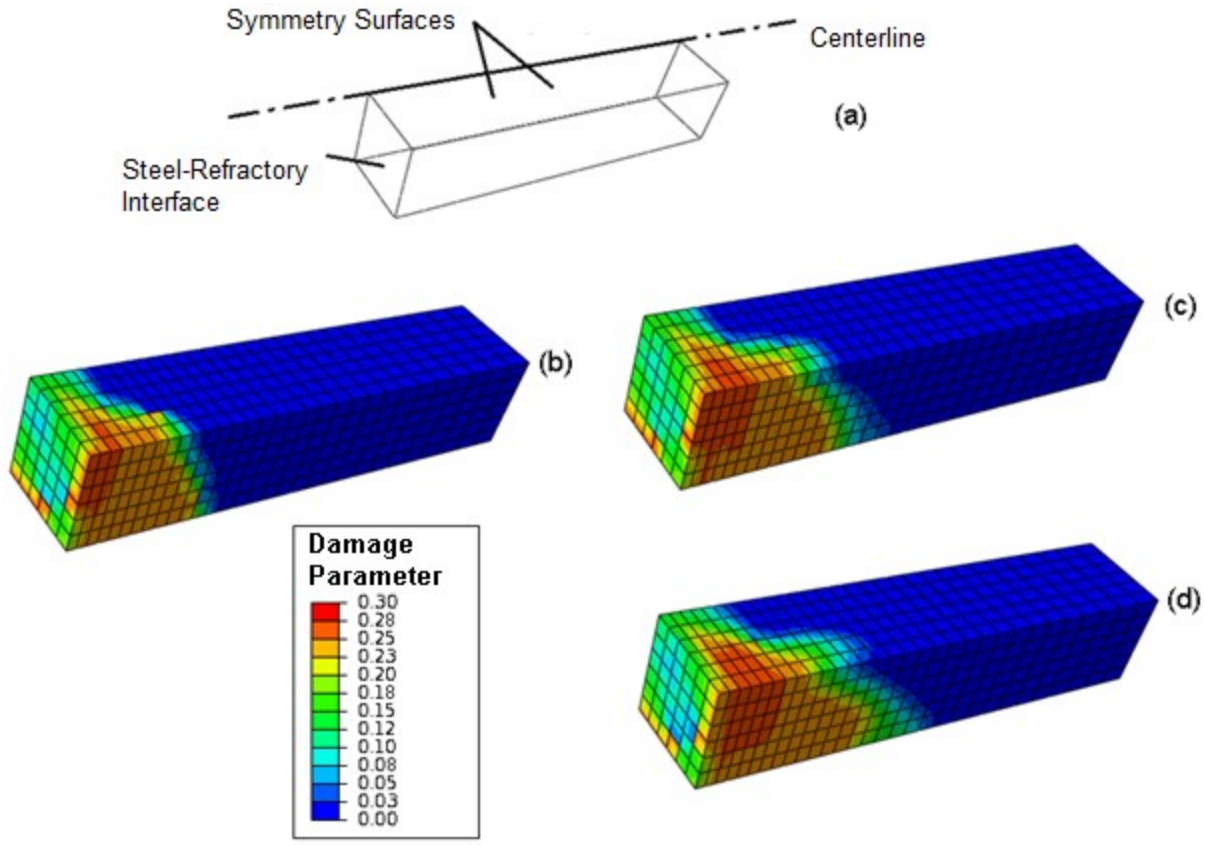

Figure 7.33: (a) Schematic of the computation domain and mechanical boundary conditions. Contour plots of predicted distribution of the damage variable during 3-cycle cold-refractory experiment after (b) 100s (c) 200s and (d) 300s into heating.

It should be noted that, SDEG is a scalar quantity; hence, the predicted damage does not indicate the direction of cracking. However, during operation, failure of the refractory (thermal

spalling) always occurs due to the cracks parallel to the hot surface. This indicates that refractory failure is due to the stresses in the direction of the heat flow (longitudinal stress) and that temperature changes in this direction should be controlled to minimize refractory losses. Following this logic, the results of the stress analysis will be mainly focussed on the stresses in the longitudinal direction.

As mentioned before, as the heat penetrates, the "compressive-tensile" zone moves further into the specimen. This effect can be observed by plotting the longitudinal stress along the centerline and along the edge at various times during the heating stage (Figure 7.34).

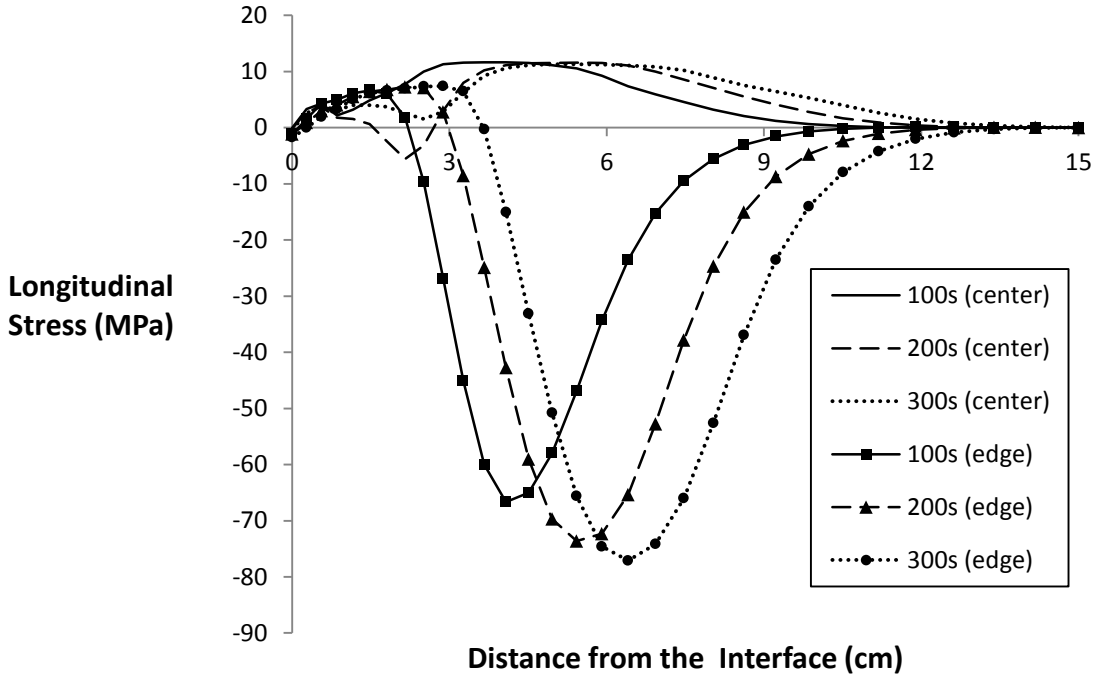

Figure 7.34: Longitudinal stress along the length of the refractory specimen during the heating stage predicted with the thermal-stress model at various times in the 3-cycle cold-refractory experiment.

Figure 7.34 shows that as heating progresses the magnitude of the maximum compressive stress increases, however, the magnitude of the maximum tensile stress does not increase. This is attributed to the fact that the damage in refractories occurs at lower stress in tension compared to compression. The predicted damage profiles at these times are shown in Figure 7.35.

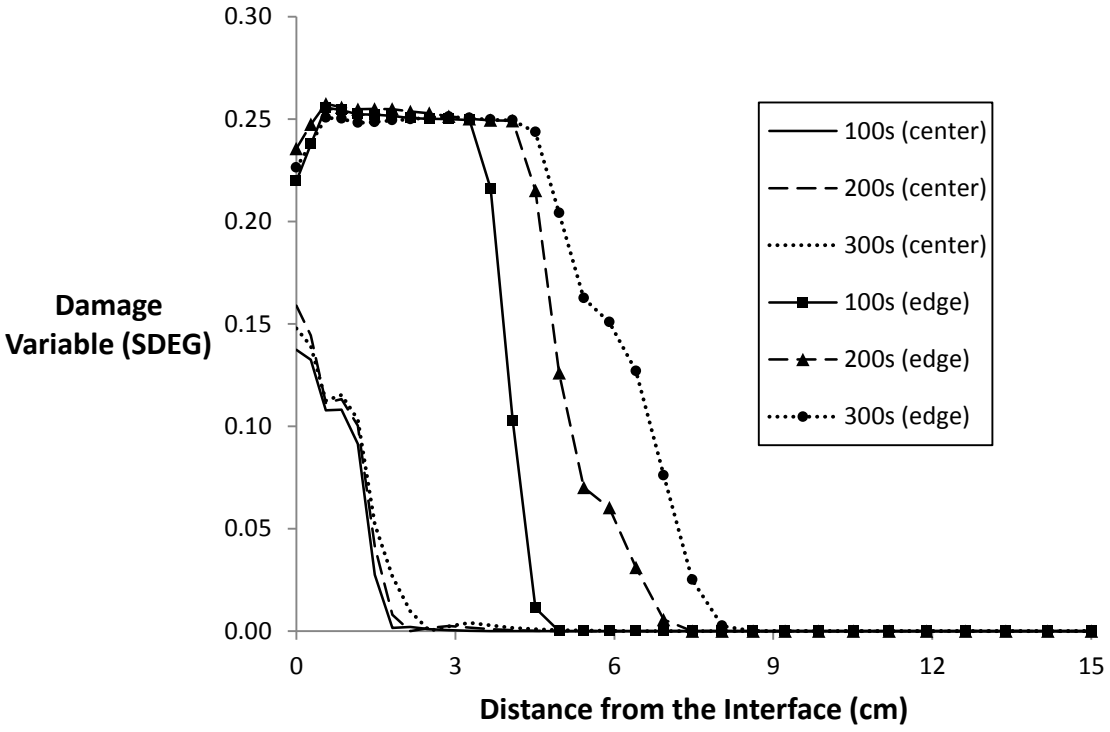

Figure 7.35: Damage variable (SDEG) across the length of the refractory specimen during heating predicted with the thermal stress model of a 3-cycle cold-refractory experiment.

Figure 7.35 shows that the damage penetrated further along the edge than along the centerline. The damage along the centerline is smaller compared to along the edge. As the heating continues the damage develops further into the specimen, however, the level of damage does not change significantly with distance from the interface.

In order to reveal the effect of the cooling during the first thermal cycle, contours of temperature, stress, and damage are illustrated in Figure 7.36.

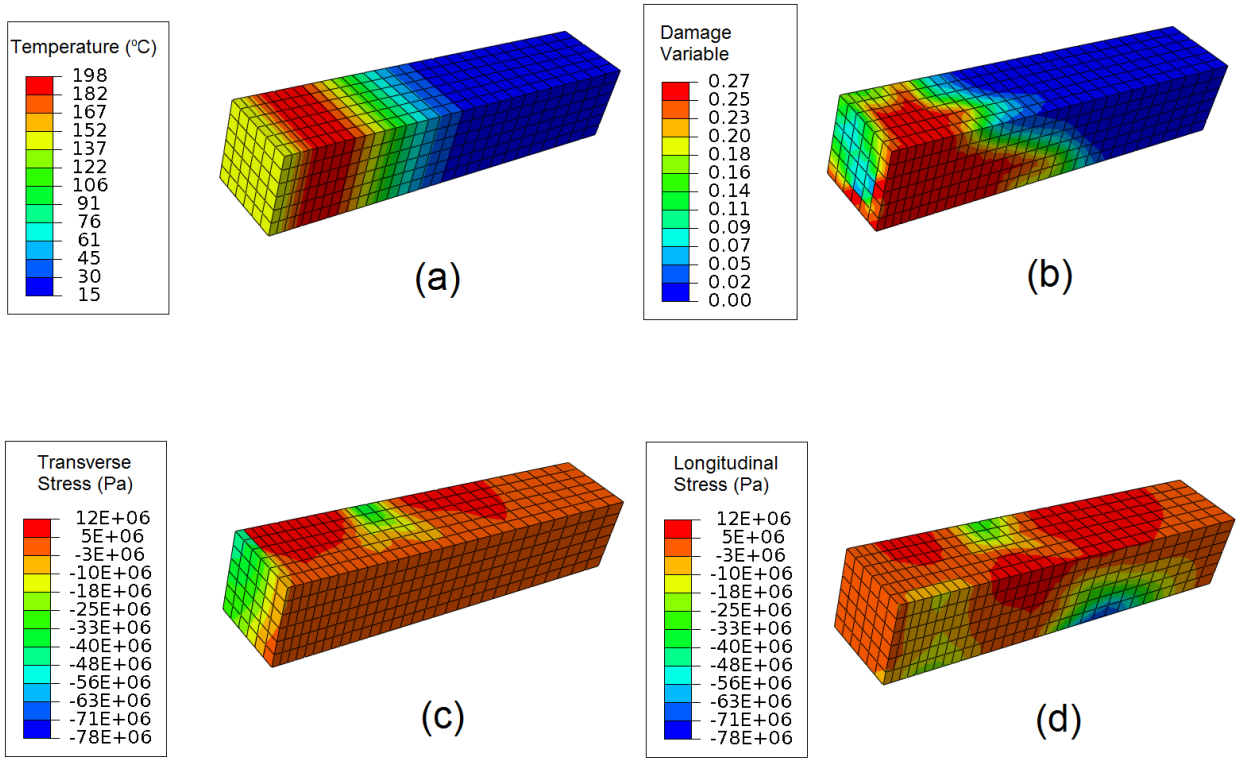

Figure 7.36: Predicted results of the stress model for a 3-cycle cold-refractory experiment after the first heating-cooling cycle (a) Temperature distribution (b) Distribution of the damage variable (c) Transverse stress distribution (d) Longitudinal stress distribution

Figure 7.36(a) shows the thermal gradient in the material after one complete heating-cooling cycle. Note that the temperature, stress and damage effects have penetrated further into the refractory specimen compared to the results after the heating stage as shown in Figures 7.31-7.32. It should also be noted from Figure 7.36(a) that the effects of the heat transfer conditions are significant only up to about half the length of the specimen from the interface. The temperature in the rest of the specimen (in blue) has not changed and is at room temperature.

However, Figures 7.36(c-d) show that the stress effects have penetrated further than the temperature as a response to the stresses in the material undergoing the temperature changes. Comparing Figures 7.32 and 7.36(d), it can be seen that, because of cooling, another tensile-compressive zone has developed next to the existing compressive one at the edge. A similar effect can be observed along the centerline. This effect is also observed in the transverse stress distribution in Figure 7.36(c). The extent of the damaged region in the refractory has also extended further into the material (see Figure 7.36(b)), but the damage distribution is similar to that shown in Figure 7.33.

With multiple heating-cooling cycles, the temperature effects penetrate further into the specimen forming alternating zones of tensile and compressive stresses. The damage profile after three heating-cooling cycles evolves as the thermal-stress effects penetrate into the specimen. Figure 7.37 shows the variation of damage with length along the centerline and edge of the refractory specimen after each cycle. It is observed that damage is more prevalent along the edge of the refractory and that it extends further along the edge than the centerline of the specimen. The results also indicate that at the center, the level (magnitude) of damage increases by a small amount after each cycle up to 3 cm from the interface, however, it does not increase significantly past 3 cm into the specimen. At the edge, the level (magnitude) of damage after each cycle does not increase significantly. Additionally, the area of damage increases with the number of cycles.

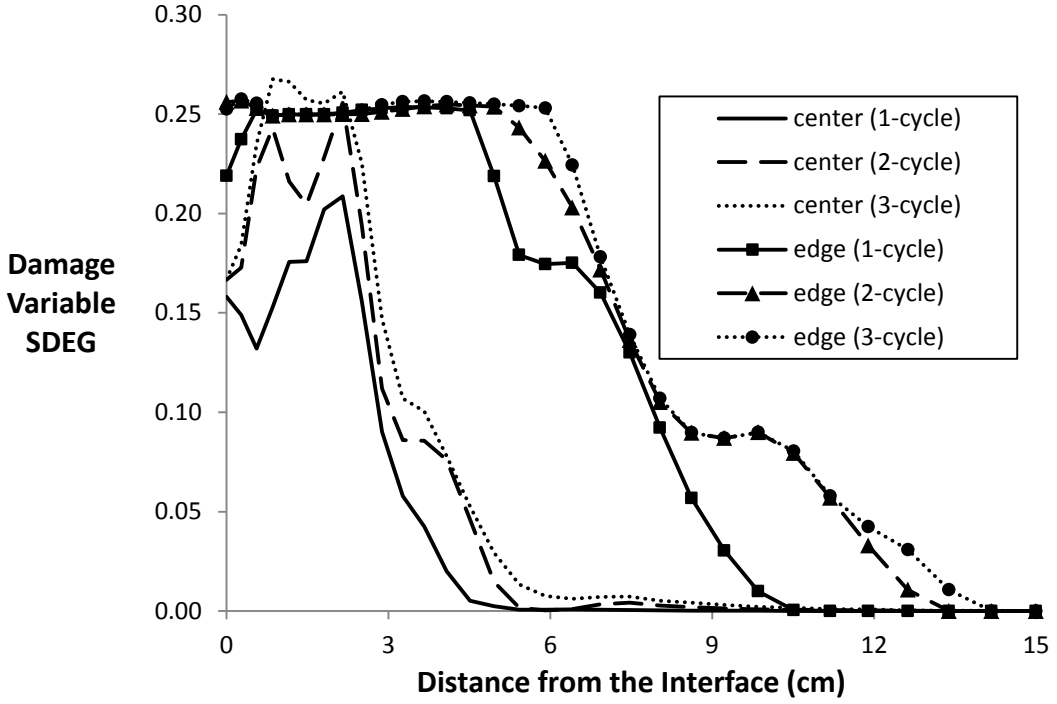

Figure 7.37: Predicted profile of the damage variable (SDEG) of the refractory specimen after 1, 2, and 3 heating-cooling cycles.

7.4.2. Ultrasonic Testing Results for Cold-Refractory Experiments

The results of the ultrasonic tests were compared with the model predictions of damage. The ultrasonic test measures the overall damage, in terms of the reduction in the elastic modulus, in the volume of material between the transducers. To facilitate comparison with this data, the average value of the damage variable (SDEG) over the volume of material corresponding to the location where the transducers were placed (i.e. $1/3^{rd}$ of the specimen) was calculated based on predictions at the end of each cycle.

As mentioned earlier, multiple experiments were performed in order to produce the thermal data necessary to analyze 1, 2, and 3-cycle cold-refractory experiments. The specimens

produced during the tests where a thermocouple failed (i.e. thermal data was not be acquired, but thermal cycling was performed) were also characterized with ultrasonic measurement. Table 7.2 shows the damage indicated by the ultrasonic testing and the predicted damage for all the three experiments discussed above. The ultrasonic testing results in terms of velocities are given in APPENDIX A. It can be seen that for the 1-cycle and 2-cycle experiments one extra sample was tested.

Table 7.1: Results of the ultrasonic tests and the predicted damage at various locations of the refractory specimens for the cold-refractory experiments.

Distance from the Interface (cm)	**Damage (%)**							
	1-Cycle Experiment			**2-Cycle Experiment**			**3-Cycle Experiment**	
	Measured "a"	Measured "c" *	Predicted	Measured "d"	Measured "e" *	Predicted	Measured "g" *	Predicted
0-5	~12	~12	~14	~21	21	~21	~26	~23
5-10	0	0	0	0	0	~4	~12	~6
10-15	0	0	0	0	0	0	~3	~0.5
Along the length of the specimen	18	~4	~5	26	~14	~8	~18	~10

* indicates the refractory specimens for which the thermal data is available.

The damage (which indicates the percent change in the elastic modulus) is calculated as the change in the square of the sound-velocity in the material because the elastic modulus is proportional to the square of the sound-velocity in the material (See Eq. (4.1)).

It can be seen from the table that with additional cycles, the predicted overall damage in the section closest to the interface (within 0-5cm from interface) does not increase significantly after the second cycle. In this section of the specimen, the predicted values are close to the experimental values for both samples following the 1-cycle and 2-cycle experiments and the difference between the predicted and the experimental values is 3% for the 3-cycle experiment. At the other cross-sections (5-10 cm and 10-15 cm from the interface), the model predictions are in agreement with the tests carried out on both the samples for 1-cycle experiment. However, for the 2-cycle experiment, the measured value shows no damage but the model predictions show 4% damage. In addition, for the 3-cycle experiments, the agreement exhibits a maximum difference of 6% between the predicted and measured damage.

The results in the longitudinal direction show significant scatter. For the 1-cycle experiment, the experimental value of damage for sample "B" (5%) is in agreement with the predicted value (4%). However, the value for sample "A" is 18%. The same trend is observed in the data from the 2-cycle experiments. In general, the measured values in the longitudinal direction are larger than the predicted values.

There are various reasons for the discrepancies between the predicted and measured damage values:

1) Ultrasonic testing - The ultrasonic velocity measured at a particular location was observed to vary within ±75m/s. The damage variation associated with this could be as high as 6% relative to the range of velocities observed in the current samples.
2) Thermal model - The thermal model is accurate to within ~60°C. Depending on the corresponding stress, the associated variation in damage could be significant for a temperature change of ~60°C.
3) Stress model – For compression, the material properties used for the damage model at high temperature were assumed to be the same as that of room temperature. At high temperatures, the propensity for damage in compression would increase, thus the associated damage predicted by the model would increase.
4) Material inhomogeneity - The material properties applied in the model assume a homogeneous material, however, uneven distributions of porosity, aggregates and various phases makes it inhomogeneous. The inhomogeneity of the material could affect the measured damage.

The results of the ultrasonic testing indicate that given the uncertainty in the factors discussed above related to stress modeling of refractories, the model predictions are in a reasonable agreement. The ultrasonic test only gives an idea about the magnitude of damage in terms of the loss of elastic modulus. It does not specify the crack direction. Attempts to use optical microscopy, image correlation and dye penetrant inspection were not successful in revealing further details on the nature of the damage experienced by the specimens.

7.4.3 Hot-Refractory Experiments

The predicted temperature and the longitudinal stress distribution after 3 thermal-cycles starting with hot refractory samples are shown in Figure 7.38. It can be seen that the thermal cycling has resulted in a temperature change in more than half of the length of the specimen. However, the multi-axial stress distribution indicates that the effects of thermal cycling are significant along the entire length of the specimen. The predicted damage is also significant along almost the entire length of the specimen and the magnitude of the damage is larger than that predicted for the cold-refractory experiments.

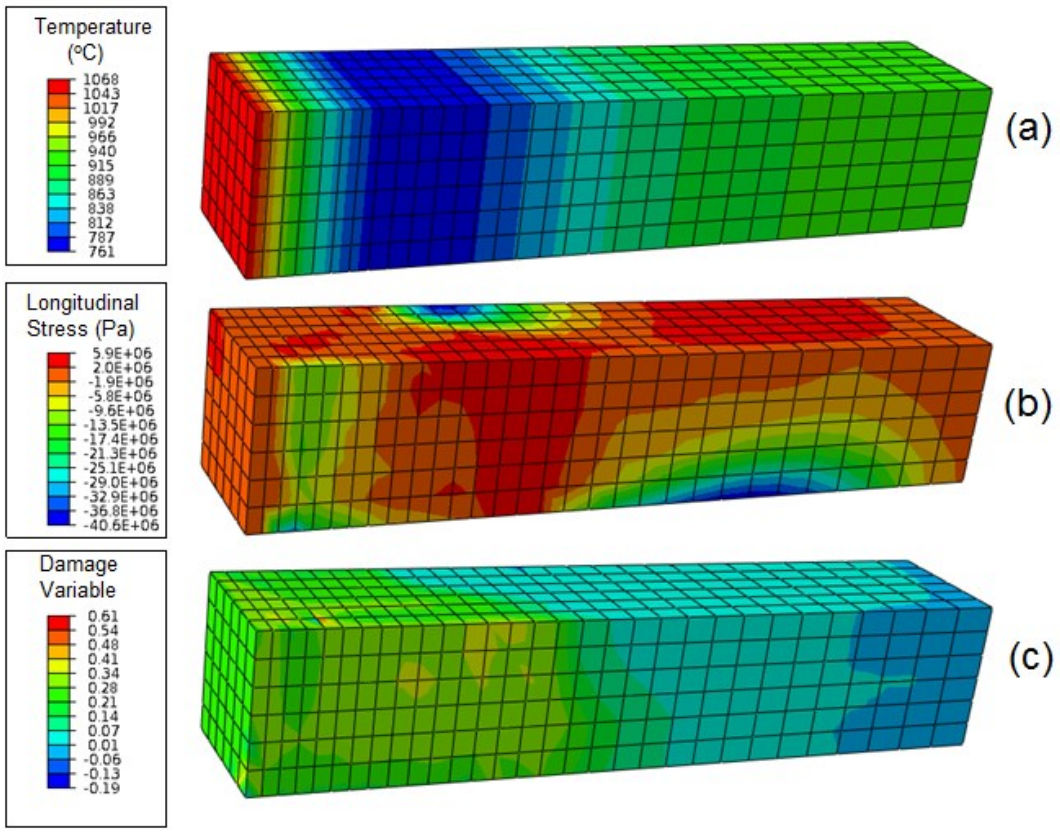

Figure 7.38: Predicted results for a 3-cycle hot-refractory experiment after the 3 thermal-cycles (a) Temperature distribution (b) Longitudinal stress distribution (c) Damage distribution.

7.4.4. Ultrasonic Testing Results for Hot-Refractory Experiments

The damage predictions for each of the hot-refractory experiments are compared with the ultrasonic measurements in Table 7.3. It can be seen from the table that the ultrasonic measurements indicate that significantly higher damage has occurred in the refractory sample as compared to that predicted. It can also be seen that for the 1-cycle experiment, even though the thermal changes are significant only up to half the length of the specimen, the entire length of the specimen has experienced some damage. The same trend can be seen in the 2-cycle and 3-cycle experiments where the ultrasonic measurements indicate more damage than predicted. This suggests that some form of uniform damage has occurred along the length of the specimen. One potential cause of uniform damage may be high thermal gradients resulting from high rate of heating in the furnace to the target temperature of 1000°C.

Table 7.2: Results of the ultrasonic tests and the predicted damage at various locations of the refractory specimens for the hot-refractory experiments.

Distance from the Interface (cm)	**Damage (%)**					
	1-Cycle Experiment		**2-Cycle Experiment**		**3-Cycle Experiment**	
	Measured "a"	Predicted	Measured "c"	Predicted	Measured "f"	Predicted
0-5	53	~20	65	~25	~68	~25
5-10	42	~4	56	~5	~59	~6
10-15	42	0	45	~1	~53	~2
Along the length of the specimen	68	~8	~64	~10	~71	11

In order to experimentally check if furnace heating is responsible for the high overall damage in these refractory specimens, a heating test was conducted. The ultrasonic tests were carried out before and after heating a refractory specimen to 1000°C in the furnace. The results

show that the damage in transverse direction was ~39% (V_{bef}=4210m/s, V_{aft}=3280m/s) and the damage along the length of the specimen was ~51% (V_{bef}=4720m/s, V_{aft}=3290m/s). This confirms that the furnace heating was responsible for a significant damage. It should be noted that even though the damage caused by heating in the furnace was significant, the ultrasonic results show that the damage effects penetrate further into the specimen with increasing numbers of cycles. This effect was also predicted by the model.

To conclude, the modeling results of the tests on hot refractories indicate that heating in the furnace prior to thermal cycling caused significant damage in the refractory. However, the predicted damage data shows an expected trend of increasing the length of damage penetration with increasing number of cycles. Comparing to the overall experimental and predicted damage values for the cold-refractory experiments in Table 7.2 with those in Table 7.3 it can be seen that hot-refractory experiments show higher values. This is because of the expected reasons mentioned in section 7.2.2 i.e. higher thermal cycling in the case of hot-refractory experiments and also due to the fact that the refractories exhibit higher damage at higher temperatures for the same amount of thermal stress.

In the next chapter, the application of the thermo-mechanical model presented here to the industrial process conditions is discussed.

8. Application to the Industrial Conditions

The thermal-stress modeling methodology developed in this work can be applied to any refractory material used in the pyrometallurgical industry to predict the damage. The refractory material considered in this work is used in the steel-industry. More specifically, it is used in secondary steel-making vessels e.g. tundish as a safety lining. In this chapter, the thermo-mechanical model is applied to predict damage in refractories used in a tundish application.

8.1 Thermal Conditions in Tundish Refractories

The tundish acts as a reservoir of molten steel transferred from the ladle furnace and helps to facilitate smooth flow to the continuous casting machine (CCM). The thermal cycles experienced by a tundish involves three steps, preheating, casting and idling before the next operating cycle starts. The timespan for each of these steps varies from plant to plant. It is therefore of interest to an operator to find the optimum processing conditions and times to minimize refractory loss for their plant. Prior to normal operation, a tundish must be preheated to between 500 and 1100°C, typically over a time period of 12 to 27 hours [77]. Preheating is followed by casting where molten steel of ~1580°C is poured into the tundish and supplied to CCM. Casting operations can take place for as long as ~15 hours, during which time, the liquid metal in the tundish is periodically replenished. The tundish experiences an idle period thereafter for 10 to 22 hours depending on the availability of the molten steel for the next cycle of operation. During the idle time, the refractory lining loses heat to the surrounding environment.

8.2 Effect of Preheating Conditions on Damage in Refractories

If the tundish is not preheated for long enough or does not reach a high enough temperature, large thermal shock may occur in the refractory lining leading to subsequent refractory cracking and losses. On the other hand, preheating for too long or to too high a temperature results in large energy consumption. Depending on a variety of factors, the preheating schedules that are followed can vary from plant to plant. As a result, the heating rates during preheating also vary. Three types of preheating schedules similar to those shown in Fig. 8.1 are common. In schedule "A", the refractory is preheated to a surface temperature of 1100°C in 6 hours; in schedule "B", the refractory surface is preheated to 500°C in 12 hours; and in schedule "C", 1100°C in 27 hours. After preheating, the casting stage follows in which, the tundish is filled up with molten steel at ~1580°C causing the refractory surface temperature to increase rapidly. For simplicity, this increase in temperature is shown as a vertical dotted line in Figure 8.1.

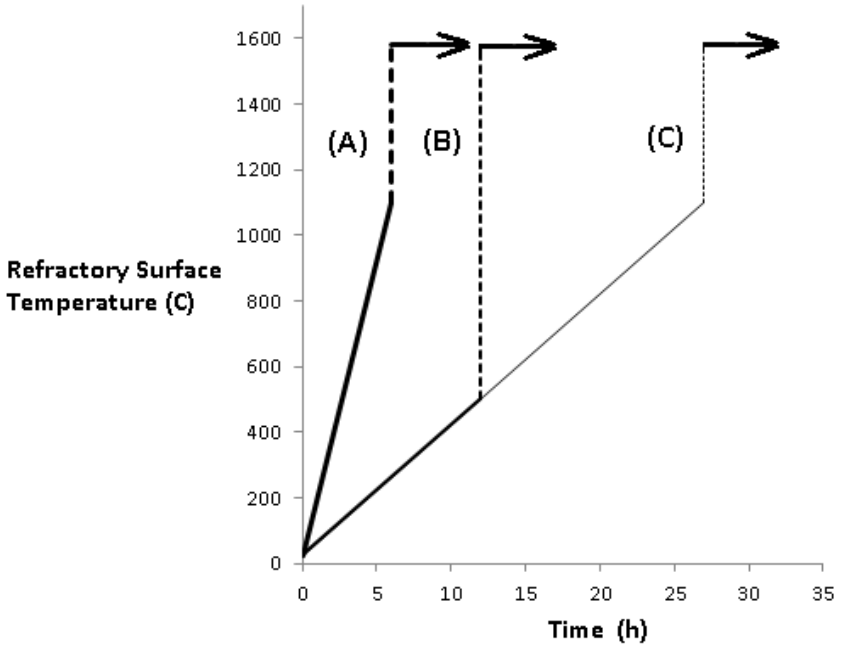

Figure 8.1: Preheating schedules in tundish operation followed by casting of 1580°C of molten steel. (A) Heating for 6 hours to reach 1100°C (B) Heating for 12 hours to reach 500°C (C) Heating for 27 hours to reach 1100°C.

The thermo-mechanical model described in Chapter 6 was used to predict the damage caused by these tundish preheating schedules. The details of the tundish geometry and boundary conditions are discussed in the next section.

8.2.1 Model Development

The refractory lining system of a tundish consists of three sections. The lining immediately in contact with the molten steel is called “working lining”, which is applied as a spray mixed slurry, and has a low thermal conductivity (20mm to 50mm in thickness). The next section of lining is the “safety lining” (100mm to 160mm in thickness) made up of the refractory material examined in this project. The next section is the “insulating lining”, which is made from

a very low thermal conductivity insulating board (~10mm in thickness). The linings that make up a tundish are supported by a steel shell of thickness ~25mm. The aim of the simulations presented here is to predict the damage accumulation in the safety lining.

Considering the entire refractory lining system as the computational domain is a complex problem due to the presence of the mortar joints and spatially changing boundary conditions on the surface of the refractory. Therefore, only a small section of the lining that is in contact with the molten steel is considered for the simulation. The computational domain consists of a composite strip of various sections of the refractory lining and the steel shell. The computation domain and the boundary conditions are shown in Figure 8.2.

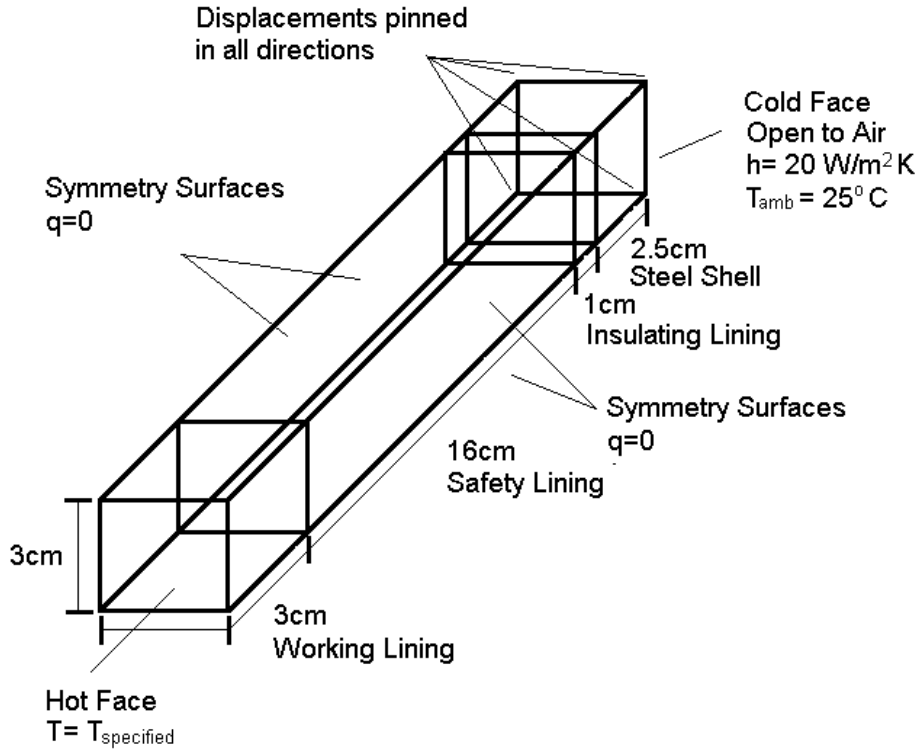

Figure 8.2: Computational domain and the boundary conditions employed to study the effect of preheating schedule on refractory damage.

The following assumptions were made while developing the model:

1. In the refractories used for the pyro-metallurgical reactors, heat flow via conduction occurs predominantly in the radial direction along the thickness of the lining. Hence, one-dimensional heat flow was assumed.
2. Because of the lack of the data needed to describe the behaviour of the mortar joints, the refractory lining was assumed continuous i.e., without any mortar joints.
3. The focus of the simulation was to predict damage due to the thermal stress in the safety lining. In order to avoid any other stresses arising at the safety lining-working lining interface and the safety lining-insulating lining interface, the mechanical properties of all the refractories were assumed to be the same as those of the material used in this project (i.e. the safety lining). Elastic-plastic material behaviour was assumed for the steel shell.
4. The thermophysical properties (conductivity, specific heat, and density) were assumed because the exact data for the properties of the working and the insulating lining are not available. The rationale for choosing these values is described below.

   For the working lining, the commercial product "Basilite spray mix" (manufactured by Vesuvius) with a density of 1400kg/m^3 was assumed. The thermal conductivity of this product is not available. Since, the working lining has lower thermal conductivity than the safety lining, a thermal conductivity of 1W/mK was assumed. For the insulating lining, the commercial product "HZ RCF Board" (manufactured by KT Refractories) with density 350kg/m^3 and temperature dependent thermal conductivity [78] was assumed. The specific heats of the insulating and working linings were assumed to be the same as that of the safety lining.

A model of the composite section through the furnace was run for three cases following the preheating schedules shown in Figure 8.1. The temperature distribution through the wall of the furnace at the end of the preheat is plotted for each case in Figure 8.3.

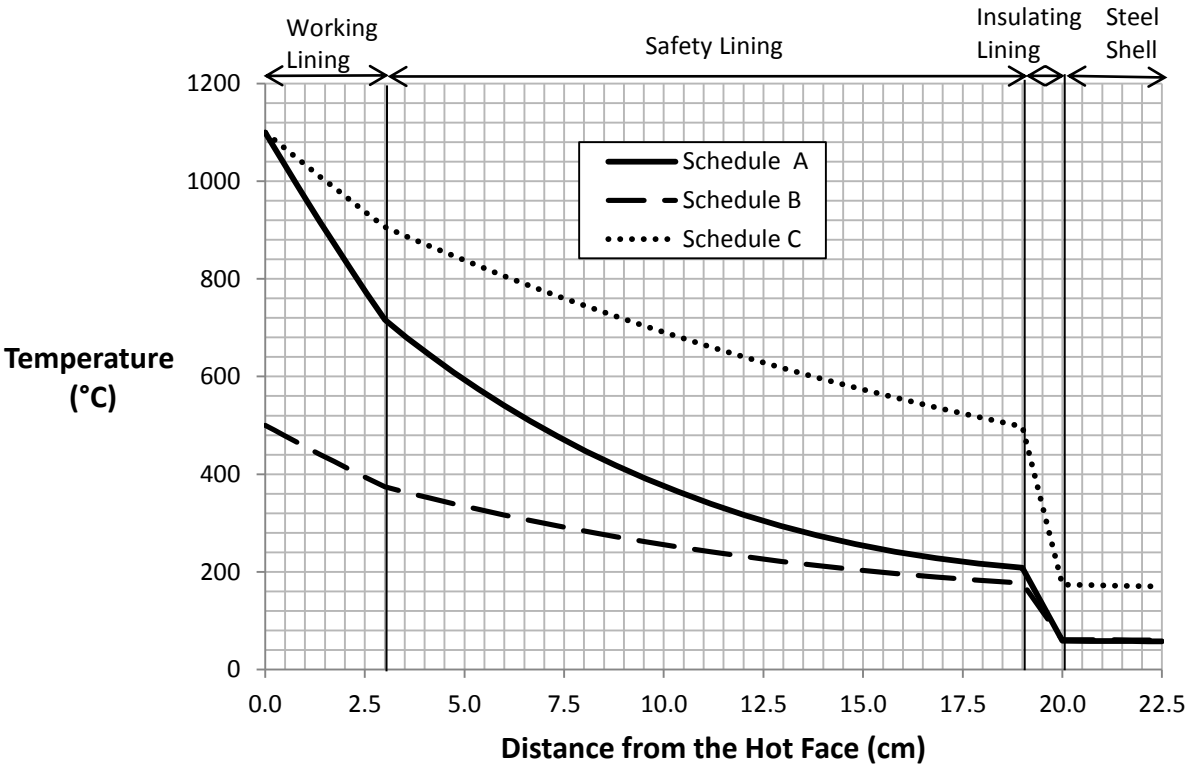

Figure 8.3: Predicted temperature profile of tundish sections (refractory linings and steel support) following different preheat schedules.

Figure 8.3 indicates that, for each preheating schedule, the thermal gradients in the lining vary with the preheating schedule and the thermal diffusivity of the various sections of the lining. The highest thermal gradient is observed for schedule A, followed by schedule C and then schedule B. Due to the increased duration of heating, preheating schedule C results in a higher

average wall temperature than schedule A even though the temperature at the hot face is approximately the same.

The existing model that considers only the preheating stage was extended to include the casting stage that lasts for 15hours. During this stage, the heat transfer coefficient between the metal and the lining and the temperature of molten steel were assumed to be 1000W/m^{2}K and 1580°C, respectively. On the exterior surface of the support steel, which is exposed to the atmosphere, the heat transfer coefficient and the atmospheric temperature were assumed to be 20W/m^{2}K and 25°C, respectively. The predicted temperature profiles at the end of the casting stage for the various preheating schedules do not show any significant difference (Figure 8.4). This indicates that the thermal conditions existing during the casting operation and the duration of this stage are sufficient to reach a thermal profile very close to the steady-state thermal profile in the furnace wall, eliminating the gradients achieved during the preheat.

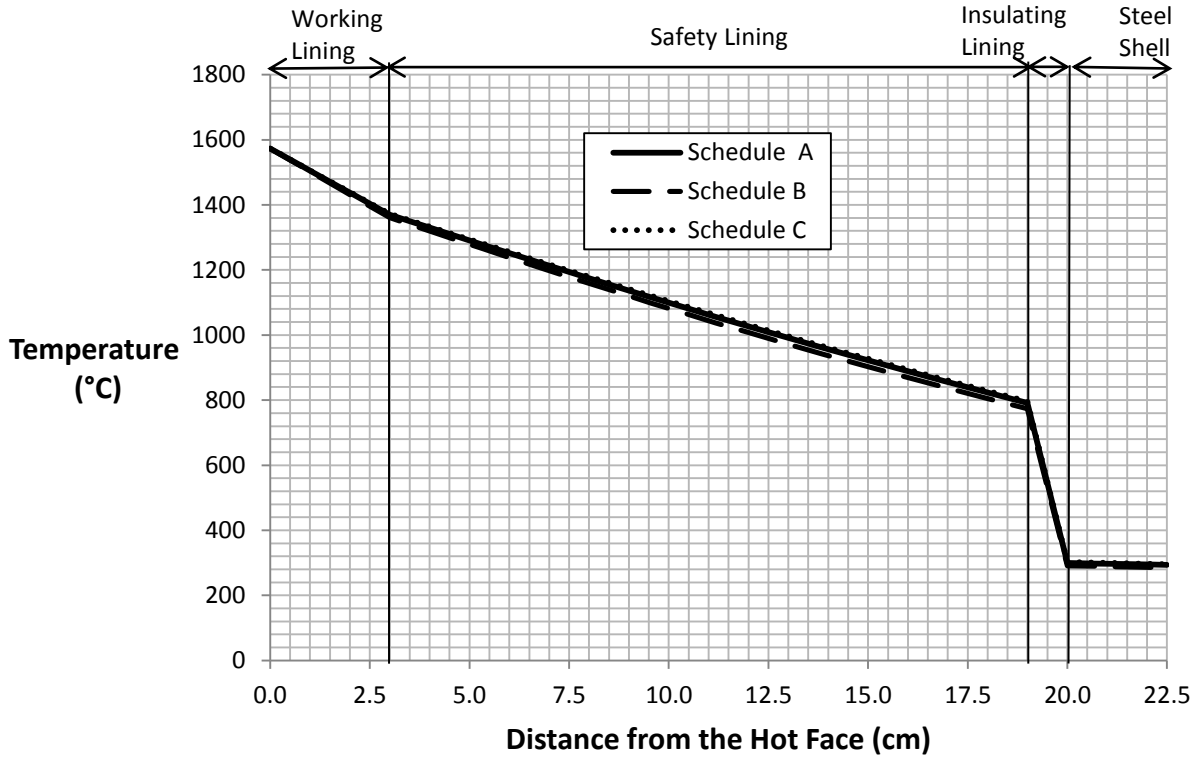

Figure 8.4: Predicted temperature profile of tundish sections (refractory linings and steel support) after different preheat schedules followed by the casting stage.

During the initial period of the casting stage, the thermal conditions are not close to the steady-state conditions. Thus, prior to steady state conditions being reached, the thermal history of the furnace lining will be dependent on the preheating schedule. Figure 8.5 shows the temperature profile after 5hr into the casting stage. It can be seen that the difference between the thermal gradients is not as significant as the one observed after the preheating (shown in Figure 8.3). Schedule B has the largest thermal gradient followed by schedule A that shows slightly smaller thermal gradient than schedule B and then schedule C.

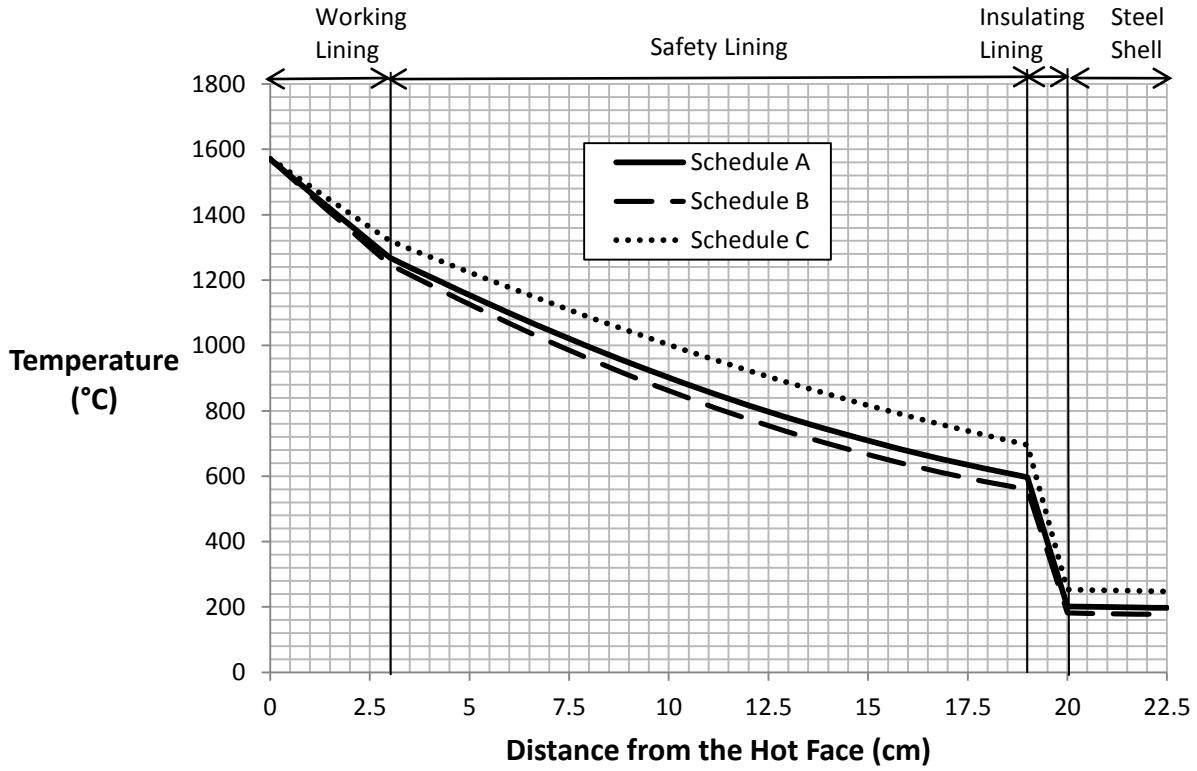

Figure 8.5: Predicted temperature profile of tundish sections (refractory linings and steel support) after different preheat schedules followed by 5hr into the casting stage.

The profile of damage occurring in the safety lining after 5hr into the casting stage is shown in Figure 8.6. It can be seen that at distances greater than ~15cm from the hot face, the damage is almost uniform (~25%) for all three cases. Even though, schedule B shows the largest thermal gradient, the damage within ~15cm from the hot face shows that Schedule C experiences the largest damage followed by Schedule A and then B. This is due to the temperature dependence of damage in the refractory materials. Damage occurs more readily (i.e. at lower stresses) at higher temperatures. Since the lining temperature after pre-heating with schedule C has a higher average temperature than occurs with schedule A or B, higher damage results after

casting following pre-heat schedule C. The results indicate that the influence of higher thermal gradient in the cases of schedule A and B compared to schedule C is not as significant as the influence of the higher average temperature in case of schedule C.

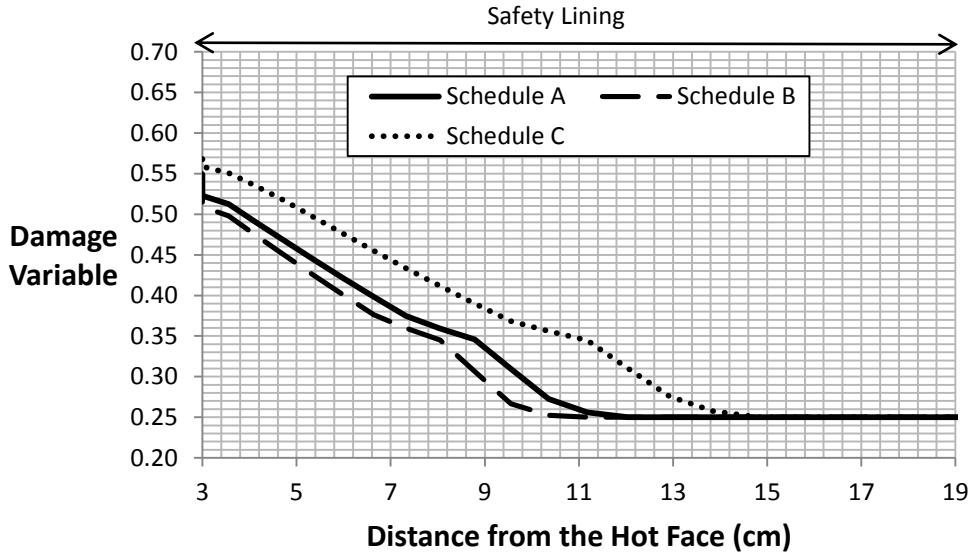

Figure 8.6: Predicted damage profile of tundish safety lining after different preheat schedules followed by 5hr into the casting stage.

Figure 8.7 shows the predicted damage profile at the end of the casting stage. As expected, the results show that the differences in the damage profiles for various preheating schedules is negligibly small due to similar temperature profiles at the end of the casting stage (shown in Figure 8.4). It can also be seen that as with the progress of the casting stage the effects of temperature are penetrated further resulting into an increase in damage along the entire length of the working lining.

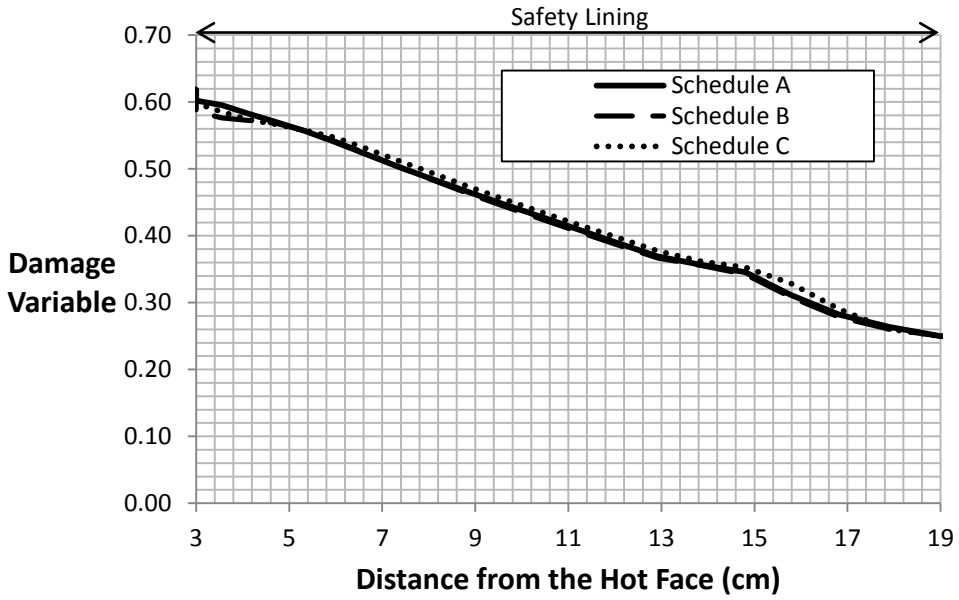

Figure 8.7: Predicted damage profile of tundish safety lining after different preheat schedules followed by the casting stage.

The analysis indicates that the difference in damage for various schedules is initially significant but it is negligibly small at the end of the casting stage. The choice of schedule is important during the initial period. The results indicate that Schedule B shows the least damage in the material. It is therefore desirable to follow schedule B.

One of the other ways to improve life of the lining would be to control the idle time between two processing cycles. The next section discusses the effect of idle time on the refractory damage.

8.3 Effect of Idle Time on Damage in Refractories

The thermo-mechanical model discussed in the last section was used to predict damage in the refractory safety lining while idle time of tundish operation. Three different idle periods of 10, 15 and 20hours were considered.

Considering the long duration (~15 hours) of the casting operation, steady-state conditions were assumed to have been achieved at the end. The steady-state temperature at the end of casting was used as the initial thermal condition to study the effect of idle time. For the steady-state analysis, convective boundary conditions consistent with liquid metal in contact with the interior surface of tundish were assumed. The heat transfer coefficient and the temperature of molten steel were assumed to be 1000 W/m^2K and 1580°C, respectively. On the exterior surface of the support steel, which is exposed to the atmosphere, the heat transfer coefficient and the atmospheric temperature were assumed to be 20 W/m^2K and 25°C, respectively. During the idle time, the heat transfer coefficient and the atmospheric temperature were assumed to be $20W/m^2K$ and 50°C, respectively on the interior surface. The boundary conditions at the exterior surface during the idle time were not changed.

The predicted temperature distribution through the thickness of the tundish is plotted for various idling times in Figure 8.8. As expected, the results show that the highest thermal gradient is observed for the case with a 10 hour idle time and the gradient reduces with increasing idle time. The maximum thermal gradients for the case of 10 hour idle time is about 28°C/cm and 12°C/cm in the working and safety lining, respectively. For the cases of 15 hour and 20 hour idle time, the maximum thermal gradients change to about 14°C/cm and 7°C/cm, respectively for the

working lining but in the case of safety lining they change only to about 6°C/cm and 3°C/cm, respectively. This shows that in the safety lining, the thermal gradient does not reduce as significantly as that in the working lining with increasing the idle time.

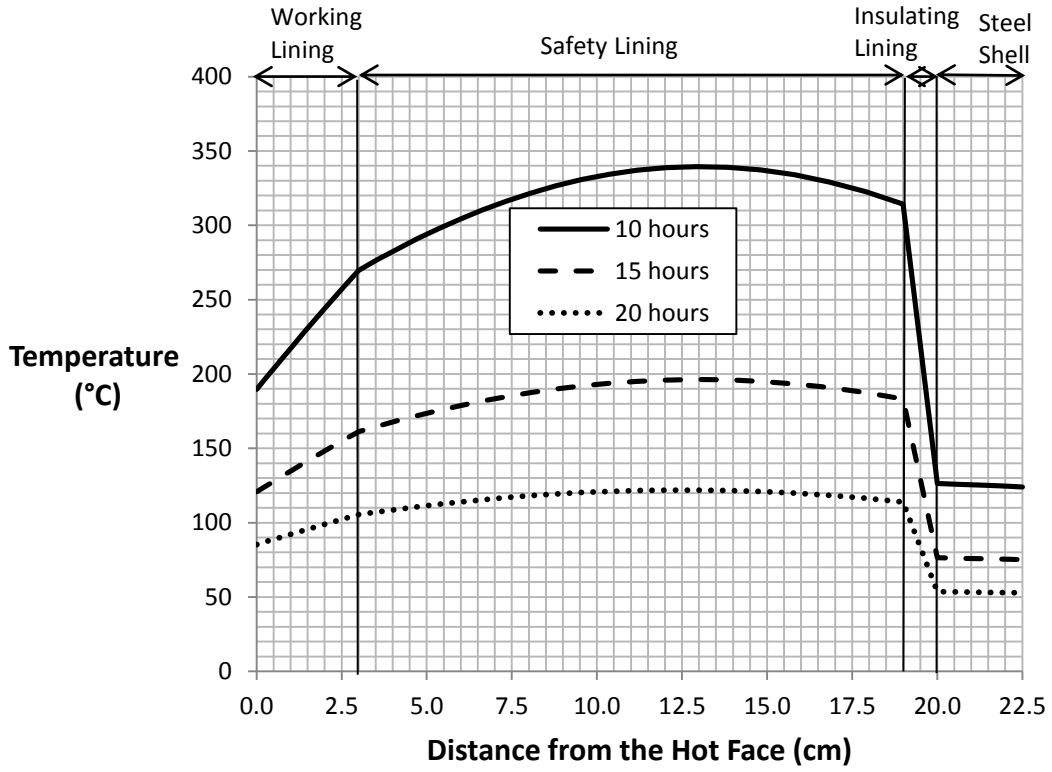

Figure 8.8: Temperature profile of refractory lining after different idling periods.

To further examine the effects of idle time, the variation of the damage variable across the length of the safety lining is plotted in Figure 8.9. The variation of the damage variable across the safety lining after 10hours does not change significantly with increasing idle time. This is attributed to the fact that even though the magnitude of thermal gradient in the working lining reduces with

idle time, the change in the magnitude is not significant enough to cause a significant change in damage.

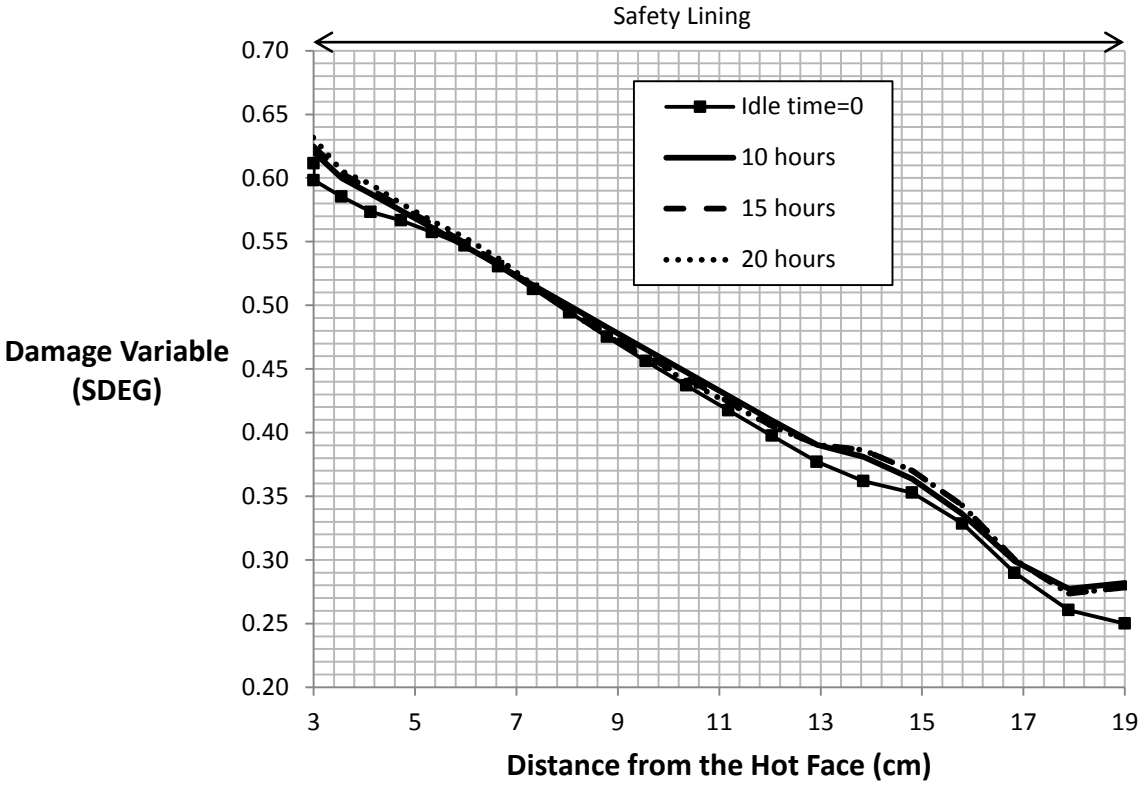

Figure 8.9: Damage variation across the safety lining after different idling periods.

Even though in practice long idle times are avoided due to additional energy consumption during the next preheating cycle, the results in this section indicate that increasing the idle time longer than 10 hours does not cause additional significant cooling, nor any additional significant damage in the lining. Since the tundish operates on a cyclic basis, the effect of multiple cycles on the state of stress in refractories is discussed in the next section.

8.4 Effect of Multiple Thermal Cycles

To see the effects of multiple cycles, a case where a tundish at room temperature undergoes preheating followed by 3 thermal cycles is considered. Each cycle consists of a casting stage followed by idle time. The casting time and idle time of 15hours were assumed. The computational domain and boundary conditions are the same as the ones previously discussed in this chapter. The simulations were run for the three cases of preheating schedules shown in Figure 8.1. Since, the temperature profiles for the different preheating schedules after the first casting stage are the same (Figure 8.4), the temperature profiles after following the idle time and the subsequent cycles are also the same. For the sake of simplicity, the results of only one preheating schedule (schedule A) are discussed.

The temperature profile of the tundish section at the end of each stage is plotted for schedule A (Figure 8.10). It can be seen that the temperature profiles after the casting stage and after the idle time does not change significantly with the number of cycles.

The damage profiles of the safety lining after the preheating and at the end of the idle time of every cycle are plotted (Figure 8.11). It can be seen that the damage after 13cm into the safety lining increases after the 2^{nd} cycle. However, the damage does not increase further with the subsequent cycles. This is attributed to the temperature changes shown in Figure 8.10. It can be seen that at the start of the first casting stage, the material is at an elevated temperature due to the preheating. However, due to the idle time after the first casting stage, the material is at a lower overall temperature than the one after the preheating. Therefore, the second casting stage involves larger temperature increase than the first one. This is the cause of an increase in damage seen in Figure 8.11 after the 2^{nd} cycle. Figure 8.10 also indicate that the temperature change for

the third casting stage is the same as the one for second casting stage. Therefore, the damage after the 3rd cycle is the same as the one after the 2nd cycle.

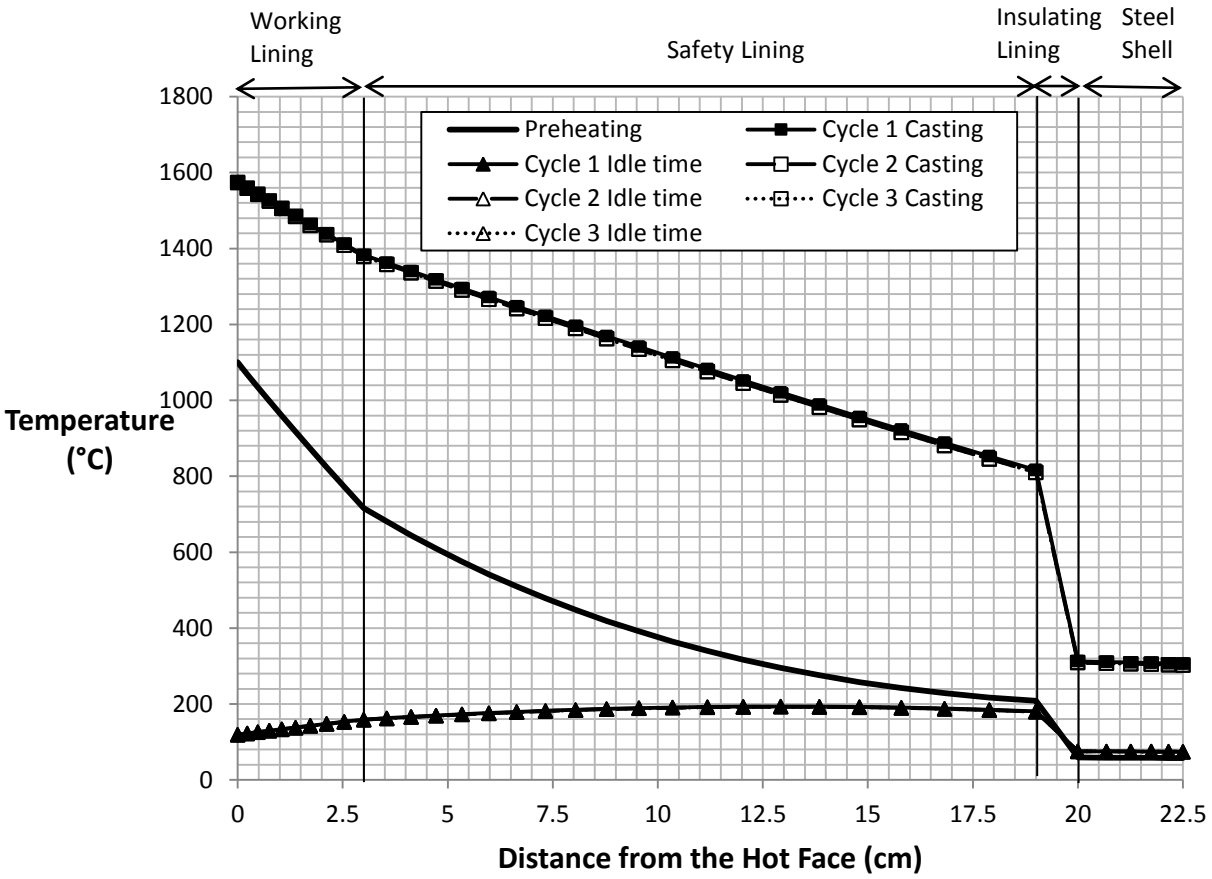

Figure 8.10: Predicted temperature profile of tundish sections (refractory linings and steel support) after various stages of the tundish operation.

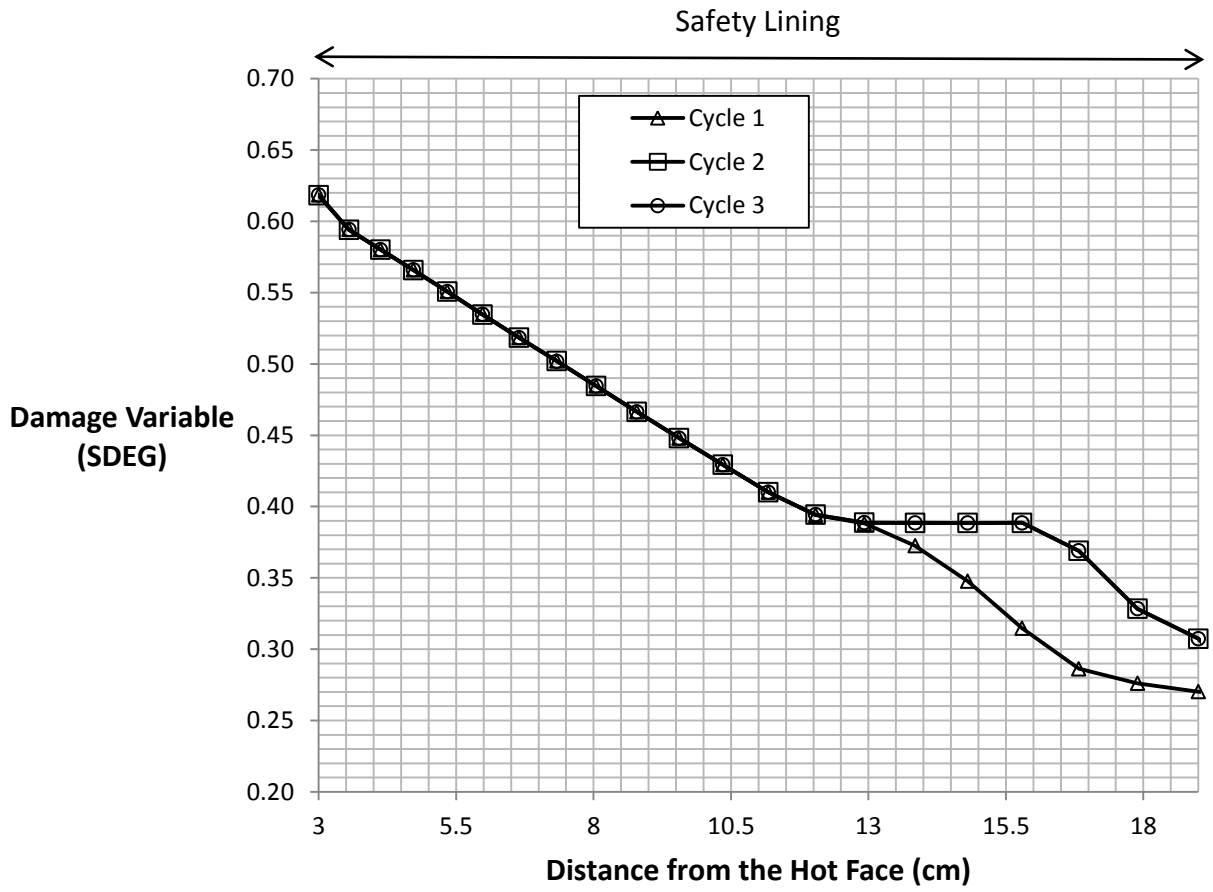

Figure 8.11: Predicted damage variation in the safety lining after 1,2, and 3 thermal cycles with different preheat schedules.

To conclude, the analysis presented in this chapter shows that the modeling methodology discussed in this project can be readily applied to industrial operating conditions to predict damage occurring due to thermal stress in the refractory linings. This analysis could be used to minimize the refractory loss due to the thermal stress by examining different operational scenarios and materials.

9. Conclusions and Future Work

In this chapter, the results are summarized and conclusions are discussed. The future scope of this work is also discussed thereafter.

9.1 Summary and Conclusions

Previous work shows the need for analyzing refractory degradation due to thermal stress by means of mathematical modeling because of its practical significance to the industrial applications. Further work in this area from the modeling and experimental perspectives has been hampered because: 1) precise material models require detailed material property data, which can only be acquired with testing machines specifically designed for this purpose; 2) limited experimental validation of models that have been developed. Additionally, the control and quantification of the heat transfer conditions in thermal cycling experiments on refractories has not been achieved successfully. The work done in this thesis provides a new approach to study refractory degradation due to cyclic heating and cooling and attempts to provide a solution to the above-mentioned issues.

The work presented in this thesis highlights some important aspects about refractory behaviour during thermal cycling. In the last three decades of work on refractory performance simulation, the assumption of the constitutive behaviour has changed. The initial work assumed a simple “linear-elastic” material behaviour and more recent work considers more complex “temperature-dependent damageable” material behaviour. The thermo-mechanical model considered in this work predicts damage in terms of a material property (elastic modulus) which

can be measured by the non-destructive testing (ultra-sonic testing). Although this model has been used previously for refractories, it has not been validated against data from thermal cycling experiments.

Thermal shock tests are commonly used as an approximate measure to test refractories for their resistance to thermal cycling. Refractories are tested before, during and after the thermal shock tests and the material properties are compared. In most of the tests, a hot or cold refractory specimen is immersed in a liquid medium such as water, salt bath, oil and so forth. The control of the heat flux and its quantification is very difficult in these methods. In this work, the "contact" method of thermal cycling was employed to overcome these problems and, was used to validate a thermal-mechanical model including "damage" behaviour. Use of this method also appears to have the potential to become a standard thermal shock testing method for the refractories due to the control over its thermal boundary conditions. These thermal cycling experiments using the "contact" method were successful in inducing significant thermal gradients in the refractory specimens. The start-to-finish temperature change was ~500°C for experiments starting with cold (room temperature) refractory specimens and was ~575°C for experiments starting with hot refractory specimens. However, these experiments did pose some experimental issues such as detachment of spot-welded thermocouples, oxidation of the threads in the steel block and so forth. Due to this, more than one attempt was required to perform each experiment successfully.

The temperature data from the steel was used in the inverse heat conduction model to calculate the heat flux entering into the refractory. The refractory temperatures were predicted using the heat flux values. The predicted refractory temperatures during the heating stage in both

cold- and hot-refractory experiments were significantly higher than the experimental values. This could have been due to the heat loss to the surrounding either from the refractory specimen or from the steel block. An experiment with multiple thermocouples attached to the refractory specimen indicated that the heat loss from the refractory to the surrounding was negligibly small. Hence, it was concluded that the heat loss must have been from the steel block. After compensating for the heat loss from the steel block in the thermal model, the predicted temperatures were within ~60°C of the experimental values for all thermal-cycling experiments. The predicted refractory temperatures during the cooling stage were in agreement owing to negligibly small heat loss from the steel block that is at low (room) starting temperature. The thermal model also predicted that large thermal gradients develop across the length of the refractory specimen during the experimentation.

The temperature data from the refractory specimen was used to run the thermal-stress model that predicts thermal-stress and damage in terms of loss in elastic stiffness. The model predicted the time variation temperature and thermal stress as they penetrate further into the specimens during multiple thermal cycle experiments. It was also shown that the effects of thermal-stress penetrate further into the specimen than the effects of temperature due to the transmission of force. The model also shows that even though the temperature variation is one-dimensional, the stress and damage variation is three-dimensional. The predicted damage variation indicate that the magnitude of damage along the edge of the specimen is larger than that at the center. With multiple cycles, the overall damage in the specimen does not increase significantly, however, the damage penetrates further into the specimen with each cycle.

To validate the predicted damage results from the thermal-stress model, ultrasonic testing was carried out at various locations on the refractory specimen. The results of the tests indicate percentage loss of elastic stiffness (damage) at those locations. Ultrasonic testing on specimens that had experienced cold-refractory experiments indicates that the model was capable of predicting the damage within a reasonable agreement. The small discrepancy in the agreement is attributed to the factors such as heterogeneity of the refractory material, assumption of the "damage" properties in compression at elevated temperatures, discrepancy of about 60°C in the thermal model predictions, and the inherent error associated with the ultrasonic tests. Ultrasonic testing on specimens that had experienced hot-refractory experiments exhibited significantly higher damage than that predicted. This was determined to be due to the damage associated with the high rate of preheating of the refractory material in the furnace prior to the thermal cycling experiments.

These refractories are mostly used in the secondary steel-making operations. They are widely being used in the tundish furnace. The current model was applied to examine the tundish operations. Three preheating schedules that are commonly used in the tundish operation were considered and the model was run to predict damage in the refractory. The models predictions show that the schedule with preheating time of 12hours and temperature of 500°C will cause the least amount of refractory damage during the early stages of casting. However, the damage after the casting is the same regardless of the preheating schedule. This is due to the long duration (15hours) of the casting stage that results near steady-state thermal profiles. The model also considered other aspects of the tundish operation such as the effect of the idle time and the effect of multiple operating cycles. The model predictions show that even though the idle time cause

damage in refractories, the damage resulting from increasing the idle time by more than 15 hours is not significant. When the model is run for multiple operating cycles, it was seen that the increase in damage was significant only until the 2nd thermal cycle. The damage did not increase with multiple cycles after the 2nd cycle. The results show that this work can be applied to any reactor with known heat transfer conditions and based on the results suggestions could be made for the best operating practices.

9.2 Future Work

Current work provides tools to model refractory damage by means of a new modeling and experimental methodology. However, areas remain that require further improvement.

1. Design of the experiment – The current work was the first and the only attempt so far to use the "contact" method to carry out multiple thermal cycling experiments. Experimental issues were experienced that were not anticipated. The experimental results show that 1-D heat flow was achieved in the refractory specimen. However, 1-D heat flow was not achieved in the steel block. In addition, thermocouples in the refractory specimens as well as steel blocks were susceptible to breaking while heating in the furnace. The thermocouple contacts had to be spot welded quite frequently. A methodology to mitigate this issue needs to be developed.
2. Temperature dependent constitutive data that is used is crucial in the stress / damage models. This data is available for a very limited number of refractory materials due to the requirement of specially designed testing equipment. Further work is needed for mechanical characterization of other refractory materials.

Apart from these points, this work also hints at other new areas of work, which should be investigated.

To apply this modeling methodology successfully to industrial conditions, understanding the thermal and mechanical boundary conditions is important. The stress experienced by a single refractory originates from thermal as well as mechanical factors such the presence of mortar joints, movement of molten metal due to the movement of reactor and so forth. Strains can arise from the chemical reactions between the molten metal and the refractories, which may lead to spalling of refractory material. Research has been done on individual mechanisms or the combination of thermal and chemical factors however, there is a need to develop an integrated model, which combines all the three factors (thermal, mechanical and chemical) together.

References

[1] M. A. Deneen and A. C. Gross, “Refractory Materials: The Global Market, The Global Industry”, Bus. Econ., 45 (4), (2010), pp. 288-295.

[2] N. Kreuels, “A view on the European Refractory Industry”, Bol. Soc. Esp. Ceram, (48), (2009), pp 245-254.

[3] M. S. Moats and W. G. Davenport, Treatise on Process Metallurgy: Volume 3-Industrial Processes Part A, (2014), Ringgold Inc., Beaverton, (2014), p. 646.

[4] D. H. Hubble, R. O. Russell, H. L. Vernon and R. J. Marr, “Steelmaking Refractories”. In “The making Shaping, and Treating of Steel, 11th edition, Steelmaking and refining volume, R. J. Fruehan, Ed., AISI Steel Foundation, Pittsburgh, PA, (1991), pp. 227-290.

[5] A. A. Bustos, J. K. Brimacombe and G. G. Richards, “Heat Flow in Copper Converter”, Metall. Trans. B, 17 (4), (1986), pp. 677-685.

[6] I. P. Tsibin and A. T. Kuznetsov, “A Physical Model of Thermal Failure of Refractory Concretes”, All-Union Refract. Inst., 29 (1-2), (1988), pp. 43-48.

[7] G. X. Wang, A. B. Yu and P. Zulli, “Three-dimensional Modelling of the Wall Heat Transfer in the Lower Stack Region of a Blast Furnace”, ISIJ Int., 37 (5), (1997), pp. 441-448.

[8] A. O. Nieckele, M. F. Naccache and M. S. P. Gomes, “Numerical Modelling of an Industrial Aluminum Melting Furnace”, J. Energ. Resour-ASME, 126 (1), (2004), pp. 72-81.

[9] A. R. Khoei, I. Masters and D. T. Gethin, “Numerical Modelling of the Rotary Furnace in Aluminum Recycling Processes”, J. Mater. Process. Tech., 139 (1-3), (2003), pp. 567-572.

[10] V. I. Shubin, “The Effect of Temperature on the Lining of Rotary Cement Kilns”, Refra. Ind. Ceram., 42 (5-6), (2001), pp. 216-221.

[11] O. Volkova and D. Janke, “Modelling of Temperature Distribution in Refractory Ladle Lining for Steelmaking”, ISIJ Int., 43(8), (2003), pp. 1185-1190.

[12] J. L. Xia and T. Ahokainen, “Transient Flow and Heat Transfer in a Steelmaking Ladle During the Holding Period”, Metall. Mater. Trans. B, 32 (Aug), (2001), pp. 733-741.

[13] A. Zimmer, A. N. C. Lima, R. M. Trommer, S. R. Braganca, and C. P. Bergmann, “Heat Transfer in Steelmaking Ladle”, J. Iron Steel Res. Int., 15 (3), (2008), pp. 11-14.

[14] A. R. Hanifi, A. Eilaghi, A. Salary, F. Golestani-Fard and W. L. Headrick, "Influence of Covers on Thermomechanical Performance of Steelmaking Ladles", Refra. Appl. Trans., 2(2), (2006). pp. 1-5.

[15] T. P. Fredman, "Heat Transfer in Steelmaking Ladle Refractories and Steel Temperature–A Literature Review", Scand. J. Metall., 29, (2000), pp. 232-258.

[16] A. K. Kyllo and G. G. Richards, "Accretion Growth on Single-Pipe Tuyeres: Part II. Model Results and Discussion", Metall. Trans. B, 24 (4), (1993), pp. 583-591.

[17] W. A. Krivsky and R. Schuhmann Jr., "Heat Flow and Temperature Distribution around a Copper Converter Tuyere", Trans. Metall. Soc. AIME, 215, (1959), pp. 82-86.

[18] K. Datta, S. Chandra and A. Chatterjee, "Fundamental and Operational Aspects of Submerged Gas Injection into Steel Melts", Trans. Indian Inst. Met., 48 (4), (1995), pp. 309-328.

[19] W. D. Kingery, "Factors Affecting Thermal Stress Resistance of Ceramic Materials", J. Am. Ceram. Soc., 38 (1), (1955), pp. 3-15.

[20] W. S. Chang, C. E. Knight, D. P. H. Hasselman and R. G. Mitchiner, "Analysis of Thermal Stress Failure of Segmented Thick-Walled Refractory Structures", J. Am. Ceram. Soc., 66 (10), (1983), pp. 708-713.

[21] B. K. Ganguly, Karl R. McKinney, and D. P. H. Hasselman, "Thermal-Stress Analysis of Flat Plate with Temperature-Dependent Thermal Conductivity", J. Am. Ceram. Soc., 58 (9-10), (1975), pp. 455-456.

[22] Y. Joliff, J. Absi, J.C. Glandus, M. Huger and N. Tessier-Doyen, "Experimental and Numerical Study of the Thermomechanical Behaviour of Refractory Model Materials", J. Eur. Ceram. Soc., 27 (2-3), (2007), pp. 1513-1520.

[23] A. S. Nikiforov and E. V. Prekhod'ko, "Thermal Stresses Generated in the Lining of a Steel Ladle", Refract. Ind. Ceram., 46 (5), 2005, pp. 360-363.

[24] D. Gruber, K. Andreev, and H. Harmuth, "FEM Simulation of the Thermomechanical Behaviour of the Refractory Lining of a Blast Furnace", J. Mater. Process. Tech., 155-156, (2004), pp. 1539-1543.

[25] X. Liang, W. L. Headrick, L. R. Dharani and S. Zhao, "Transient Stresses in Refractory Lining of a High Temperature Black Liquor Gasifier", Refract. Applic. Trans., 1 (3), (2005), pp. 1-8.

[26] B. Schwartz, "Thermal Stress Failure of Pure Refractory Oxides", J. Am. Ceram. Soc., 35 (12), (1952), pp. 325-333.

[27] C. Aksel and P. D. Warren, "Thermal Shock Parameters [R, R''' and R'''']' of Magnesia-Spinel Composites", J. Eur. Ceram. Soc., 23 (2), (2003), 301-308.

[28] D. P. H. Hasselman, “Elastic Energy at Fracture and Surface Energy as Design Criteria for Thermal Shock”, J. Am. Ceram. Soc., 46 (11), (1963), pp. 535-540.

[29] D. P. H. Hassleman, “Thermal Stress Parameters for Brittle Refractory Ceramics- A Compendium”, Am. Ceram. Soc., 49 (12), 1970, pp. 1033-1037.

[30] D. P. H. Hasselman, “Unified Theory of Thermal Shock Fracture Initiation and Crack Propagation in Brittle Ceramics”, J. Am. Ceram. Soc., 52 (11), (1969), 600-604.

[31] D. A. Ivanov, A. S. Balabanov, G. A. Fomina, N. A. Alad’ev, and G. E. Val’yano, “The Problem of Thermal Stability of Ceramic Materials”, Refract. Ind. Ceram., 39 (3-4), (1998), pp. 80-84.

[32] G. V. Kulokev and I. I. Nemets, “The Theory of Thermal Shock in Heterogeneous Refractory Materials”, Refractories-USSR, 6 (7-8), (1965), pp. 394-401.

[33] H. Hencke, J. R. Thomas Jr., and D. P. H. Hasselman, “Role of Material Properties in the Thermal-Stress Fracture of Brittle Ceramics Subjected to Conductive Heat Transfer”, J. Am. Ceram. Soc., 67 (6), (1984), pp. 393-398.

[34] F. Bradley, A. C. D. Chakladar, and A. Mitchell, “Thermal Stress Fracture of Refractory Lining Components: Part I. Thermoelastic Analysis”, Metall. Trans. B, 18, (1987), pp. 355-363.

[35] F. Bradley, A. C. D. Chakladar, and A. Mitchell, “Thermal Stress Fracture of Refractory Lining Components: Part II. Safe Heating and Cooling Rates”, Metall. Trans. B, 18, (1987), pp. 365-370.

[36] F. Bradley, A. C. D. Chakladar, and A. Mitchell, “Thermal Stress Fracture of Refractory Lining Components: Part III. Analysis of Fracture”, Metall. Trans. B, 18, (1987), pp. 371-380.

[37] V. R. Salvini, V. C. Pandolfelli, R. C. Bradt, “Extension of Hasselman’s Thermal Shock Theory for Crack/Microstructure Interactions in Refractories”, Ceram. Int., 38, (2012), pp. 5369-5375.

[38] H. Harmuth, K. Rieder, M. Krobath, and E. Tschegg, “Investigation of the Non-Linear Fracture Behavious of Ordinary Ceramic Refractory Materials”, Mat. Sci. Eng. A, 214, (1996), pp. 53-61.

[39] H. Harmuth, and E. K. Tschegg, “A Fracture Mechanics Approach for the Development of Refractory Materials with Reduced Brittleness”, Fatigue Fract. Engng. Mater. Struct., 20 (11), (1997), pp. 1585-1603.

[40] D. N. Boccaccini, M. Cannio, T. D. Volkov-Husoviæ, I. Dlouhy, M. Romagnoli, P. Veronesi, and C. Leonelli, “Assessment of Viscoelastic Crack Bridging Toughening in Refractory Materials”, J. Euro. Ceram. Soc., 28, (2008), pp. 1941-1951.

[41] N. Rendtorff and E. Aglietti, “Mechanical and Thermal Shock Behaviour of Refractory Materials for Glass Feeders”, Mater. Sci. Eng. A, 527 (16-17), (2010), pp. 3840-3847.

[42] W. O. Soboyejo, C. Mercer, J. Schymanski, and S. R. van der Laan, “Investigation of Thermal Shock in a High-Temperature Refractory Ceramic: A Fracture Mechanics Approach”, J. Am. Ceram. Soc., 84 (6), (2001), pp. 1309-1314.

[43] C. Aksel, “Mechanical Properties and Thermal Shock Behaviour of Alumina-Mullite-Zirconia and Alumina-Mullite Refractory Materials by Slip Casting”, Ceram. Int., 29, (2003), pp. 311-316.

[44] B. A. Latella, and T. Liu, “The Initiation and Propagation of Thermal Shock Cracks in Graphite”, Carbon, 44, (2006), pp. 3043-3048.

[45] J. P. Singh, Y. Tree, and D. P. H. Hasselman, “Effect of bath and specimen temperature on the thermal stress resistance of brittle ceramics subjected to thermal quenching”, J. Mater. Sci., 16(8), (1981), pp. 2109-2118.

[46] T. Ozyener, K. Satyamurthy, C. E. Knight, J. P. Singh, D. P. H. Hasselman, and G. Ziegler, “Effect of ΔT-and Spatially Varying Heat Transfer Coefficient on Thermal Stress Resistance of Brittle Ceramics Measured by the Quenching Method”, J. Am. Ceram. Soc., (1983),66 (1), pp. 53-58.

[47] A. A. Ogacho, B. O. Aduda, F. W. Nyongesa, “Thermal shock behaviour of a kaolinite refractory prepared using a natural organic binder” J. Mater. Sci., (2006), 41 (24), pp. 8276-8283.

[48] D. Lewis, “Comparison of Critical ΔTc Values in Thermal Shock with the R Parameter”, J. Am. Ceram. Soc., 63 (11-12), (2006), pp. 713-714.

[49] M. Posarac, M. Dimitrijevic, T. Volkov-Husovic, A. Devecerski, and B. Matovic, “Determination of Thermal Shock Resistance of Silicon Carbide/Cordierite Composite Material using Nondestructive Test Methods”, J. Eur. Ceram. Soc., 28 (6), (2008), pp. 1275-1278.

[50] N. Rendtorff, L. Garrido, E. Aglietti, “Mullite–zirconia–zircon composites: Properties and thermal shock resistance”, Ceram. Int., 35(2), (2009), pp. 779-786.

[51] M. Posarac, M. Dimitrijevic, J. Majstorovic, T. Volkov-Husovic, and B. Matovic, “Nondestructive Testing of Thermal Shock Resistance of Cordierite/Silicon Carbide Composite Materials after Cyclic Thermal Shock”, Res. Nondestruct. Eval., 21 (1), (2010), pp. 48-59.

[52] N. S. Koksal and M. Toparli, “Calculation of Temperature and Thermal Stress in Refractory Materials Quenched in Water Using Finite Element Methods”, Key. Eng. Mater., 264-268, (2004), 1783-1786.

[53] I.D. Katsavou, M.K. Krokida, and I.C. Ziomas, "Determination of mechanical properties and thermal treatment behavior of alumina-based refractories", Ceram. Int., 38(7), (2012), pp. 5747–5756.

[54] F. Damhof, W. A. M. Brekelmans and M. G. D. Geers, "Non-local Modelling of Thermal Shock Damage in Refractory Materials", Eng. Fract. Mech., 75 (16), (2008), 4706-4720.

[55] F. Damhof, W.A.M. Brekelmans and M.G.D. Geers, "Non-Local Modelling of Cyclic Thermal Shock Damage Including Parameter Estimation", Eng. Fract. Mech., 78(9), (2011), pp. 1846-1861.

[56] P. K. Panda, T.S. Kannan, J. Dubois, C. Olagnon and G. Fantozzi, "Thermal Shock and Thermal Fatigue Study of Ceramic Materials on a Newly Developed Ascending Thermal Shock Test Equipment", Sci. Technol. Adv. Mater., 3(4), (2002), pp. 327-334.

[57] A. G. Tomba Martinez, M. A. Camerucci and A. L. Cavalieri, "Thermal Stress Analysis of Cordierite Materials Subjected to Thermal Shock", J. Mater. Sci., 43 (8), (2008), pp. 2731-2738.

[58] W. P. Rogers and A. F. Emery, "Contact Thermal Shock Test of Ceramics", J. Mater. Sci., 27 (1), (1992), pp. 146-152.

[59] Z. P. Bazant and J. Planas, Fracture and Size Effect in Concrete and Other Quasibrittle Materials, CRC Press, (1998), Madrid, pp. 103-104.

[60] K. Andreev and H. Harmuth, "FEM Simulation of the Thermo-Mechanical Behaviour and Failure of Refractories- A case Study", J. Mater. Process. Tech., 143-144, (2003), pp. 72-77.

[61] A. Gasser, P. Boisse, Y. Dutheillet, and J. Poirier, "Experimental and Numerical Analysis of Thermomechanical Refractory Lining Behaviour", Proc. Instn. Mech. Engrs., 215 (L), (2001), pp. 41-54.

[62] X. Liang, W. L. Headrick, L. R. Dharani and S. Zhao, "Modeling of Failure in a High Temperature Black Liquor Gasifier Refractory Lining", Eng. Fail. Anal., 14 (7), (2007), pp. 1233-1244.

[63] X. Liang, W. L. Headrick and L. R. Dharani, "Continuum Damage Mechanics Modeling of the Failure of Refractory Cup under Thermal Loading and Chemical Shrinkage", Refract. Appl. News., 11 (3), (2006), pp. 17-23.

[64] Ron H. J. Peerings, "Enhanced Damage Modeling for Fracture and Fatigue", PhD Thesis, Technische Universiteit Eindhoven, The Netherlands, (1999).

[65] D. Henneberg, A. Ricoeur and P. Judt, "Multiscale Modeling for the Simulation of Damage Processes at Refractory Materials under Thermal Shock", Comp. Mater. Sci., 70, (2013), pp. 187–195.

[66] E. W. Washburn, "Refractory Materials as a Field for Research", J. Am. Ceram. Soc., 2 (1), (1919), pp. 3-31.

[67] C. A. Schacht, Refractories Handbook, CRC Press, (2004), New York, pp. 435-474.

[68] P. Laugier and G. Haiat, Introduction to the Physics of Ultrasound, P. Laugier and G. Haiat (eds.), Bone Quantitative Ultrasound, Dordrecht: Springer (2011), pp. 29-45.

[69] R. H. Bogaard, "Thermal Conductivity of Selected Stainless Steels", Therm. Cond., 18, (1985), pp. 175-185.

[70] R. H. Bogaard, P. D. Desai, H. H. Li and C. Y. Ho "Thermophysical Properties of Stainless Steels", Thermochim. Acta., 218, (1993), pp. 373-393.

[71] M. M. Rathore and R. R. A. Kapuno, Engineering Heat Transfer, 2nd edition, Ringgold Inc., (2010), Portland, pp. 353-446.

[72] K. N. Prabhu and A. A. Ashish, "Inverse Modeling of Heat Transfer with Application to Solidification and Quenching", Mater. Manuf. Process., 17 (4), (2002), pp. 469-482.

[73] A. Buhr, "Refractories for Steel Secondary Metallurgy", CN-Refract., 6(3), (1999), pp.19-30.

[74] T. Jankowiak and T. Lodygowski, "Identification of Parameters of Concrete Damage Plasticity Constitutive Model", Found. Civil. Env. Eng., 6, (2005), pp. 53-69.

[75] M. G. Kakroudi, "Tensile Thermomechanical Behavior of Refractory Concrete: Influence of the Nature of the Aggregates and Their Thermal Treatment" (in French), Doctoral dissertation, Faculty of Sciences University of Limoges, (2007).

[76] E. Ouedraogo, M. Roosefid, N. Prompt and C. Deteuf, "Refractory Concretes Uniaxial Compression Behaviour Under High Temperature Testing Conditions", J. Eur. Ceram. Soc., 31(15), (2011), pp. 2763-2774.

[77] T. Auer, D. Gruber and H. Harmuth, "Numerical Failure Analysis for the Refractory Lining of a Tundish", 49th International Colloquium of Refractories, Aachen, Germany, (2006), pp. 194-196.

[78] "Ceramic Fiber Board Data Sheet", n.d. Web. 24 Mar. 2016, Retrieved from http://www.ktrefractories.com/ceramic-fiber-board.cfm

Appendix A

This section shows the results of the ultrasonic testing used to calculate damage. The test gives the velocity of sound through the material. The refractory specimens were tested before and after the thermal cycling experiments. The results for cold-refractory experiments and hot-refractory experiments are shown in Table A and in Table B, respectively.

Table A: Results of the ultrasonic tests and the predicted damage at various locations of the refractory specimens after the cold-refractory experiments.

Distance from the Interface (cm)	1-Cycle Experiment		2-Cycle Experiment		3-Cycle Experiment
	Specimen "a" V_{bef}=4480m/s	Specimen "c" V_{bef}=6320m/s	Specimen "d" V_{bef}=4700m/s	Specimen "e" V_{bef}=6320m/s	Specimen "g" V_{bef}=6320m/s
0-5	V_{aft}=4200m/s	V_{aft}=5940m/s	V_{aft}=4175m/s	V_{aft}=5610m/s	V_{aft}=5420m/s
5-10	V_{aft}=4480m/s	V_{aft}=6320m/s	V_{aft}=4700m/s	V_{aft}=6320m/s	V_{aft}=5940
10-15	V_{aft}=4480m/s	V_{aft}=6320m/s	V_{aft}=4700m/s	V_{aft}=6320m/s	V_{aft}=6210
Along the length of the specimen	V_{bef}=4800m/s V_{aft}=4340m/s	V_{bef}=5760m/s V_{aft}=5640m/s	V_{bef}=4950m/s V_{aft}=4250m/s	V_{bef}=5380m/s V_{aft}=4980m/s	V_{bef}=5120 V_{aft}=4640

Table B: Results of the ultrasonic tests and the predicted damage at various locations of the refractory specimens after the hot-refractory experiments.

Distance from the Interface (cm)	1-Cycle Experiment Specimen "a" V_{bef}=4230m/s	2-Cycle Experiment Specimen "c" V_{bef}=4480m/s	3-Cycle Experiment Specimen "f" V_{bef}=4380m/s
0-5	V_{aft}=2890m/s	V_{aft}=2650m/s	V_{aft}=2460m/s
5-10	V_{aft}=3230m/s	V_{aft}=2970m/s	V_{aft}=2790m/s
10-15	V_{aft}=3230m/s	V_{aft}=3310m/s	V_{aft}=3000m/s
Along the length of the specimen	V_{bef}=4410m/s V_{aft}=2500m/s	V_{bef}=4210m/s V_{aft}=2520m/s	V_{bef}=4240m/s V_{aft}=2300m/s